University of Stavanger

Faculty of Science and Technology

MASTER'S THESIS

Study program/ Specialization: **Marine and Subsea Technology**	Spring semester, **2017** **Open access**
Writer: **Ying Chang**	Ying Chang (Writer's signature)
Faculty supervisor: **Prof. Muk Chen Ong and Dr. Lin Li** External supervisor(s): **Msc. Li Li**	
Title of thesis: **Dynamic analysis of gravity based fish cage**	
Credits (ECTS): **30**	
Key words: **Dynamic response,** **fish cage,** **numerical simulation,** **wave and current**	Pages: **107** Stavanger, **06/07/2017** Date/year

Front page for master thesis
Faculty of Science and Technology

Abstract

With the development of economy and growth of population, we are constantly facing the challenge of decreasing fish population and increasing needs in the fish market. Aquaculture is a practical way to fulfill this demand. Due to limited coastal area for fish farming, the fish farms are moving to deeper sea with harsher wave and current condition.

This thesis focuses on the numerical analysis on the responses of the most commonly used gravity based fish cage under various wave and current conditions using ABAQUS program.

Firstly, the behavior of a simple beam element and the single circular floater in waves and currents are investigated before studying the complex responses of the fish cage. The purpose is to understand the dynamics of the simple fish cage components and lay a foundation for modelling of the whole fish cage system.

Secondly, the responses of a model scaled fish cage are studied using two commonly used numerical models for fish cage modelling: truss model and mass spring model. Convergence study and sensitivity study are conducted and responses in terms of volume reduction and hydrodynamic forces are compared using the two models. These numerical results are also validated with the numerical and experimental results from previous study.

Thirdly, truss model is further applied to the full scale fish cage. The interaction of the net and the floater are studied. More sensitivity studies related to solidity ratio, bottom weight and wave-current condition are performed with the improved truss model to study the responses of volume reduction, hydrodynamic force, mooring tension, and critical stresses.

The conclusions are that the current velocity is the dominating factor which affects the responses of the fish cage. The hydrodynamic force and deformation are closely influenced with each other, so the hydrodynamic force in reality may have some deviations with that calculated from Morison's equation. The interaction of the floater to the net should not be overlooked when studying the responses of the whole fish cage. The solidity ratio, bottom weight, wave condition can also influence the responses of the fish cage.

Key words: fish cage, numerical simulation, dynamic responses, wave and current

Acknowledgement

I would like to express my appreciation to all those who have helped me to complete this thesis. Special thanks go to Prof. Muk Chen Ong and Dr. Lin Li who have answered my questions timely and helped me to finalize this thesis within the limited time frame. Particularly, they have inspired me in many ways and continuously encouraged me with the belief that I can do better than I have thought. Furthermore, I'd like to thank Msc. Li Li, who has provided support and shared his expertise with me.

Two years' happy student life finally comes to an end, and it is a great experience that has already changed my life. I would like to express my deepest gratitude to University of Stavanger that has provided me with an opportunity to study. As I finish the thesis and exams at the University, I recognize the importance of research skills, and I believe my ability and expertise will serve me well as a qualified master.

Last but not least, I want to thank my fellow friends for their generous help, especially Bin Du, Hui Zhu and Akinyemi Akinsanya, and my families who have supported me through the hardships. Thanks to all who have helped and cared about me.

List of figures

List of tables

Contents

1. Introduction

1.1 Background

Ever since the late 1980s, aquaculture has represented the growth in the supply of fish for human consumption. As we can see from figure 1-1, in 1974 aquaculture industry provides only 4 million tonnes fish for human consumption (3% of the total fish consumption), this share has increased to 26 million tonnes in 1994 (17% of the total fish consumption) and 82 million tonnes in 2014 (47% of the total fish consumption). China has played a major role in this growth as it represents more than 60 percent of world aquaculture production.

Aquaculture is the fastest growing sector of the world food economy. It is estimated by 2030 aquaculture will provide nearly two thirds of global food fish consumption (Msangi et al., 2013). That is because wild fish resources are being over exploited, and very challenging for sustainable development. At the same time, with the growth of the world population, demands are increasing rapidly.

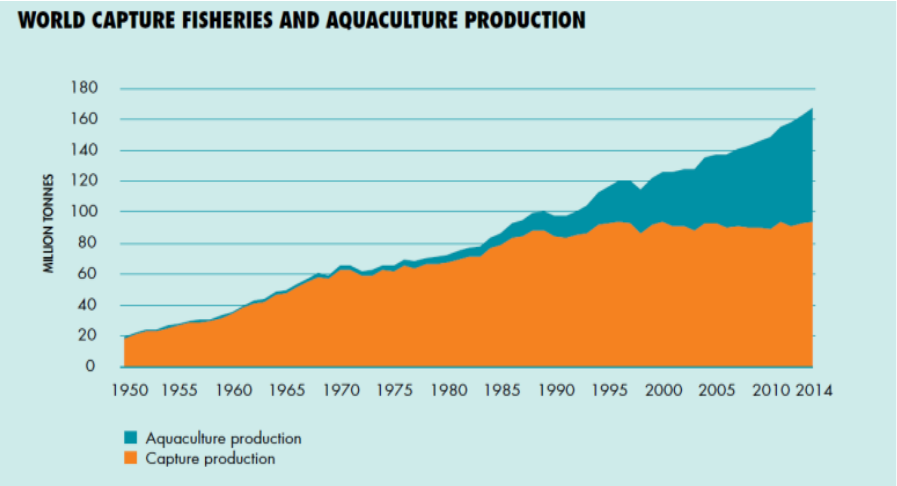

Figure 1-1 Production of captured fish and aquaculture (Fisheries, 2016)

With the pollution and more frequent human activity of near sea area, the fish farm is moving to deep sea, where the sea water is cleaner with no frequent human activities, and the fishes are of high survival rate. However, deep sea is usually with harsh environmental conditions, thus more severe dynamic response for the fish cage will be induces. This is a big challenge for the design of the cage structure.

Norway has a coast with 21,000 km of length, and 90,000 km^2 of sea, compared to approximately 1/3 of the total land area, so the potential for aquaculture is huge. Norway is the world's leading producer of Atlantic salmon and the second largest seafood exporter in the world. The Norwegian aquaculture industry is a major industry for the country. Norway's long coastline is surrounded by cold seawater which provides excellent conditions for

aquaculture activities (Eurofish, 2014).

1.2 Structure and type of floating fish cages

The fish cages are mainly composed of the floater, the net structure, weight system and mooring system. Now the most widely used anti-storm types are gravity type cages, saucer-shaped cages and tension leg cages. Below is the introduction of these types of cage.

1.2.1 Gravity type fish cage

As in figure 1-2, gravity based fish cage is a cylinder shaped fish cages composed of floater, net, weight system and mooring system. Gravity cages mainly rely on the weight system and the buoyancy of floater to tension the net and maintain a certain volume.

The net structure is made of nylon and HDPE (abbreviation for high-density polyethylene), very flexible and easy to deform under wave and current. The floater is made up of 2 to 3 high-strength HDPE pipe of around 0.25m diameter to provide the buoyancy for the whole cage. The operators can walk on it for daily operations and maintenances. Usually it has a perimeter of 60 to 110 meters, the maximum can reaches up to 180 m. The maximum depth is 40 m, and the fish cage with capacity of 200 tons can be used up to 10 years.

This type of fish cage is widely used in China, US, Canada, Japan and some other countries, for its simple structure, easy operation and limited investment. It also has its limitations, as it cannot withstand too harsh environment condition, for example, the relative volume will reduce more than 60% in current (v≥1m/s) when the fishes inside are hard to survive (Fei, 2014).

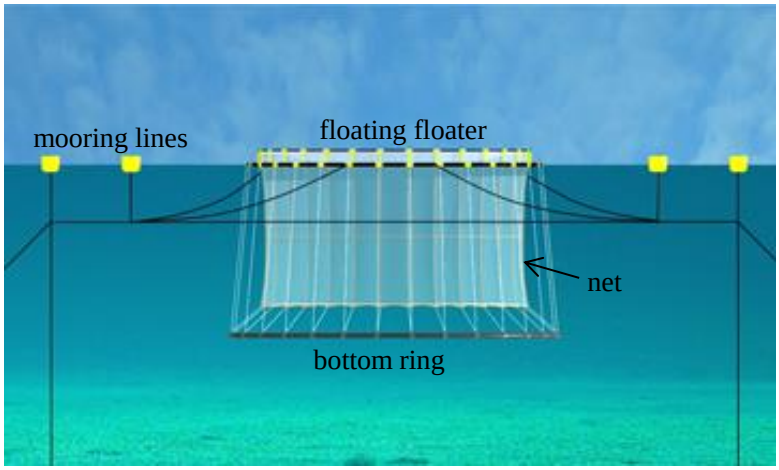

Figure 1-2 Gravity based fish cages (BadinottiGroup, 2011)

1.2.2 Saucer-shaped fish cage

Saucer-shaped fish cage is also known as Marine station cages or double cone-shaped settlement cages. It consists floating ring, floating bar, net system, weight system, offshore

work platforms and lifting control system. Typically, a rigid floating rod in the middle of the cage is 15 meters in length, the diameter of the floating ring is 25 meters. Cage maintains its shape through its resilience and self-supporting. The working platform can slide along the central floating rod, therefore change the capacity of the cage. Floating ring can also float to sea surface in order for fish feeding and harvesting (Fei, 2014). It can withstand larger wave and current than gravity based fish cage, so in harsh ocean area, marine station is the first choice to raise fish. However, it is not so widely applied because of its limited effective volume. With the same height and diameter, the effective volume is only 1/3 of the gravity based fish cage, so it is not so economical.

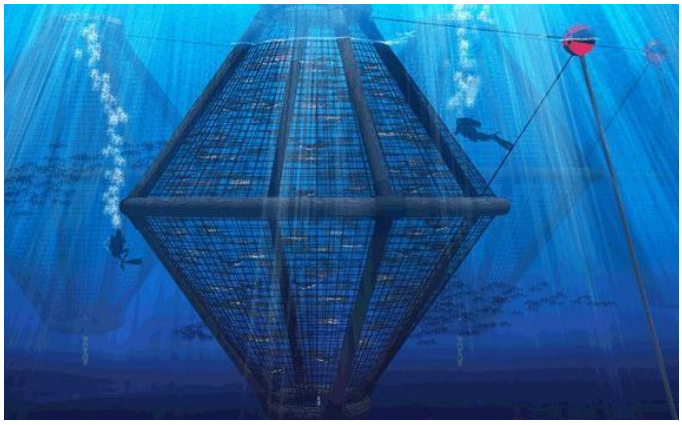

Figure 1-3 Saucer-shaped cage (Ellmer, 2011)

1.2.3 Tension leg cage

Tension leg cage (TLC) is proposed in Norway. It has the same mooring lines as the tension leg oil platform. It consists of six telescopic ropes, which are connected with six piles of the seabed through the tension leg. Each corner of the hexagon cage connects to a pillar to ensure a stable volume. Tension leg cage is strong in resisting extreme wind, wave and current condition. In storm and large current condition, the TLC submerges by itself, and the volume reduction is less than 10% (Refamed, 2010). Usually, the dimension of the cage volume is 16 meter in diameter, 20 meter in depth. Its limited size makes it only stay in early commercial stage.

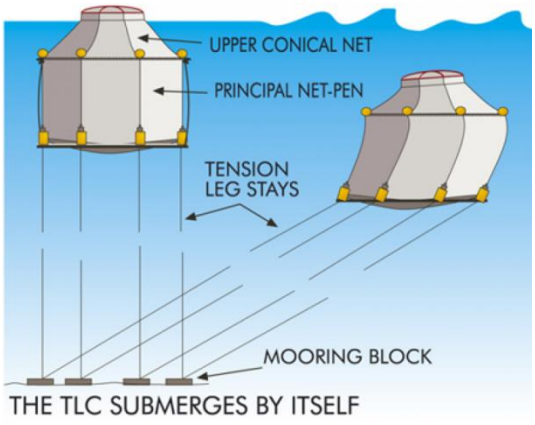

Figure 1-4 Tension leg cage (Refamed, 2010)

There are also other new concepts of fish cage, such as flexible floating cages or egg shaped fish cage. However, currently these concepts are not so economical to apply. Gravity based fish cage is still in the dominating place, taking up nearly 90% of the fish cages now being used worldwide (Li, 2013). It is very practical to study the dynamic responses under various environmental conditions in order to design the reliable cage structure under harsh wave and current condition. This thesis focuses on the dynamic responses of the gravity based fish cage.

1.3 Previous work on dynamic response study of the fish cage

The dynamic response of the fish cage in deep ocean area is a very complex problem. Norway is the leading country in fish farm research, and now it is still a very hot topic in the universities and companies.

The most significant influence of the fish cage comes from wave and current. The current can reduce the net pen volume, thus endanger the fish inside. The floater constrained by the mooring line, deforms with the wave and current. The wave can give the cage structure with a force variation, leading to possible fatigue damage of the structure. The adding bottom weight can reduce the responses caused by the wave and current. Therefore, we can see responses under wave and current is the primary concern when designing the cage structure. Lots of researchers have devoted their attentions on different research topics of the fish cage under wave and current. The main conclusions from their studies are summarized as follows:

1) Hydrodynamic force on the floater under wave and current will induce the deformation and fatigue problem to the floater.

2) The current force on the flexible net will cause deformation, thus reduce the net volume.

3) Bio-fouling increases the drag on the net and decreases the net volume.

4) Max mooring tension is the key operational parameter to choose the suitable mooring line.

5) Bottom weight (or bottom ring) has an impact on the hydrodynamic force and net volume.

6) The responses of the fish cage under wave and current separately and concurrently are also a big issue when designing the fish cage.

There are mainly two ways to study dynamic responses of the fish cage system: model experiment and numerical analysis. These two methods need to be validated with each other in various conditions. In numerical analysis of the flexible fish nets, 3 typical models are widely applied: truss model, mass spring model (also known as lumped mass model) and net panel model (also called as screen model). There are also other FEM methods to study the responses of fish cage, such as Aqua FE program.

Moe et al. (2010) modeled the net as truss model and performed the analysis on the drag force and volume reduction under influence of the current speed, weight and gravity. They compared the simulation results with the model experiment done by Lader and Enerhaug (2005), and got similar results with experiment. Then they applied the truss model to predict the hydrodynamic force and relative volume with the full size fish cage. They found that drag load was dependent on the net cage size and weight system. Both drag and lift force were proportional to the current velocity when the velocity was larger than 0.2 m/s.

Lee et al. (2008) modeled the fish cage as a mass spring model (figure 1-5). They verified the model with the experiments by Lader and Enerhaug (2005). Then they validated the numerical model by experiments in the water tank. The validations were performed focusing on four aspects: the velocity reduction ratio under various attack angles, the cage deformation under different current speed, responses from the wave with different heights and periods, the volume reduction ratio and drag forces under various current speeds and sinkers. The comparisons successfully proved the reliability of the mass spring model.

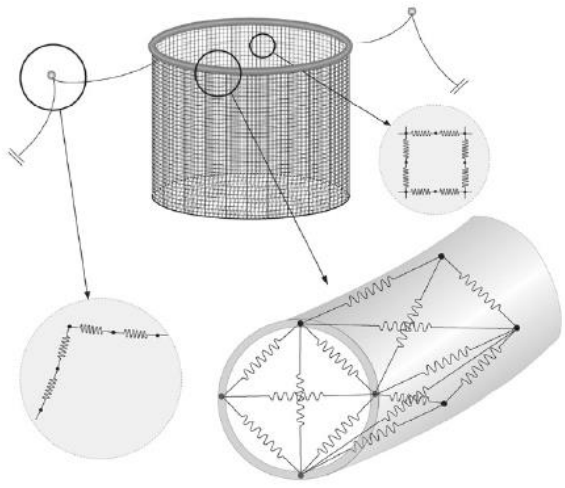

Figure 1-5 Model of fish cage, net, mooring line and floater

Zhao et al. (2007) modeled the net system as a mass spring model and the floater as a

double-column pipe system. Then the wave and current force were calculated on each mini-segment of the floater model by Morison's equation. The results from numerical simulations (hydrodynamic forces and displacements) were very close to those from experiments. They also found that the forces and motions of the floater were dependent on the net responses by the mutual mass points that were attached to both the net and the floater.

Huang et al. (2008) investigated the combined effect of wave and current on the gravity-type cage using lumped-mass method. They found that the responses from current on the volume of net-cage system was more important than those due to waves only. They concluded that farming sites should not be situated in areas where the current speed exceeds 1 m/s, and recommended that the ideal water depth for net-cage implementation in the open sea is between 30 and 50 m.

Lader and Fredheim (2006) used the numerical net panel model which was to divide the net model into super elements (figure 1-6), and to calculate the structural and hydrodynamic forces for each element. They also proposed five critical parameters in studying the responses of fish cage under wave and current: floater movement, wave period/height, current velocity, net solidity and bottom weight. In addition, he found that the current tended to enlarge the effect of the wave loads. Increasing net solidity would result in larger force on the net. The increase of the bottom weight would increase the hydrodynamic force.

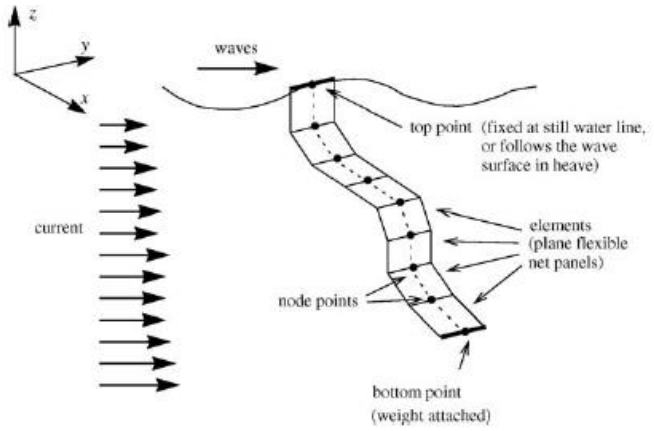

Figure 1-6 Plane net model (Lader and Fredheim, 2006)

Kristiansen and Faltinsen (2012) applied the screen model to look into the viscous hydrodynamic load on nets. The screen model assumed that the net was divided into a number of flat net panels, or screens. The net structure was modeled as a truss model as in figure 1-7. They presented comparisons to experiments with circular net cages in steady current, and got satisfactory agreement between experimental and numerical prediction of the drag and lift.

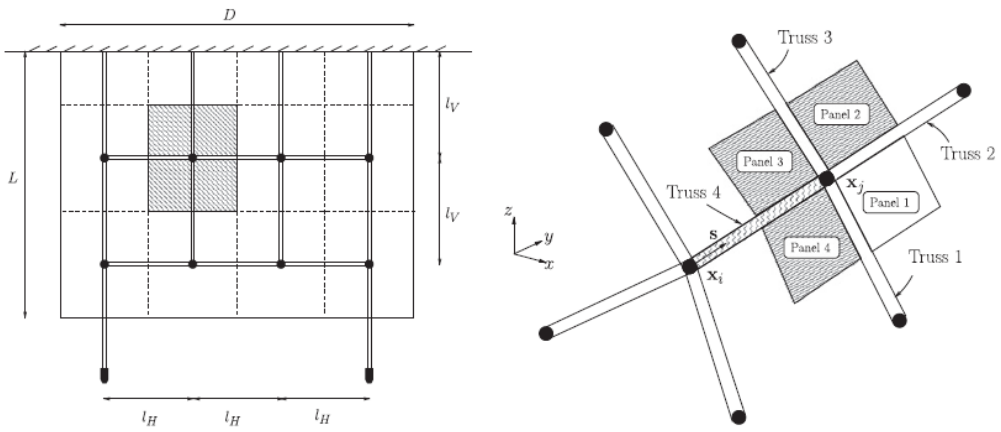

Figure 1-7 Division of a planar net into an equivalent truss model and net panels represented by shaded areas of arbitrary quadrilateral shape

Berstad et al. (2005) used the AquaSim program to simulate the model of fish cage. They studied the load and stress of mooring lines and the volume change with currents and waves. At last, they proposed some practical suggestions for operation by conducting preliminary risk assessment. They concluded that the force and stress increased significantly when the mooring system was skewed. The current played an important role on the volume reduction, as also verified in other papers. The effect whether the wave could induce the volume deduction needed to be verified. Some hazardous operations related the net change, such as boat operation needed to be observed.

Another effective analysis method is model experiment. Model experiment is to test a small scaled fish cage in water, and measure the parameters that can predict the responses of the fish cage. There are some other researches mainly focus on the model experiment. Compared with numerical results, sometimes overlooked problems can be found.

Lader and Enerhaug (2005) investigated the force and deformation of a flexible circular net with different weights under pure current condition by experimental method. They concluded that the hydrodynamic force and deformation were mutually dependent on each other. The drag formula tended to overestimate the drag compared with the experimental results. The drag force was also dependent on Reynold number. Numerical model should take into consideration the dependence of force and deformation.

Lader et al. (2007) studied wave force on a flexible net through experiments. They made the net panel in the flume tank with 3 different solidities under regular wave of different heights and periods. They found that the horizontal force was roughly 10 times larger than the vertical force, and the force increased with increasing net solidity and increasing wave energy. The experiment measurements were also compared with the numerical simulation results, and reached a good agreement.

DeCew et al. (2010) focused on the responses of the single moored submerged fish cage

under current. They used both numerical simulation (Aqua FE) and model experiment to set the solidity ratio as a variable, and investigated the responses related to the submerged depth and mooring tension. They found that Froude scale physical testing could overestimate drag forces at high water velocities, as a larger coefficient of drag was induced in laminar flow.

Fredriksson et al. (2006) used the experimental method to collect the data of the current velocities and mooring system tensions in a 20-unit net pen fish farm near Bay of Fundy in USA. They investigated the flow characteristics in 3 distinct solidities conditions; clean nets for smolts, clean nets for standard grow out and fouled net. They also measured the loads on some important anchor legs and conducted the tidal analysis. Their studies were important for the fish farm engineering, especially for studies on combinations of nets and levels of bio-fouling.

These researches have provided a good understanding of the dynamic responses of gravity based fish cage, especially meaningful for designing the reliable structure of fish cage under rigorous deep ocean area.

1.4 Objective and scope

The thesis tends to perform numerical analysis of the gravity based fish cage under various environmental conditions. The objective is to study the response of the floater, compare the truss and mass spring model, and predict the responses of a full scale fish cage under various conditions.

The thesis is presented in 7 chapters.

Chapter 1 is the general description of the development of fish cage, and progress of research methodology on the dynamic responses.

In chapter 2, basic theory related to the hydrodynamic force calculation are presented, including application of Morison equation, force analysis related to the truss model and mass spring model, and FEM method of solving nonlinear response equations.

In chapter 3, numerical program ABAQUS is introduced. In FEM methods, the net is taken as a set of slender cylinders. This chapter begins with the hydrodynamic force calculations on a simple beam under wave and current separately, to validate the methodology in hydrodynamic force calculation and make preparation for further study. Wave properties are decided by Airy wave theory.

In chapter 4, the single floater model is simulated under wave and current, the responses of the displacement, deformation and stress are addressed.

In chapter 5, two fish cage models (truss model and mass spring model) are studied with a

model scaled fish cage, convergence and sensitive study will be presented. Numerical results will be compared with the experimental results from previous study to test which model is better for further research.

In chapter 6, a full scale fish cage is modeled and analyzed using the truss model. The interaction of the floater and the net are investigated and the truss model will be improved considering the interaction effect. Sensitivity studies on solidity ratio, bottom weight and wave-current condition will be studied. Hydrodynamic force, deformation, max mooring tension and critical stress are compared.

Chapter 7, which is the last chapter, is the conclusion, error source and future work.

The highlight of this thesis lies in that two fish cage models are applied and tested under various waves and currents conditions, equivalent calculations are used to accelerate the calculation. The numerical results are also compared with experimental results to validate the reliability of these two models.

1.5 Summary

This chapter briefly introduced the development of the aquaculture industry. The prospect is prosperous, but there are many challenges. Several main types of the fish cages were illustrated here, such as gravity based floating type, saucer-shaped, and tension leg cage. Gravity based floating fish cage is the most widely used type.

The dynamic response of the fish cage is a popular topic among researchers and scientists. Model experiment and numerical simulation are the most common methods to study the dynamic responses. They mainly focused on the responses of hydrodynamic force, mooring tension, displacement and deformation. Based on these responses, sensitivity study on bottom weight, solidity ratio, attack angles under wave and current were studied.

2. Basic theories on models and methods

2.1 Background

In this chapter, the theories related to the dynamic analysis of the fish cage will be stated. The hydrodynamic force calculation is the main issue. There are two hydrodynamic force models presented briefly in this chapter, Morison type force model and screen model. Then Morison's equation is applied to calculate the hydrodynamic force on the fish cage. Force analysis on the truss model and mass spring model are addressed separately. Morison's equation will be adjusted according to different situations in Morison type force model. Hydrodynamic coefficients are the main issues to decide the hydrodynamic force on the fish cage. Wave velocity, acceleration and stretching method are key issues to get accurate wave force. The wave properties are all based on airy wave theory. In addition, the FEM methods in solving nonlinear calculation are stated.

2.2 Hydrodynamic force calculation

To analyze the forces on the aquaculture net, two hydrodynamic force models (Morison type force model and screen model) are widely used. Then Morison's equation is applied to calculate the hydrodynamic force on slender element.

2.2.1 Morison type force model

In Morison type force model (as figure 2-1), the net can be taken as the sum of many net cylinders, hydrodynamic force on each net cylinder is calculated through Morison's equation.

According to Kristiansen and Faltinsen (2012), the total normal and drag forces predicted by the Morison formulation, $F_N \propto U_\infty^2(\cos\theta + \cos^2\theta)$ and $F_D \propto U_\infty^2(1+\cos^3\theta)$, and these two equations could not be applied in the following situations: (1) a drag model based on the cross flow principle could not be justified when the inflow angle was larger than about 45°, and (2) the interaction between the twines were not accounted into.

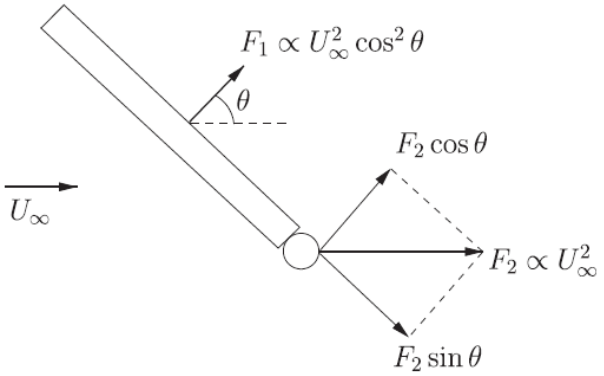

Figure 2-1 Sketch of Morison type force model of net (Kristiansen & Faltinsen, 2012)

2.2.2 Screen model

Kristiansen and Faltinsen (2012) took the fish cage as a truss model, described the truss as a number of flat panels. The geometry and the force of panel can be seen in figure 2-2, the force coefficients as functions of solidity ratio Sn, Reynolds number Re and in flow angle **y**.

$$C_D=C_D\,(Sn, Rn, y),\ C_L = C_L\,(Sn, Rn, y) \tag{2-1}$$

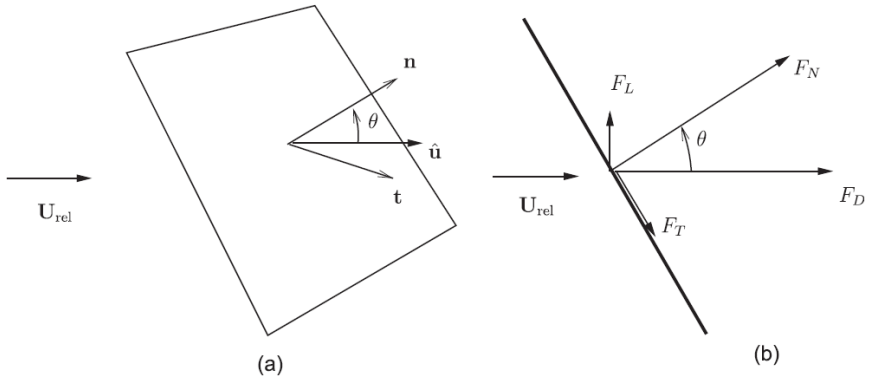

Figure 2-2 General panel with arbitrary orientation (a) and two-dimensional panel (b).
(F_D is drag force, F_L is lift force, F_N is normal component and F_T is tangential component).

The calculation results were compared with those from the experiments, and have achieved good results. However the net panel model also has its limitation. It cannot be applied when the net is highly deformed. In addition, responses under wave condition are too complicated for the screen model to get the accurate results, as the attack angle is changing all the time.

2.2.3 Application of Morison's equation

To calculate the wave and current force on slender elements, Morison's equation is applied. Induced by Morison from University of California in 1950, it is empirical equation derived from numerical experiments. In this thesis, Morison's equation is applied to calculate the force on the floater, net and bottom weights.

According to Morison equation, hydrodynamic force has two components, inertia force (F_M)

and drag force (F_D). Inertia force is induced by the added mass that additional flow which stays originally at the position of the slender cylinder. The hydrodynamic force per unit length can be written as:

$$f(z,t) = f_M + f_D = \frac{\pi D^2}{4}\rho C_M \dot{u} + \frac{\rho}{2} C_D D u|u| \quad (2\text{-}2)$$

Here, D is the diameter of the cylinder, C_M is the inertia coefficient, $\dot{u}$ is the acceleration, u is the velocity, C_D is the drag coefficient, ρ is the density.

For the steady current velocity, the inertia force is 0, there is only drag force.

In case of wave, the cylinder will experience the combination of accelerations and velocities from wave particles. So both drag force and inertia force need to be taken into consideration.

The above Morison's equation is for slender cylinder, if we take the cylinder with other cross section shape other than circle, the Morison's equation can be written as:

$$f(z,t) = f_M + f_D = \Delta\rho C_M \dot{u} + \frac{\rho}{2} C_D A u|u| \quad (2\text{-}3)$$

Here, Δ is the cross-sectional area, A is the projected area (Gudmestad, 2015).

1. Assumptions of Morison's equation

There are some assumptions needed to be fulfilled in order to use Morison's equation. In deep water regular waves break when the ratio of wave height H and wave length L is less than 0.14, a slamming load will happen. The acceleration should not change much over the cylinder. In addition, the amplitude **a** of the motion of the cylinder should not be too big. So to apply Morison's equation, the following conditions need to be satisfied (Gudmestad, 2015):

a) $H/L < 0.14$

b) $D/L < 0.2$

c) $a/D < 0.2$

Here H is the wave height, L is the wave length, D is the diameter of the beam, **a** is the motion of the cylinder.

The net twines in fish cage model are taken as slender cylinders, and the above assumptions are all satisfied.

2. Definition of C_M and C_D

There are two unknown parameters in deciding the hydrodynamic force, drag coefficient and mass coefficient.

To get the wave force by Morison's equation is only applicable for $KC \geq 2$, with C_D and C_M given as functions of the Reynold's number, the KC number and relative roughness. Figure

2-6 shows that drag coefficient C_D changes with different Re and roughness k under critical flow regime.

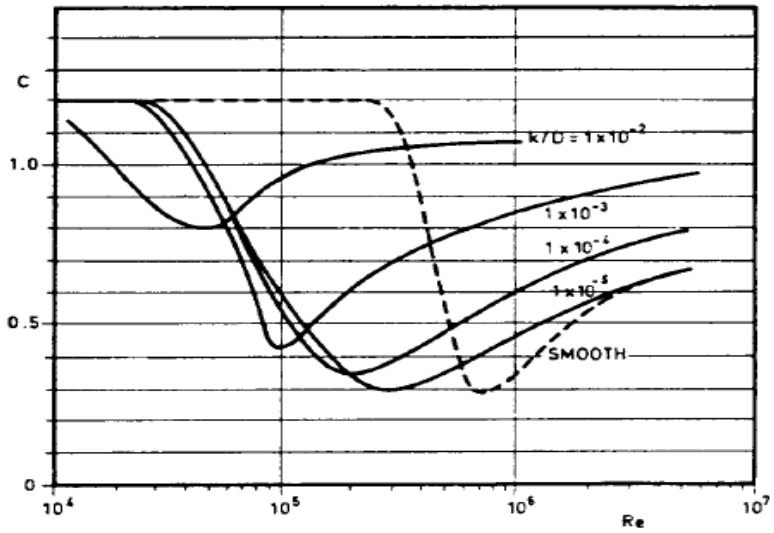

Figure 2-3 Drag coefficient for fixed circular cylinder for steady flow in critical flow regime, for various roughness (DNV, 2008).

A lot of researches related with the drag coefficients have been done. Among them, there are some typical ones in modeling and simulation, and are divided into two different kinds of C_D: C_D for net panel model and C_D for Morison model.

a) Drag coefficients of the net panel model

The drag and lift coefficients were calculated using formulas derived by Løland (1991). These formulas were based on both theoretical work and comprehensive model tests. C_D and C_L were given by:

$$C_D(S_n, \theta) = 0.04 + (-0.04 + S_n - 1.24S_n^2 + 13.7S_n^3)\cos(\alpha) \quad (2\text{-}4)$$

$$C_L(S_n, \theta) = (-0.05S_n + 2.3S_n^2 - 1.76S_n^3)\sin(2\alpha) \quad (2\text{-}5)$$

Here, Sn is the solidity of the net, α is the angle of attack. The model tests on which the formulas were based were for Reynolds numbers in the range from 1400 to 1800 and Sn within [0.13, 0.317]. Further, these formulas were strictly valid for stationary flow only.

Estimates of drag coefficient for square meshes of the net provided by Milne (1972) are :

$$C_D = 1.0 + 2.73\left(\frac{d}{L}\right) + 3.12\left(\frac{d}{L}\right)^2, \text{ for knotless net} \quad (2\text{-}6)$$

$$C_D = 1.0 + 3.77\left(\frac{d}{L}\right) + 9.37\left(\frac{d}{L}\right)^2, \text{ for knotted net} \quad (2\text{-}7)$$

Where d is the diameter of the strand and L is the mesh bar length.

b) Drag coefficients of Morison model:

Zhao et al. (2007) mentioned for cylinder, the drag coefficient could be calculated by applying the following equations:

$$C_n = \begin{cases} \frac{8\pi}{R_{e_n} s}(1 - 0.87s^{-2}), & (0 < R_{e_n} \leq 1) \\ 1.45 + 8.55R_{e_n}^{-0.9}, & (0 < R_{e_n} \leq 30) \\ 1.1 + 4R_{e_n}^{-0.5}, & (0 < R_{e_n} \leq 10^5) \end{cases} \quad (2\text{-}8)$$

$$C_\tau = \pi\mu(0.55R_{e_n}^{0.5} + 0.084R_{e_n}^{2/3}) \quad (2\text{-}9)$$

Where $Re_n=VD/\nu$, $s=-0.07721565+\ln(8/Re_n)$, C_n and C_τ are normal and tangential drag coefficients for mesh bars, V is the normal component of the fluid velocity relative to the mesh bar, ν is the kinematic viscosity, $\nu = 1.15\times10^{-6} m^2/s$ for sea water. Further, he mentioned, the drag force coefficient C_d in the combined wave-current flows was usually less than that in waves only.

c) Mass coefficient

For mass coefficient C_M,

$$C_M=1+C_A \quad (2\text{-}10)$$

Here C_A is added mass coefficients.

So to find C_M, we need to get C_A. C_A is also related to KC number and roughness k.

a) For KC < 3, C_A can be assumed to be independent of KC number, C_A = 1.0 for both smooth and rough cylinders.

b) For KC > 3, the added mass coefficient can be found from the formula

$$C_A=\max\begin{Bmatrix}1 - 0.044(KC - 3)\\0.6 - (C_{DS} - 0.65)\end{Bmatrix} \quad (2\text{-}11)$$

Where C_{DS}= 0.65 for smooth C_{DS} = 1.05 for rough cylinder, for intermediate roughness the values were found by linear interpolation between the curves for smooth and rough cylinder corresponding to C_{DS} = 0.65 and C_{DS} = 1.05. The variation of C_A with KC for smooth (C_{DS} = 0.65) and rough (C_{DS} = 1.05) cylinder is shown in Figure 2-6.

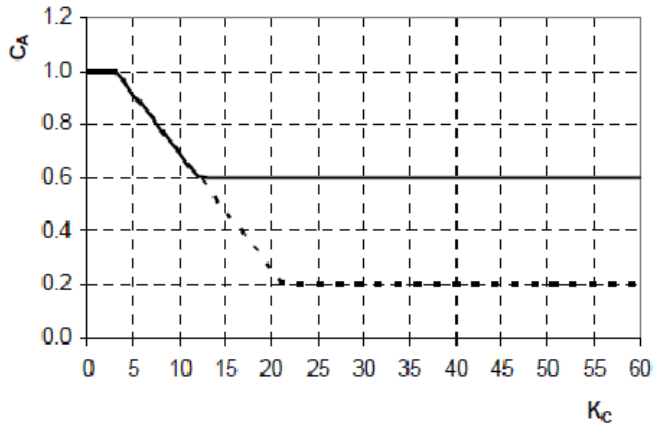

Figure 2-4 Added mass coefficient change with KC for smooth and rough cylinders (DNV, 2008)

c) For large KC-number, the drag force is dominating compared with the inertia force. Then C_A for large KC-number are:

$$C_A=\begin{cases} 0.6 & \text{for smooth cylinder} \\ 0.2 & \text{for rough cylinder} \end{cases} \tag{2-12}$$

For small cylinders, C_M can be taken as 2 according to previous experience in figure 2-5 (Gudmestad, 2015).

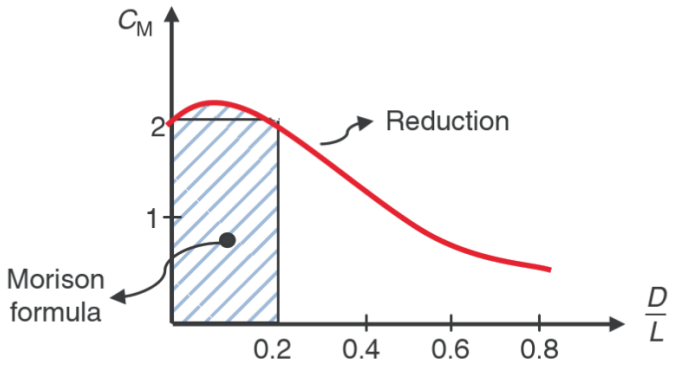

Figure 2-5 The relation between C_M and D/L

3. Forces on a moving cylinder under wave and current

When we consider the structure in the open sea, the structure is hard to stay still under large force caused by wave and current. To take consider in the relative movement of the structure, the Morison's equation about the hydrodynamic force per unit length cylinder can be modified as (Li, 2013):

$$f(z,t) = f_M + f_D = \frac{\pi D^2}{4}\rho C_M(\dot{u} \pm a_p) + \frac{\rho}{2}C_D D(u \pm v_p)\left|u \pm v_p\right| \tag{2-13}$$

Here, D is the diameter of the cylinder, C_M and C_D are inertia and drag coefficient respectively, ρ is the density of the sea water, u is the velocity of the water particle, $\dot{u}$ is the acceleration of the water particle, a_p and v_p is the vector of acceleration and velocity of

the structure respectively.

In the open sea, the wave and current usually happen at the same time. If we consider the effect of current in addition to the relative movement of the structure and water particles, Morison's equation about the hydrodynamic force in unit length cylinder can be revised continuously (Li, 2013):

$$f(z,t) = \frac{\pi D^2}{4}\rho C_M(\dot{u} \pm a_p) + \frac{\rho}{2}C_D D(u \pm v_p \pm U)\left|u \pm v_p \pm U\right| \quad (2\text{-}14)$$

Here **U** is the vector of the velocity of the current.

2.3 Force analysis on fish cage model

There are two fish cage models in the thesis, truss model and mass spring model. Forces on the model element are studied.

2.3.1 Truss model

In truss model, net twines can be seen as the slender cylinders. The hydrodynamic force on the net is equal to the sum of that on each cylinder.

The dynamic motion equation for the fish cage can be written as:

$$[M]\left[\ddot{X}\right] + [C]\left[\dot{X}\right] + [K][X] = [F_D] + [F_M] + [F_b] + [W] \quad (2\text{-}15)$$

Here [M], [C], [K] are the mass matrix, damping matrix and stiffness matrix respectively, [X] is the matrix of displacement vector, and $[F_D]$ is the matrix of drag force, $[F_M]$ is the matrix for inertia force, $[F_b]$ is the matrix for buoyance force, $[W]$ is the matrix for gravity.

1. Wave forces on a vertical slender cylinder

Assume a slender cylinder in the sea, and all the conditions are satisfied to apply Morison's equation. So the hydrodynamic force of a vertical element per unit length is:

$$f(z,t) = \frac{\pi D^2}{4}\rho C_M\dot{u} + \frac{\rho}{2}C_D D u|u| \quad (2\text{-}16)$$

Where $\dot{\mathbf{u}}$ is the acceleration of the fluid particles, u is the velocity of the fluid particles, D is the diameter of the cylinder, ρ is the density of the fluid, C_M is the inertia coefficient (or mass coefficient), C_D is the drag coefficient. C_M and C_D are different for different structures.

So the total force acting on the slender cylinder is (Gudmestad, 2015):

$$F(z,t) = \int_{-d}^{\varepsilon_0} f_M dz + \int_{-d}^{\varepsilon_0} f_D dz = \int_{-d}^{\varepsilon_0} \frac{\pi D^2}{4}\rho C_M\dot{u}dz + \int_{-d}^{\varepsilon_0} \frac{\rho}{2}C_D D u|u|dz \quad (2\text{-}17)$$

Here ε_0 is the surface elevation of the wave, d is the sea depth, C_M is the inertia coefficient,

$\dot{u}$ is the acceleration, u is the velocity, C_D is the drag coefficient, ρ is the density.

2. Wave forces on an inclined slender cylinder

When the net deforms under wave and current, the net twines will be inclined. Morison's equation can also be applied in the inclined slender cylinder. When we apply Morison's equation into the inclined cylinder, we need to take into consideration of all velocity components normal to the cylinder.

As in figure 2-6, an inclined cylinder submerged in waves, with angle θ to plane XOZ, and angle φ to Z axis, the wave velocity is U. We divide U into $U\sin\theta$ (component parallel to the cylinder plane) and $U\cos\theta$ (component normal to the cylinder plane). Then we continue divide $U\cos\theta$ into $U\cos\theta\cos\varphi$ (component parallel to the cylinder) and $U\cos\theta\sin\varphi$ (component parallel to the cylinder) (Li, 2013).

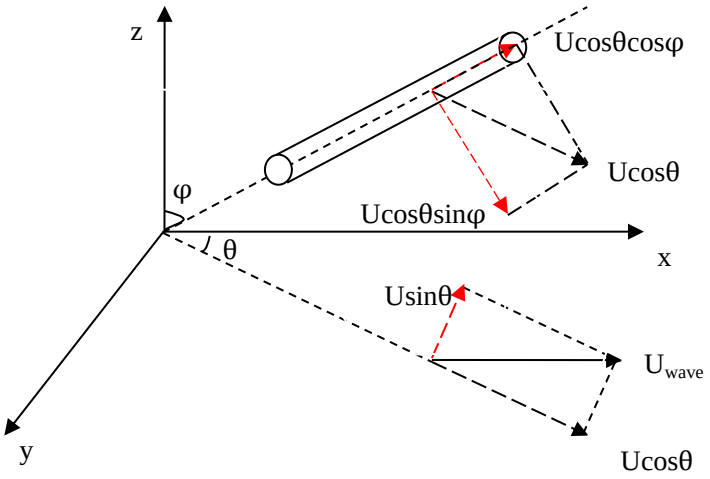

Figure 2-6 Inclined cylinder subjected to the wave, the wave velocity is finally decomposed into three velocity components (red arrows)

So now there are two velocity components $U\sin\theta$ and $U\cos\theta\sin\varphi$ that are vertical to the cylinder, and the total force per unit length in the direction in X axis is the summation of these two force vectors.

$$f_x = f_{x1} + f_{x2} = \frac{\pi D^2}{4}\rho C_M u \sin\theta + \frac{\rho}{2} C_D D u \sin\theta |u \sin\theta| + \frac{\pi D^2}{4}\rho C_M u \cos\varphi\cos\theta$$

$$+\frac{\rho}{2} C_D D u \cos\varphi\cos\theta |u\cos\varphi\cos\theta| \qquad (2\text{-}18)$$

So finally, the wave force per unit length for an inclined cylinder is:

$$f_x(z,t) = \frac{\pi D^2}{4}\rho C_M \dot{u}^2 \left(\sin^2\theta + \cos^2\varphi\cos^2\theta\right)$$

$$+\frac{\rho}{2} C_D D u|u|(\sin\theta|\sin\theta| + \cos\varphi\cos\theta|\cos\varphi\cos\theta|) \qquad (2\text{-}19)$$

2.3.2 Mass spring model

By applying lumped mass method, the net can be seen as the combination of many mass points and springs. Lumped mass points are set at the knot and in the middle of the twine. Between the mass points, springs without mass are used to connect them. Lump mass method can reduce the load of calculation compared to beam element model, thus accelerate the calculation.

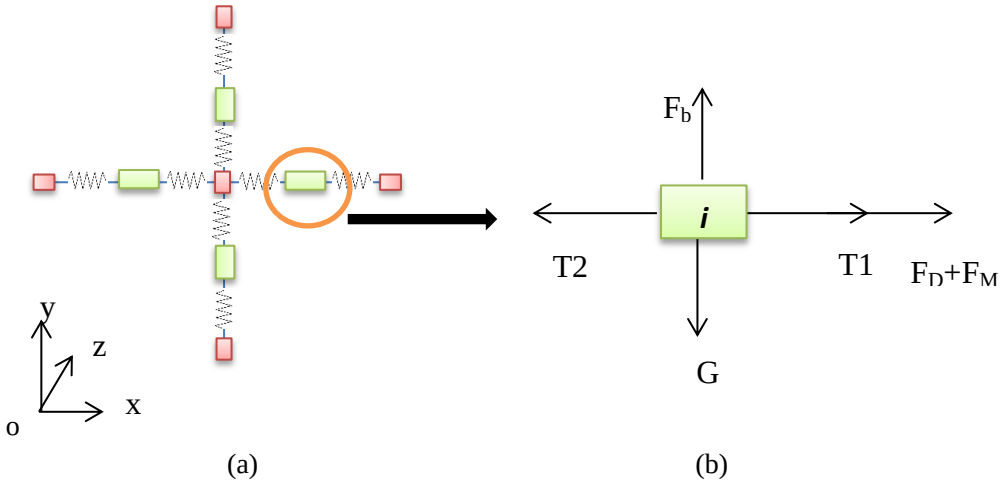

Figure 2-7 Schematic diagram of the mass spring model (a) and forces on the twine mass point ***i*** (b) (red rectangles signify the mass point of knot cylinder, green rectangles represent the mass point of twine cylinder)

In figure 2-7, T1 and T2 are the internal force of the net, which are spring forces in mass spring model. There are possible internal force T3 and T4 in Y axis or T5 and T6 in z axis for knot mass point. F_b is the buoyancy force, G is the gravity force, F_D and F_M is the drag and inertia force respectively.

According to Newton's law, the motion equation for lumped mass ***i*** can be written by

$$(M_i + \Delta M)\vec{a} = \overrightarrow{T_{int}} + \overrightarrow{F_D} + \overrightarrow{F_M} + \overrightarrow{F_b} + \overrightarrow{W} \tag{2-20}$$

Where M_i is the lumped mass, Δm is the added mass, $\vec{a}$ is the acceleration of the lumped mass point, T_{int} is the internal force act by other mass points, F_D is the drag force, F_M is the inertia force, F_b is the buoyancy force, W is the gravity force of the lumped mass. The added mass of the mass point is given as:

$$\Delta M = \rho V_m C_A \tag{2-21}$$

Here, ρ is the density of the water, V_m is the volume of the mass point, and C_A is the added mass coefficient.

Internal force T_{int} is applied to the net and the rope in the direction of tension and compression. The length of the spring elongates or reduces in the direction of tension or compression respectively, is assumed to be linearly proportional to the internal force. The internal force

applied to the mass point is as follows:

$$T_{int} = -\sum_{i=1}^{n} k_i n_i (l_i - l_{0i})$$

(2-22)

Here, k_i is the stiffness of the springs comprising the structure, n_i the unit vector along the line of the spring, l_i is the elongated spring length, l_{0i} is the initial length of the spring.

The relationship between tension and elongation on the spring can be expressed as:

$$\mathrm{k} = \frac{EA}{l_0}$$

(2-23)

Here E is the Young modulus, A is the effective area of the material, l_0 is the initial spring (or twine) length (Zhao et al., 2007).

Then the displacement of the mass point can be calculated with the following equations:

$$M_i \ddot{X} = \sum F_{xi}$$

$$\mathrm{M_i \ddot{Y}} = \sum \mathrm{F_{yi}}$$

$$M_i \ddot{Z} = \sum F_{zi}$$

(2-24)

Here, $\mathrm{M_i}$ is the point mass, $\ddot{X}$, $\ddot{Y}$, $\ddot{Z}$ are the accelerations of the mass point, X, Y, Z are the displacements of the mass point.

In this thesis, we apply Airy wave theory for all of the wave cases analysis. To get the wave force on the beam is to apply the Morison's equation and integrate from the sea bottom to the instantaneous free surface (as in as in equation 2-15).

2.4 Airy wave theory

Airy wave theory is a linearized theory based on irrotational flow of an inviscid incompressible fluid (Gudmestad, 2015). Here the velocity potential can be written as

$$\varphi(\mathrm{x,z,t}) = \frac{\varepsilon_0 g}{\omega} \frac{\cosh k(z+d)}{\cosh kd} \cos(wt - kx)$$

(2-25)

Here *d* is the water depth, *k* is the wave number, ε_0 is the amplitude, ω is the wave frequency, t is the time, *g* is the gravity constant, *x* is the horizontal position, z is the vertical position. It is assumed that the fluid is incompressible and irrotational.

The horizontal water particle velocity function is

$$u = \frac{\partial \varphi}{\partial x} = \frac{\varepsilon_0 k g}{\omega} \frac{\cosh k(z+d)}{\cosh kd} \sin(wt - kx) \tag{2-26}$$

The horizontal water particle acceleration function is

$$\dot{u} = \frac{\partial u}{\partial t} = \varepsilon_0 k g \frac{\cosh k(z+d)}{\cosh kd} \cos(wt - kx) \tag{2-27}$$

For the case of deep water, simplification is made

$$\frac{\cosh k(z+d)}{\cosh kd} = \frac{e^{k(z+d)}}{e^{kd}} = e^{kz} \tag{2-28}$$

So for deep water, the potential function can be written as

$$\varphi(\mathrm{x}, \mathrm{z}, \mathrm{t}) = \frac{\varepsilon_0 g}{\omega} e^{kz} \cos(wt - kx) \tag{2-29}$$

The horizontal water particle velocity function is

$$u_{deep} = \frac{\partial \varphi}{\partial x} = \frac{\varepsilon_0 k g}{\omega} e^{kz} \sin(wt - kx) \tag{2-30}$$

The horizontal water particle acceleration function is

$$\dot{u}_{deep} = \frac{\partial u}{\partial t} = \varepsilon_0 k g e^{kz} \cos(wt - kx) \tag{2-31}$$

For shallow water, $e^{kz} \approx 1$, the potential function can be written as

$$\varphi(\mathrm{x}, \mathrm{z}, \mathrm{t}) = \frac{\varepsilon_0 g}{\omega} \cos(wt - kx) \tag{2-32}$$

The horizontal water particle velocity function is

$$u_{shallow} = \frac{\partial \varphi}{\partial x} = \frac{\varepsilon_0 k g}{\omega} \sin(wt - kx) \tag{2-33}$$

The horizontal water particle acceleration function is

$$\dot{u}_{shallow} = \frac{\partial u}{\partial t} = \varepsilon_0 k g e^{kz} \cos(wt - kx) \tag{2-34}$$

As the instantaneous free surface is uneven, to get the wave force accurate above the wave trough, linear stretching is applied. There are two linear stretching methods mentioned here.

The linearization is achieved by assuming the wave height is small compared to the wave length and the still water depth. It is also assumed that the fluid is of uniform depth; however, the wave amplitude can be large compared with the size of a structure. Therefore we must make an assumption about the wave kinematics below a crest and above the mean water level.

Above the mean surface level the velocity, and acceleration are extrapolated from their values at the mean surface level (linear stretching 1 in figure 2-8). Hence, for $z_s<z<\eta$,

$$v = v|_{z_s},\ a = a|_{z_s} \tag{2-35}$$

Here z_s is the mean surface level (Systèmes, 2013).

There is another linear stretching method (linear stretching 2 in figure 2-8). Velocity, acceleration, and dynamic pressure are extrapolated to the wave crest.

When a gravity wave is defined, the penetration of the structure into the fluid must be calculated. Although the Airy wave theory assumes that the fluid displacements are small with respect to the wavelength and the fluid depth, they cannot be small with respect to the dimensions of the structure immersed in the fluid. Hence, the instantaneous water surface is used to determine if a point on the structure sees loads due to the presence of the water (Systèmes, 2013). These two linear stretching methods will be verified later.

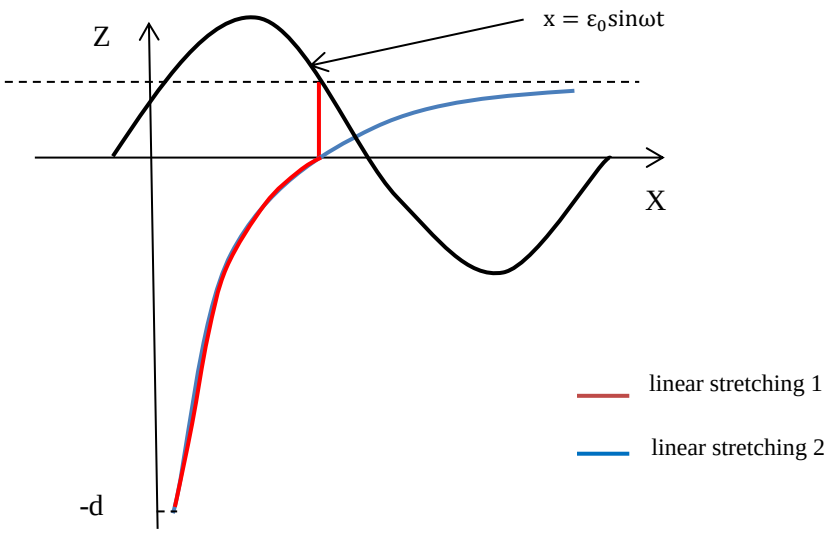

Figure 2-8 Two different stretching methods used to get wave force

2.5 Method of solving nonlinear dynamic equations

The method presented in this section is used to solve nonlinear dynamic equations (Systèmes, 2013).

The dynamic response of the structure can be solved by:

$$[M][\ddot{X}]+[C][\dot{X}]+[K][X]=[F(t)] \tag{2-36}$$

Here [M], [C], [K] are the mass matrix, damping matrix and stiffness matrix respectively, [X] is the matrix of displacement vector, and [F(t)] is the matrix of force vector.

The deformed structure will cause damping, either linear or non-linear. Normally we use

Rayleigh damping assumption to express as follows (Cook et al., 2002):

$$[C]= \alpha[M] + \beta[K] \tag{2-37}$$

Here α is the mass-proportional damping coefficient, β is the stiffness-proportional damping coefficient. That means the damping is the linear combination of mass matrix and stiffness matrix.

$$\xi_n = \frac{1}{2\omega_n}\alpha + \frac{\omega_n}{2}\beta \tag{2-38}$$

Where ξ_n is the critical-damping ratio, and ω_n is the natural frequency ($\omega_n = 2\pi f_n$). Here, the critical-damping ratio varies with natural frequency. The values of α and β are usually selected, according to engineering judgement.

ABAQUS/Standard uses Newton's method and modified Newton (quasi-Newton methods), to solve the nonlinear equilibrium equations.

The finite element models generated in ABAQUS are usually nonlinear and involve a lot of variables. The equilibrium obtained from the virtual works equation is:

$$F^N(u^M) = 0 \tag{2-39}$$

Where F^N is the force component conjugated to the N^{th} variable in the problem and u^M is the value of the M^{th} variable.

Many of the problems which ABAQUS will be applied to are history-dependent, so the solution must be developed by a series of "small" increments. Two issues arise: how the discrete equilibrium statement (equation 2-26) is to be solved at each increment, and how the increment size is chosen.

2.5.1 Newton's method

In this thesis, the displacement of fish cage is large, and the displacement and force relations are no longer linear. ABAQUS/Standard generally uses Newton's method as a numerical technique for solving the nonlinear equilibrium equations. The basic formalism of Newton's method is as follows:

Assume that, after an iteration ***i***, an approximation u_i^M, to the solution has been obtained. Let c_{i+1}^M be the difference between this solution and the exact solution to the discrete equilibrium equation 2-29. This means that

$$F^N(u_i^M + c_{i+1}^M) = 0 \tag{2-40}$$

Expanding the left-hand side of this equation in a Taylor series gives

$$F^N(u_i^M) + \frac{\partial F^N}{\partial u^P}(u_i^M)c_{i+1}^P + \frac{\partial^2 F^N}{\partial u^P \partial u^Q}(u_i^M)c_{i+1}^P c_{i+1}^Q + \cdots = 0 \tag{2-41}$$

If u_i^M is a close approximation to the solution, the magnitude of each c_{i+1}^M will be small, and so all but the first two terms above can be neglected giving a linear system of equations:

$$K_i^{NP}\left(u_i^M + c_{i+1}^P\right) = -F_i^N \tag{2-42}$$

Where $K_i^{NP} = \frac{\partial F^N}{\partial u^P}\left(u_i^M\right)$ is the Jacobian matrix and $F_i^N = F^N\left(u_i^M\right)$.

The next approximation to the solution is then

$$u_{i+1}^M = u_i^M + c_{i+1}^M \tag{2-43}$$

and the iteration continues.

F_i^N and all entries in c_{i+1}^N have to be sufficiently small in Newton's method. There is a disadvantage of applying this method: it is usually avoided in large finite element codes, apparently for two reasons. First, the complete Jacobian matrix is sometimes difficult or impossible to formulate. Secondly, the method is expensive per iteration, because the Jacobian must be formed and solved at each iteration. The most commonly used alternative to Newton is the modified Newton method, in which the Jacobian is recalculated only occasionally or not at all. This method is attractive for mildly nonlinear problems but not suitable for severely nonlinear cases.

2.5.2 Quasi-Newton method

Another alternative is the quasi-Newton method, in which Eq. (2-37) is symbolically rewritten:

$$c_{i+1}^P = -[K_i^{NP}]^{-1} F_i^N \tag{2-44}$$

and the inverse Jacobian is obtained by an iteration process.

There are a wide range of quasi-Newton methods. The method applies very well even the most extremely nonlinear cases. While the savings in forming and solving the Jacobian might seem large, the savings might be offset by the additional arithmetic involved in the residual evaluations (that is, in calculating F_i), and in the cascading vector transformations associated with the quasi-Newton iterations. Thus, for some practical cases quasi-Newton methods are more economic than full Newton.

When any iterative algorithm is applied to a history-dependent problem, the intermediate, non-converged solutions obtained during the iteration process are usually not on the actual solution path; thus, the integration of history-dependent variables must be performed completely over the increment at each iteration and not obtained as the sum of integrations associated with each Newton iteration, c_i. In ABAQUS/Standard this is done by assuming that the basic nodal variables, u, vary linearly over the increment, so that

$$u(\tau) = \left(1 - \frac{\tau}{\Delta t}\right) u(t) + \frac{\tau}{\Delta t} u(t + \Delta t) \tag{2-45}$$

Here $0 \leq \tau \leq \Delta t$ represents "time" during the increment. Then, for any history-dependent variable, g(t), we compute Eq. (2-45) at each iteration.

$$g(t + \Delta t) = g(t) + \int_t^{t+\Delta t} \frac{dg}{d\tau}(\tau) d\tau \tag{2-46}$$

Quasi-Newton method is the fundamental and improvement of Newton's method in solving practical non-linear problem. Here in this thesis, quasi-Newton is applied to solve the non-linear calculations.

2.6 Summary

The general method to solve the engineering problem is to set up the model, establish the theoretical formula and solve the formula. Chapter 2 introduced the theory of two hydrodynamic force models, Morison type force model and screen model. They both need to apply Morison's equation to get the hydrodynamic force. Morison's equation has different forms in different conditions. Drag coefficient and mass coefficient were the key parameters to decide the hydrodynamic force. Forces and motion on the truss and mass spring models were analyzed. The waves in the thesis were based on airy wave theory. Finally the method of solving nonlinear dynamic equations (Newton's method) was presented.

3. Hydrodynamic force verification

3.1 Background

The main topic of the thesis is to discuss the dynamic responses of the fish cage under waves and currents. As the net is slender and flexible, the dynamic responses under waves and current are much more complicated. Here are some ways to simply the problem. Before studying the complex responses of the fish cage, a simple beam is considered to calculate hydrodynamic force by ABAQUS and MATLAB. So this chapter will begin with calculating the wave and current force on a vertical beam, then use MATLAB to verify the results from ABAQUS. The hydrodynamic force calculations are all based on non-linear equations.

3.2 Brief introduction about the software

To analyze dynamic responses of the fish cage, ABAQUS program are applied. Finite element applications in MATLAB are used to check the ABAQUS results.

MATLAB is widely used in difficult calculation in the research and industry. MATLAB is particularly useful for solving linear algebra, differential equations and numerical integration. MATLAB also has powerful graphic tools and can produce nice pictures in both 2D and 3D (MathWorks, 2009).The computer program CALFEM is a MATLAB toolbox for finite element applications. It is mainly used for the finite element calculation. Here, we use the CALFEM to calculate the current force effect on the beam.

ABAQUS is a software suite for finite element analysis and computer-aided engineering. ABAQUS is a suite of powerful engineering simulation programs, based on the finite element method, which can solve problems ranging from relatively simple linear analyses to the most challenging nonlinear simulations. ABAQUS offers a wide range of capabilities for simulation of linear and nonlinear applications. ABAQUS is widely used in the automotive, aerospace, and industrial products industries (SIMULIA, 2016).

AQUA is a subset of ABAQUS. It is used to apply steady current, wave, and wind loading to submerged or partially submerged structures in problems such as the modeling of offshore piping installations or the analysis of marine risers. It can also be performed using the static, direct-integration dynamic, explicit dynamics, or eigen frequency extraction procedures. The AQUA can calculate drag, buoyancy, and inertia loading only for beam, pipe, elbow, truss, and certain rigid elements; In addition, it can include elements that model spud cans for jack-up foundation analysis in ABAQUS/Standard (Version, 2013).

Here displacement induced by current force is calculated by ABAQUS/AQUA, and then verify the result in MATLAB/CALFEM program. The wave force of a beam calculated from

ABAQUS/AQUA program is checked with MATLAB results. To be clear, the program here is only valid for the beam, not for the floater and net.

Hydrodynamic forces on the simple beam are shown in the programs mentioned above.

3.3 Examples of calculating wave forces

Assume a cylinder with diameter D=0.1m is fixed in the sea bottom on the seabed, the length of the cylinder is 12 meter. The water depth is chosen as w_d=10m (figure 3-2). The cylinder is subjected to the wave force in horizontal direction. Three wave heights H_1=1.5m, H_2=0.5m, H_3=0.15m with the same wave lengths L=12m are used for calculation.

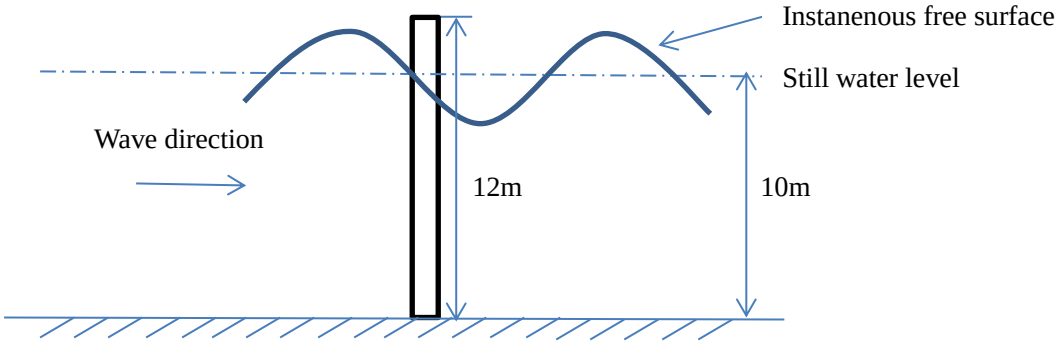

Figure 3-1 Vertical cylinder subjected to wave

According to the description above, to apply Morison's equation for wave force, first we need to investigate whether the assumptions are fulfilled (Gudmestad, 2015).

a. Check whether it is deep water and decide velocity equation, for the velocity equation of the water particle in deep water is different from that in mediate or shallow water.
   The criterion for deep water is given with:

$$\frac{w_d}{L} = \frac{10}{12} > \frac{1}{2}$$

b. Check whether the Morison's equation is valid, we also need to find:

$$\frac{D}{L} = \frac{0.1}{12} = 0.009 < 0.2$$

c. Check the breaking wave criterion:

$$\frac{H1}{L} = \frac{1.5}{12} = 0.125 < 0.14,$$

$$\frac{H2}{L} = \frac{0.15}{12} = 0.025 < 0.14,$$

$$\frac{H3}{L} = \frac{0.5}{12} = 0.083 < 0.14,$$

All these three waves do not break.

d. Check whether a/D<0.2. Here as the beam is reinforced, so we assume the motion of the cylinder is less than 0.02 m.

So Morison's equation applies in all these three situations.

Velocity in deep water: $$u=\frac{\varepsilon_0 kg}{\omega}e^{kz}\sin(\omega t), \quad (3\text{-}1)$$

Acceleration: $$\dot{u} =\varepsilon_0 kge^{kz}\cos(\omega t), \quad (3\text{-}2)$$

$$f_M(x,t) = \frac{\pi D^2}{4}\rho C_M \dot{u}, \quad (3\text{-}3)$$

$$f_D(x,t) = \frac{\rho}{2}C_D Du|u| \quad (3\text{-}4)$$

$$F = \int_{-d}^{\varepsilon_0 \sin wt}\left(\frac{\pi D^2}{4}\rho C_M \dot{u} + \frac{\rho}{2}C_D Du|u|\right)dz$$

$$= \int_{-d}^{\varepsilon_0 \sin wt}\left\{\frac{\pi D^2}{4}\rho C_M(\varepsilon_0 kg/\omega)e^{kz}\cos(\omega t) + \frac{\rho}{2}C_D D(\varepsilon_0 kg/\omega)^2 e^{2kz}\sin(\omega t)|\sin(\omega t)|\right\}dz$$

FigureAccording to DNV R205, C_D for rough cylinder is approximately 1.05, here for simplification we assume $C_D = 1$, inertia coefficient $C_M = 2$ based on previous experience according to figure 2-5.

Figure 3-3 and 3-4 show the results from MATLAB (without any stretching) and ABAQUS when the wave height is 0.5m and 0.15m respectively, table 3-1 demonstrates the extreme values in the time domain analysis with two methods.

wave force F/N	Wave 3/H=0.5m	Wave 2/H=0.15m
MATLAB/max	39.4409	11.7558
ABAQUS/max	39.5909	11.8257
MATLAB/min	-39.1991	-11.7597
ABAQUS/min	-40.8138	-11.8315

Table 3-1 Wave force results from MATLAB (no stretching) and ABAQUS (H=0.5m, 0.15m)

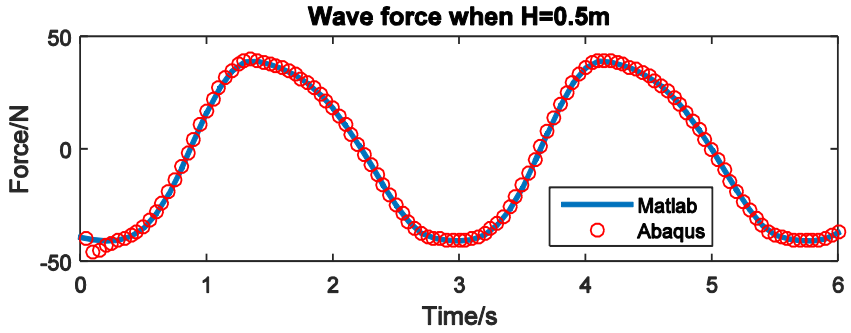

Figure 3-2 Wave force Comparison of MATLAB (no stretching) and ABAQUS results (H=0.5m)

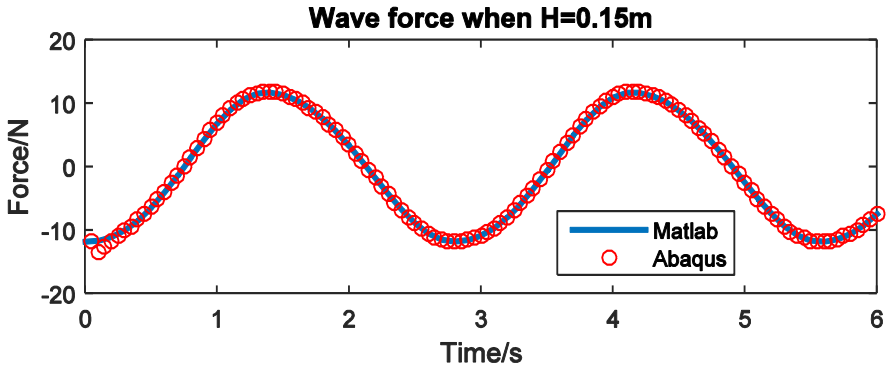

Figure 3-3 Wave force Comparison of MATLAB (no stretching) and ABAQUS results (H=0.15m)

In table 3-1, the maximum and minimum wave forces from MATLAB and ABAQUS are quite similar, the difference is less than 1%. Figure 3-3 and 3-4 shows that MATLAB (integrate to still water level) results and ABAQUS results fit very well.

Figure 3-5 shows the wave force results under wave (H=1.5m). ABAQUS results are compared with MATLAB (no stretching) results. There exists large difference between the results of MATLAB (no stretching) and ABAQUS results. When the wave is large, the wave force without stretching is no longer accurate.

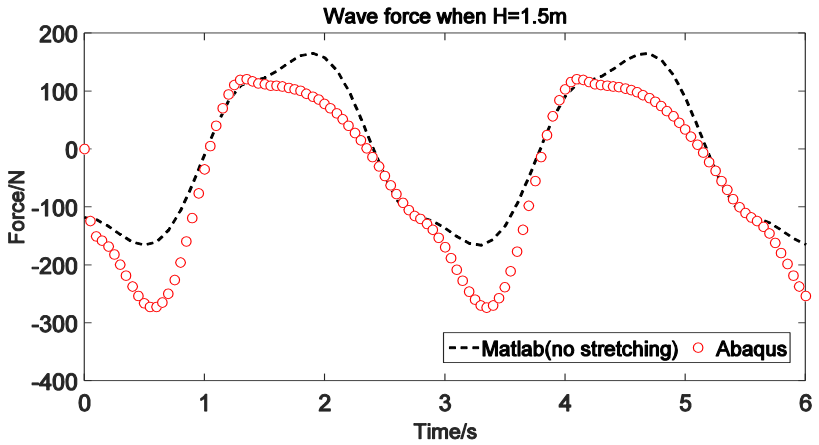

Figure 3-4 Wave force comparison of MATLAB (no stretching) and ABAQUS results when H=1.5m

The results from the MATLAB (two stretching methods mentioned in chapter 3.3) and ABAQUS are plotted in figure 3-6 respectively, and table 3-2 only shows the extreme values of the wave force (MATLAB scripts of two stretching methods are in Appendix 2).

Wave 1/H=1.5m	Wave force F/N
MATLAB(linear streaching1)/max	118.4
MATLAB(linear streaching2)/max	118.6
ABAQUS/max	120.1
MATLAB(linear streaching1)/min	-273.8
MATLAB(linear streaching2)/ min	-327.3
ABAQUS/min	-273.3

Table 3-2 Wave force from MATLAB and ABAQUS (H=1.5m)

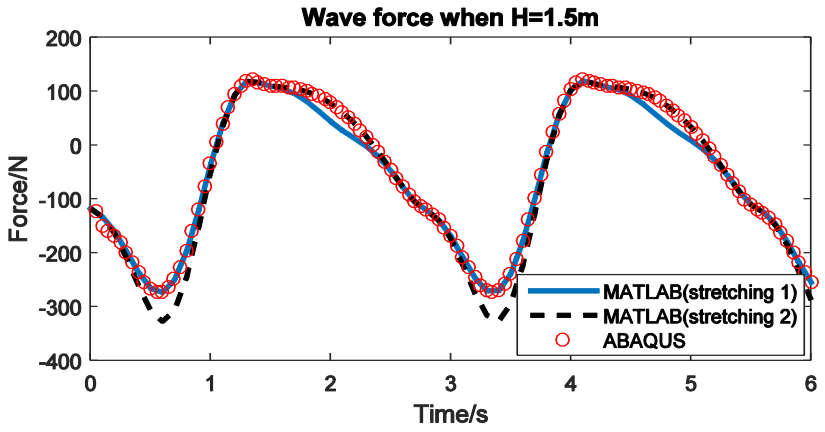

Figure 3-5 Wave force comparison of MATLAB (stretching) and ABAQUS results when H=1.5m

Compared with MATLAB (no stretching) results, the wave forces calculated from stretching methods are much closer to the ABAQUS results. Table 3-2 shows that three maximum values matched very well. However, there exists a nearly 20% deviation in the minimum values between MATLAB linear stretching 1 and 2, although MATLAB linear stretching 1 and ABAQUS result are quite similar. This can also be seen in figure 3-2. In the crest of the curves, the results of these two stretching methods fit well with ABAQUS results except a little deviation. The ABAQUS results have less difference with MATLAB stretching 1, yet have a little more difference with MATLAB stretching 2.

It can be concluded that ABAQUS applies linear stretching 1 to calculate the wave force. When the wave height is small compared with the structure size (H=0.15m or 0.5m in this thesis), the wave force can also be calculated by integrating to the still water level (no stretching). For the large wave problem (H=1.5m in this thesis), linear stretching 1 is more accurate for wave force calculation.

3.5 Current force

A vertical beam with both ends fixed is subjected to the uniform current force, the beam has a circular cross section. The diameter of the beam D=0.2m, and the length of the beam L=10m, C_D=1. We define coordinate system as the vertical direction is Y axis, and horizontal direction is X axis, and the coordinate of bottom end is x=0, y=0. Assume the current speed is 0.5m/s.

We can get the uniform pressure induced by the current from the following equation:

$$q = C_D \frac{1}{2} \rho D u^2 = 1 \times \frac{1}{2} \times 1025 \times 0.2 \times 0.5^2 = 25.625 \text{ N/m}$$

The maximum displacement happened in the center of the beam is 0.4053e-4 meter.

The maximum shear force happened in both ends is 128.125 N. (The CALFEM transcript is

in Appendix 2)

From ABAQUS, we get the maximum displacement is in the center 0.4056e-4m.

The deformations from MATLAB and ABAQUS are shown in figure 3-5.

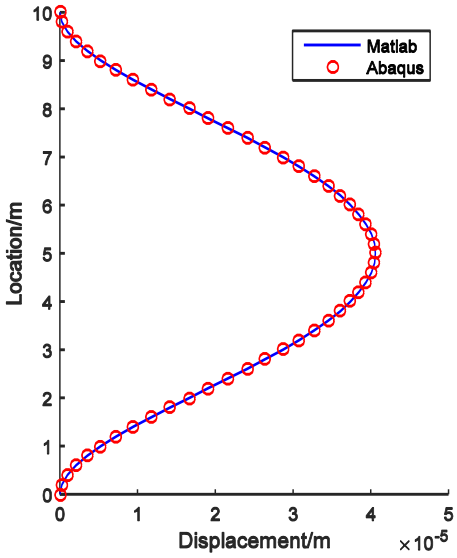

Figure 3-5 Comparison between results of MATLAB and ABAQUS

3.6 Summary

In this chapter, we got familiar with the programs MATLAB and ABAQUS, and relative modules that were best suit for these cases. To ensure the accuracy of subsequent calculations, example of hydrodynamic force calculations on a beam were proposed and verified by these two programs.

The wave force can be calculated with no stretching when the wave height is small compared to the structure. If the wave height is large, we need to apply linear stretching 1 in order not to overestimate the wave force. The effect of current force on a vertical beam can be studied through the deformation.

4. Dynamic analysis of the floater under regular wave and current

4.1 Background

For fish cage in the open sea, it is subjected to the combination of wave force, current force, buoyancy force as well as gravity, which results in the displacements and deformation. The fish cage model consists of the floater, net and bottom weight. Before we start to analyze the dynamic response of the whole fish cage, the single floater is simulated under wave and current.

4.2 Single floater model

The dimension of the single floater is shown in table 4.1 (Li, 2013).

Diameter of the floater(m)	40
Diameter of the floater pipe(m)	0.3
Thickness of the floater pipe(m)	0.048
Young's module(MPa)	950
Density(Kg/m^3)	953
Stiffness of mooring lines(N/m)	6000(tension)

Table 4-1 Properties of the single floater model

According to the properties in table 4-1, the gravity of the floater is equal to the buoyancy when it is half submerged, but the floater is not stable in ABAQUS static analysis. In ABAQUS, the buoyancy is calculated under a closed-end loading condition. It recognizes only the location of the center line whether it is higher or lower than still water level. If the center line is under the free surface, it is recognized as fully submerged, or it is 0. It cannot predict correctly the true buoyancy value when the element is partly submerged in the water. The floater will continuously move up and down the waterline in ABAQUS.

However, this problem does not affect much when the wave height is large. As when the wave height is large, the buoyancy force caused by the changing submerged cross section is much less than wave force. However, in small waves or pure current conditions when the force is small, it will be a problem. (Li, 2013) .

The single floater model in ABAQUS is shown in figure 4-1. The nylon mooring lines can be modeled as the nonlinear spring which can only take tension not compression. One end of the mooring line connected with the floater and the other end fixed. The single floater is stable at the beginning position. According to the properties of the nylon mooring line, there is a small

pretension 8-12 N when it is modeled as the nonlinear spring (Tsukrov et al., 2005). In this thesis, pretension is set to 10 N. The force and displacement relation of the nonlinear spring is shown in figure 4.2.

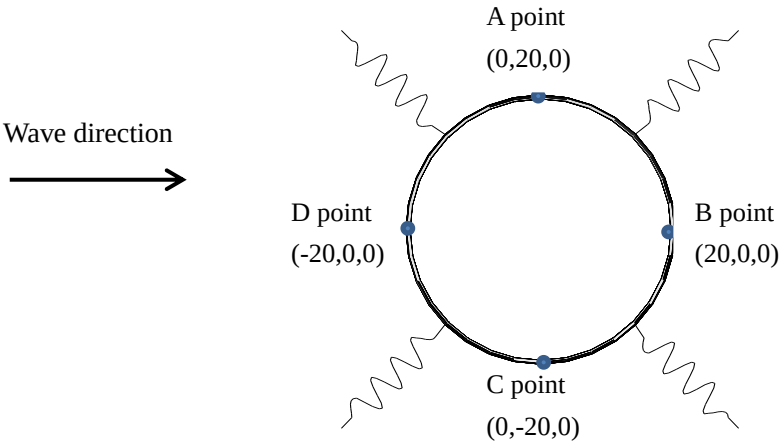

Figure 4-1 Single floater model

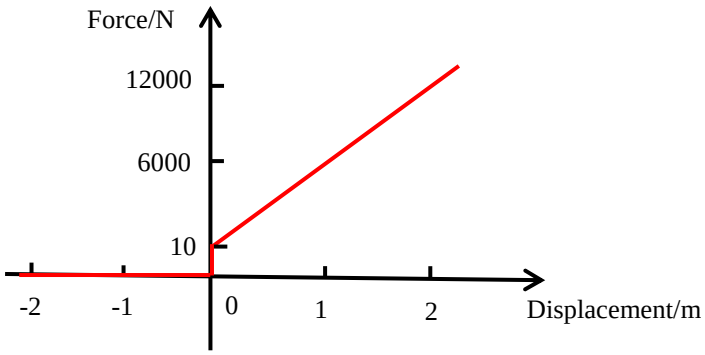

Figure 4-2 The force-displacement relation of nonlinear spring

4.3 Response of the floater under regular wave and current

The single floater model was simulated under the regular wave (H=5m, T=8s) and current (v=1m/s) separately and concurrently for 24s.

4.3.1 Responses of floater under regular wave condition

Figure 4-3 shows time domain analysis under regular wave (H=5m, T=8s). The left ones are the top views of the floater, and the right ones are the side views.

t=0s

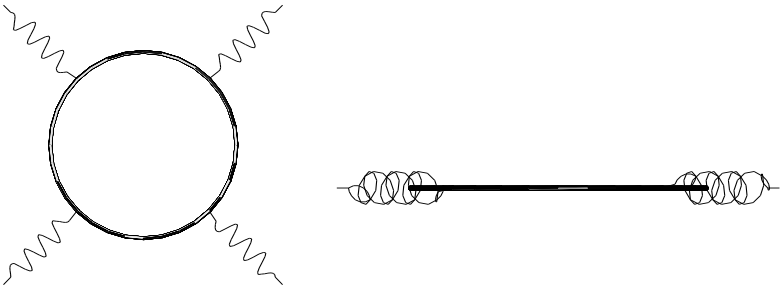

t=2s

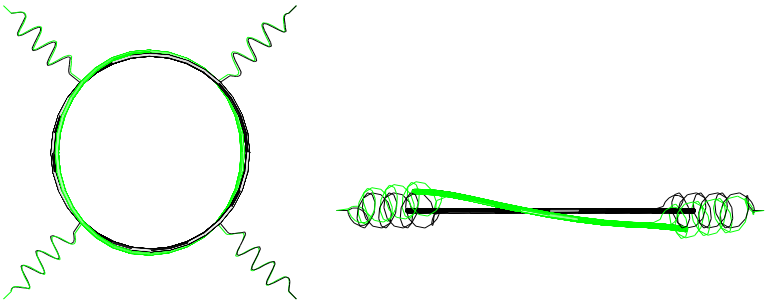

t=4s

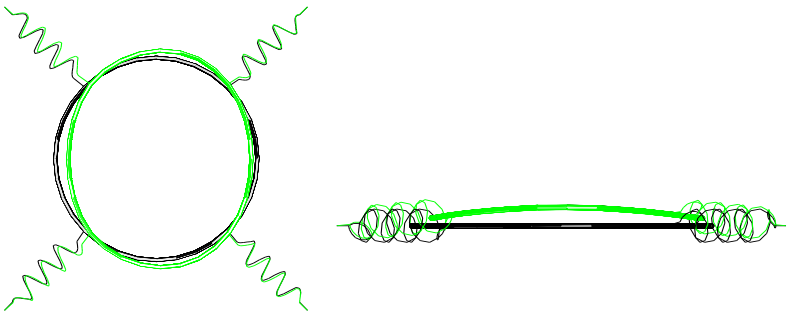

t=6s

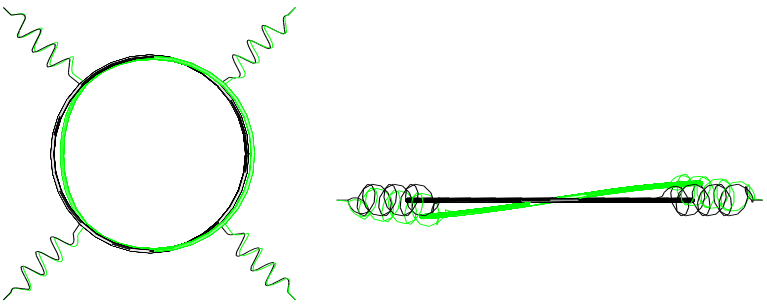

t=8s

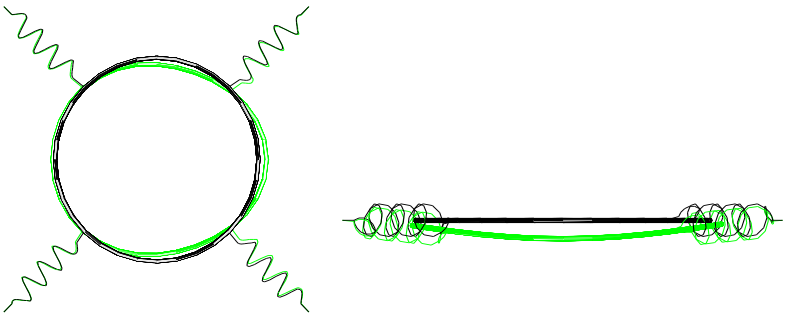

Figure 4-3 Deformation under wave in different time during a period (H=5m, T=8s)

From figure 4-3, it can be observed the floater not only moves like a rigid body, but also deforms due to the wave and spring force. To analyze the displacement of the floater, 4 points are chosen in varied positions (points show in figure 4.1). Figure 4-4 shows the displacements of point A, B, C, D on the floater.

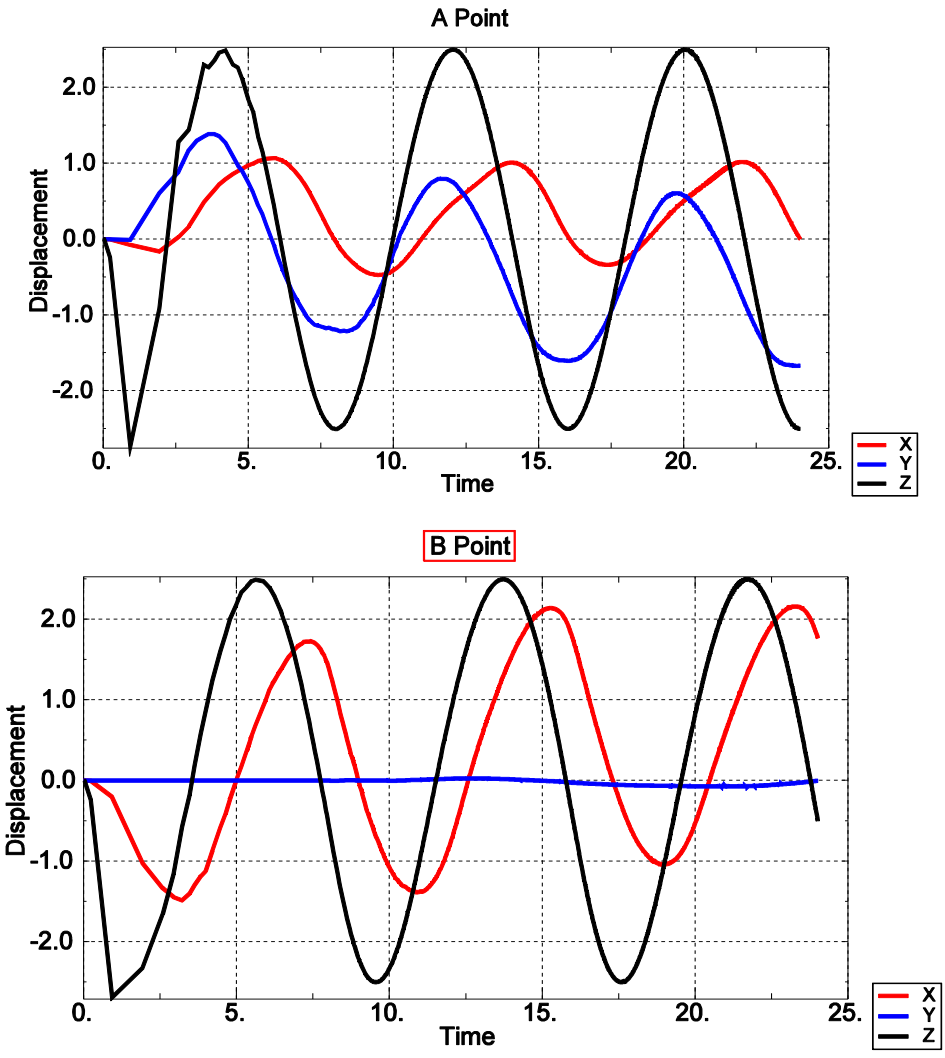

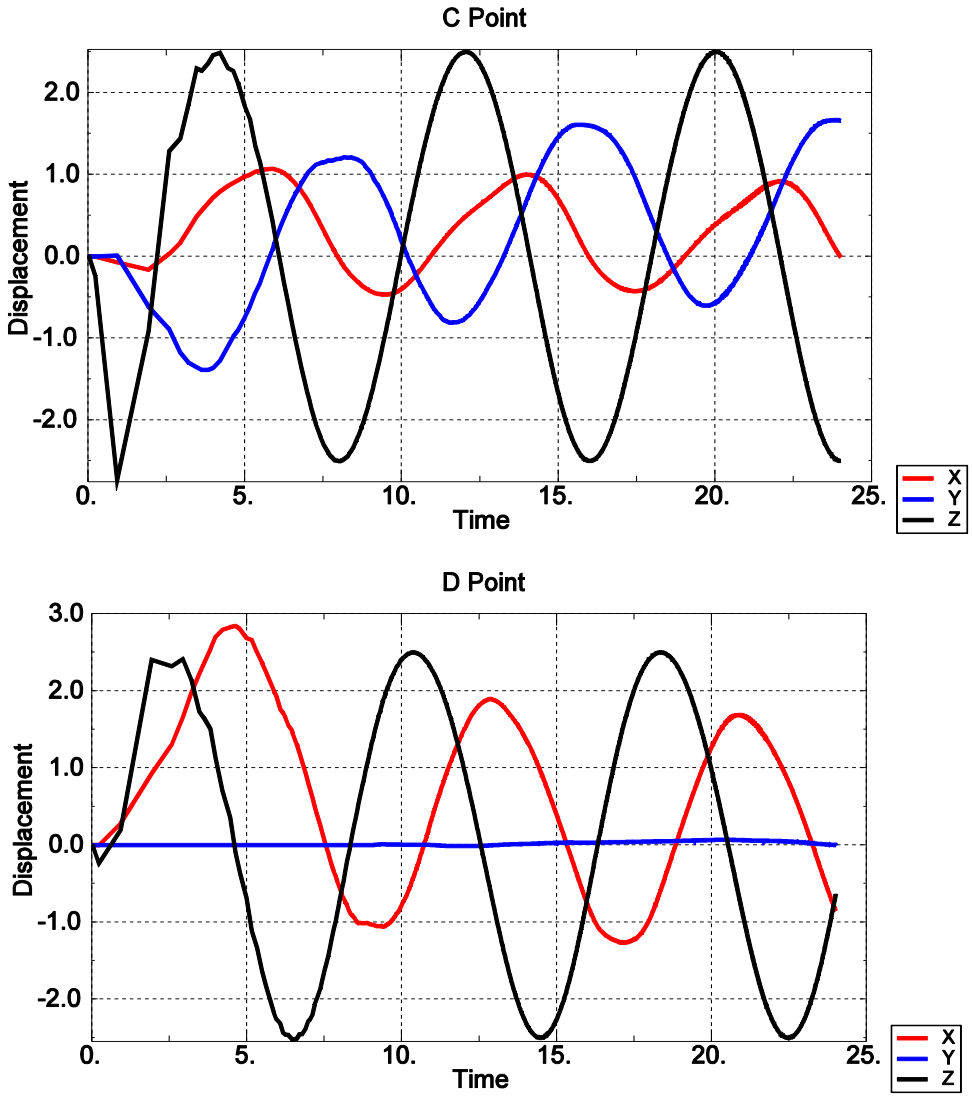

Figure 4-4 Displacements of point A, B, C, D in the floater under regular wave

In figure 4-4, it can be seen that the frequency of the floater motion is the same with the wave. In vertical direction, the displacement amplitude of the floater is identical with the wave. In horizontal direction, the floater is subjected to the nonlinear spring force and wave force, causing displacement and deformation on the floater.

Figure 4-5 shows the trajectory of wave particles and point D on the floater under pure regular wave condition. The water particle in deep water moves with a 5m-diameter circle in XZ direction. The amplitude of point D in Z axis is the same with the water particle, but not in X axis, due to the combination effect of nonlinear spring force and wave force. That is because the floater is constraint horizontally, but free to move with water particle vertically. The mean position of point D is almost 0, so we can conclude that 5m height wave is a small wave to the 40 diameter floater, the mean wave force is about 0, similar to the wave force calculation in figure 3-4 and 3-5.

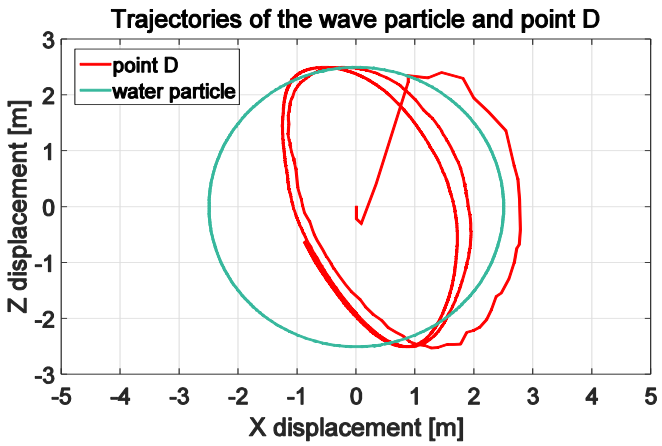

Figure 4-5 Comparison of trajectories between the wave particle motions and displacement of point D on the floater under wave

4.3.2 Responses of the floater under combined regular wave and current condition

The floater was simulated under the regular wave (H=5m, T=8s) and current (v=1m/s). Figure 4-6 shows the screen snapshots in one wave period. The left ones are the top views of the floater, and the right ones are side views. Figure 4-7 shows the displacement of point A, B, C, D on the floater.

t=2s

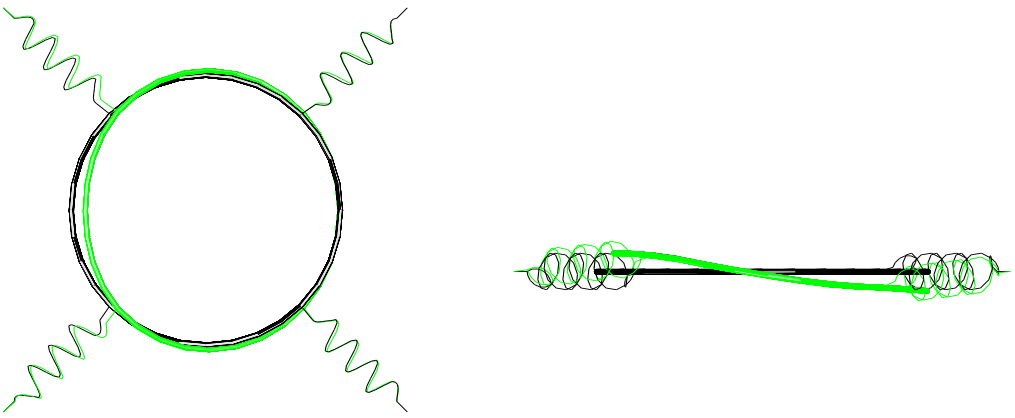

t=4s

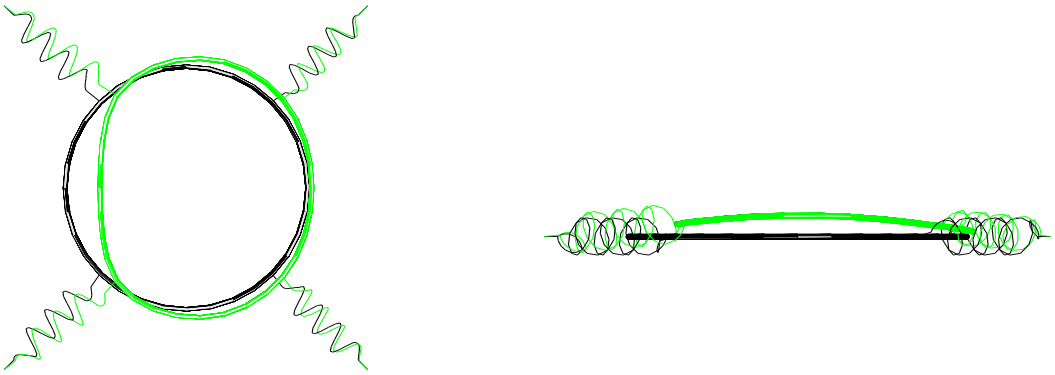

t=6s

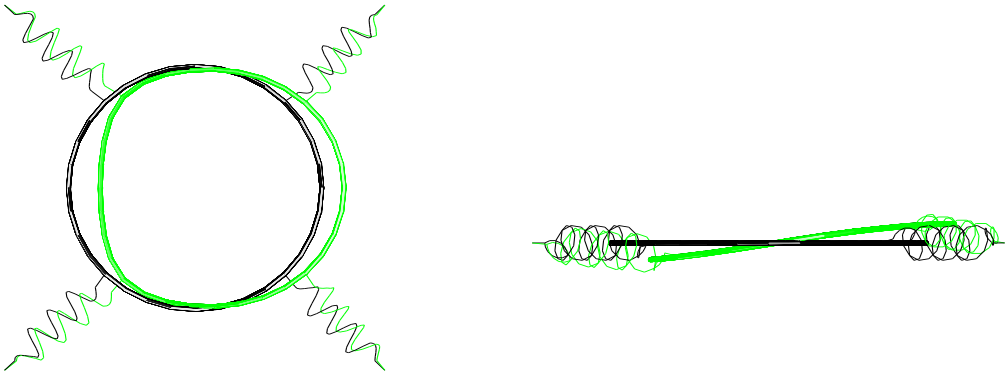

t=8s

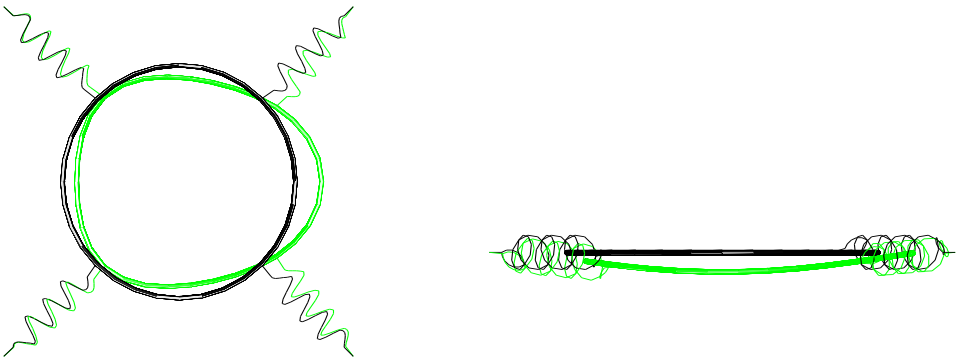

Figure 4-6 Deformation of floater under regular wave

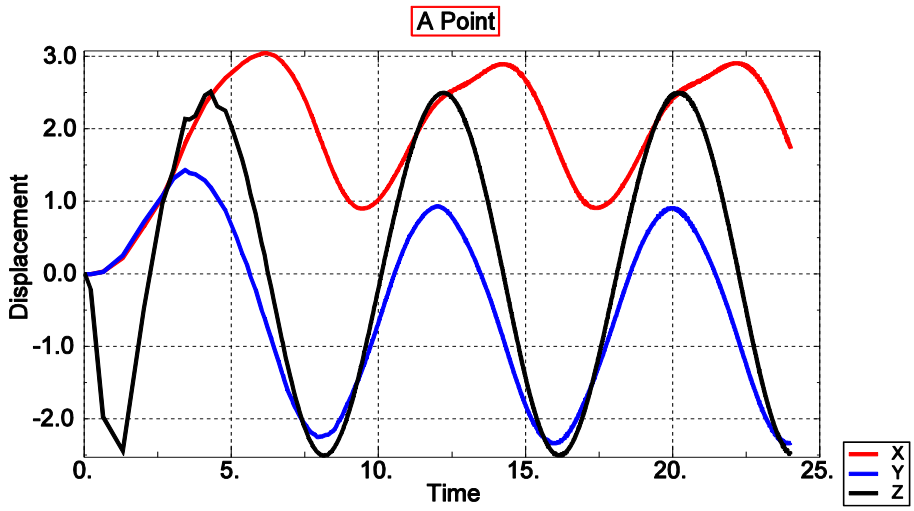
A Point
3.0
2.0
1.0
0.0
-1.0
-2.0
Displacement
0.
5.
10.
15.
20.
25.
Time
X
Y
Z

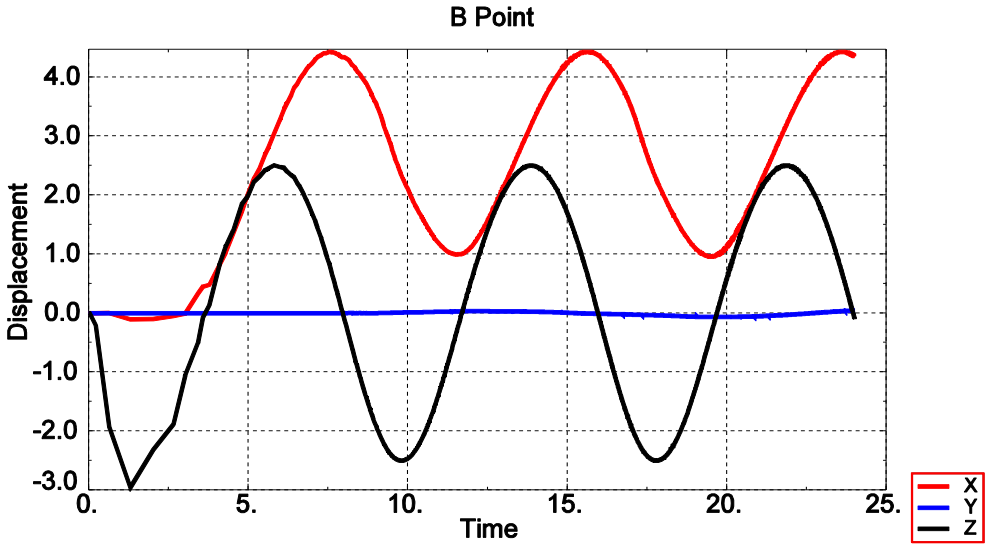
B Point
4.0
3.0
2.0
1.0
0.0
-1.0
-2.0
-3.0
Displacement
0.
5.
10.
15.
20.
25.
Time
X
Y
Z

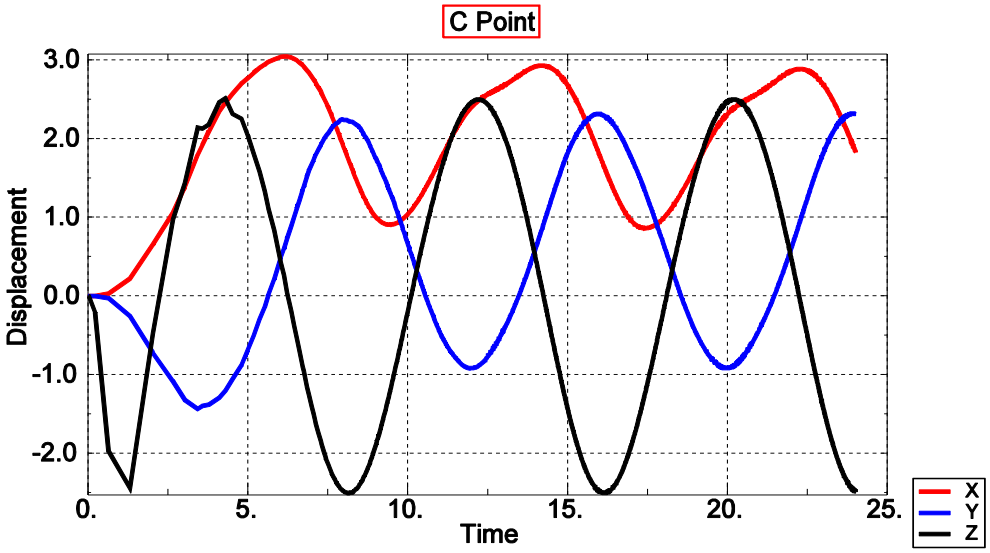
C Point
3.0
2.0
1.0
0.0
-1.0
-2.0
Displacement
0.
5.
10.
15.
20.
25.
Time
X
Y
Z

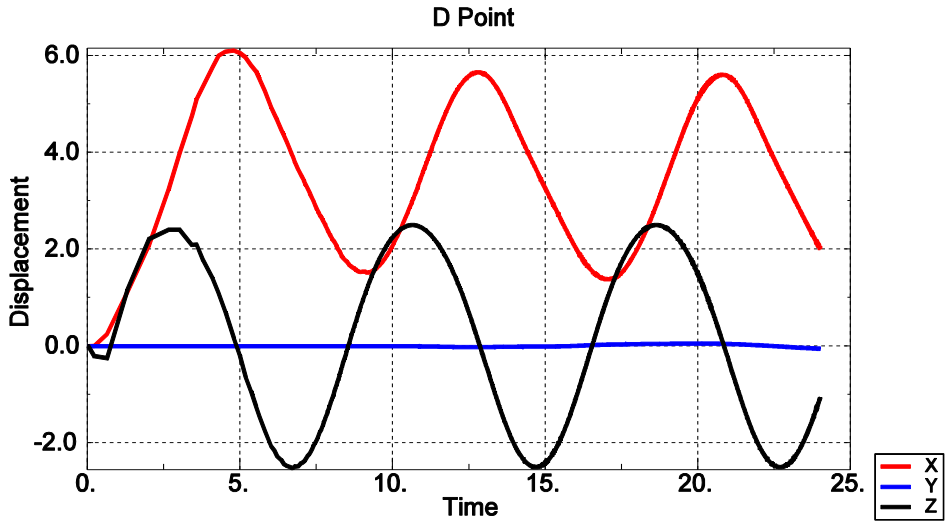

Figure 4-7 Displacements of point A, B, C, D in the floater under regular wave and current

In figure 4-6 and 4-7, the floater has larger deformation under current and wave than wave only condition. Compared the displacements between in figure 4-4 and 4-7, the current has significantly increased the displacement in X direction and aggravated the deformation. The displacements in Y and Z direction are not quite affected. Take point D for example, the maximum X displacement when the floater subjects to the wave only is 3.0 m, and the average Z displacement is around 0 m. However, when the floater is subjected to both wave and current, the maximum X displacement is 6.0m, twice of that when floater is subjectd wave only. The mean X displacement has increased approximately by 3 m.

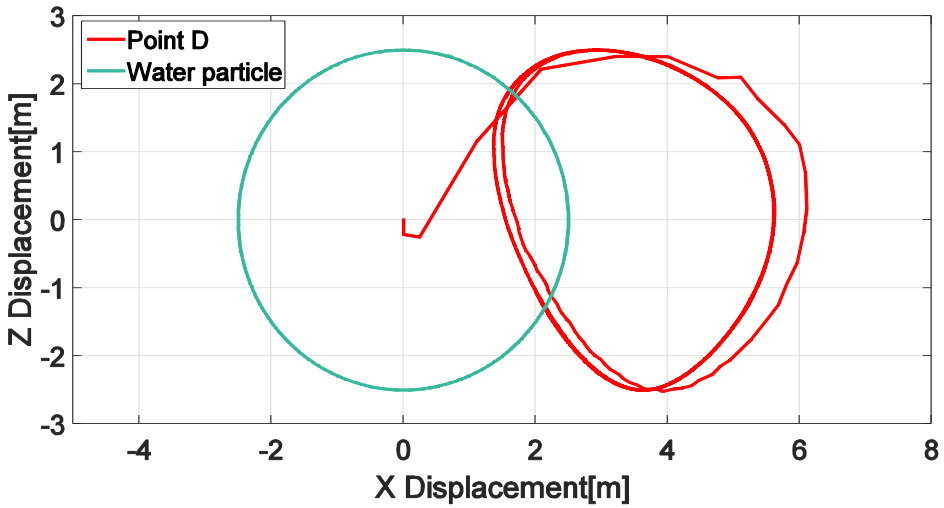

Figure 4-8 Comparison of trajectories between the wave particle motions and point D on the floater under wave and current

In figure 4-8, the trajectory of point D on the floater is quite similar with the movement of the wave particle under wave and current. The amplitude of point D is the same with the water particle. Compared with figure 4-5, mean position of point D has moved along +X direction due to current effect. The movement in X direction is much larger in wave and current

condition than that in only wave condition. The stress variations on point D under pure wave and wave-current conditions are also compared in figure 4-9.

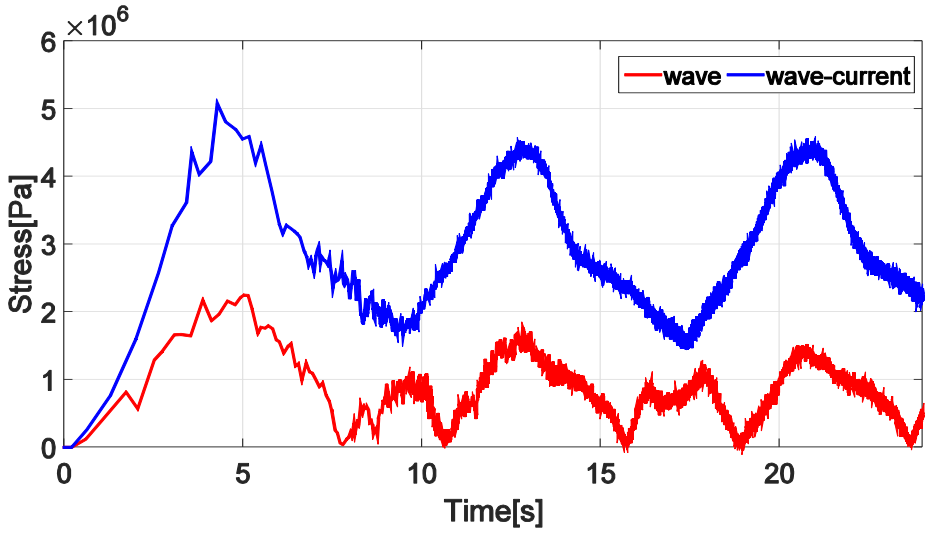

Figure 4-9 Stress on point D under pure wave and wave-current conditions

The stress variation is much larger in wave-current condition than in pure wave condition in figure 4-9. The maximum stress in wave-current condition is almost twice of that in pure wave condition. The stress in wave-current condition is more harmonic than that in wave only condition. The current has loaded the floater with more stress. The floater in wave and current combined condition is more prone to have fatigue or collapse problem than in wave only condition.

4.4 Summary

In this chapter, dynamic responses of single floater under regular wave and current has been simulated. The floater supposed to be half submerged in water was not stable during the static analysis in ABAQUS, because ABAQUS cannot give correct prediction about the buoyancy force. However, this is not a problem when the wave height is large. The floater moved with the same amplitude of the water particle vertically, but the horizontal movement varied. The current had aggravated the deformation of the floater, but it only influenced the displacement in X direction.

5. Comparison of truss model and mass spring model in model scaled size

5.1 Background

The net twine can be modeled as truss, spring and beam during numerical analysis. There are some researches that model the net as truss, for its simplicity to build and fast simulation. Some others model the net as spring, as it can solve the computational inefficiency and improve the numerical simulation accuracy when the net is modeled as beam (Ye et al., 2014). However, no one has compared these two models. In this chapter, these two models are presented and compared, the simulation results will be validated by numerical simulation and model experiment of a scaled fish cage from previous study to test which model is more accurate and efficient. In addition, convergence study will be performed to test the reliability of the equivalent process.

In the models, the floater will be fixed with respect to the earth to be consistent with the experiment and simulation from previous study. The fish cage model will be analyzed in different current conditions. Response of hydrodynamic force and volume reduction are studied to test which model is better for further study.

5.2 Numerical models

In numerical models, the floater and bottom weight were modeled as beam element, the net was modeled as truss and mass spring respectively. Hydrodynamic forces were calculated through each net element (The ABAQUS transcript can be seen in Appendix 3).

There are some principles when choosing to model the element as beam or truss. Beams can support loads and perform shear and bending. Six degrees of freedom (DOFs) including three forces and three moments, need to be taken into consideration (UX, UY, UZ, ROTZ, ROTY, ROTX). Truss is a purely axial member that can only used to transfer the loads axially. It cannot carry moment. Three DOFs need to be considered (UX, UY, UZ). There are also some other occasions that the truss element is suitable for. When the load becomes very big or the span is very long, utilizing a beam will be very expensive (Al-Hammoud, 2016).

Truss model run much faster compared to the mass spring model under the same condition (overview of the simulation is in Appendix 1), although the mass spring model is said to accelerate the simulation. The mass points in mass spring model were still beam elements, so it cannot compete with the truss element in simulation speed.

Table 5-1 shows the parameters of the fish cage.

Circumference	4.42 m	**Density of net material**	1125 kg/m^3
Cage depth	1.41 m	**Drag coefficient C_D**	1.15
Twine Diameter	2 mm	**Current velocity**	0.34 m/s
Half mesh width	17.6 mm	**Bottom weights**	16 ×800 g
Solidity	0.23	**Net stiffness**	82 Mpa

Table 5-1 Parameters of the fish cage model (Moe et al., 2010)

5.2.1 Truss model

The truss model is widely used in fish cage simulation. In truss model, the net twine is modeled as 3-D nodes truss element, as it can perform nonlinear displacement as well as bending effect (as in figure 5-1).

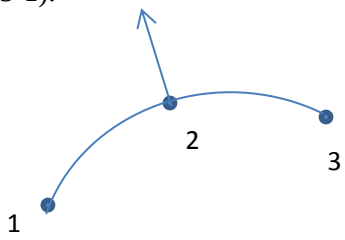

Figure 5-1 Nonlinear 3-D truss element (ABAQUS manual)

It is time consuming to model the net twine as the actual size, so we apply equivalent calculation to let one truss represent several net twines. Convergence study is conducted using different mesh size to validate the accuracy of the equivalence. Figure 5-2 illustrates how to use one equivalent truss to represent four net twines. Additional node was added in the middle of each global truss element to perform the bending effect.

The equivalent truss elements were given the combined properties of the represented four twines, i.e. the extension property of the truss element was equal to that of the represented twines combined. The hydrodynamic force and buoyancy force on the truss element were equal to that in the represent twines respectively.

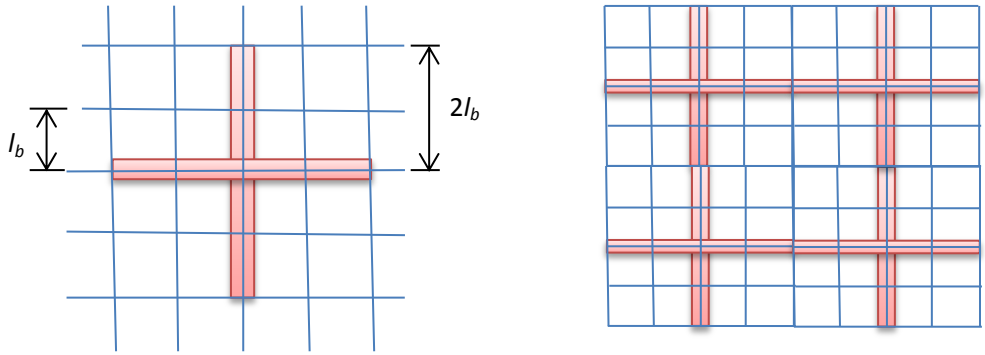

Figure 5-2 Equivalence of the net twines in truss model

(Blue lines signify the original fish net, while red lines signify the equivalent fish net)

We combined four net twines into one truss element by satisfying three equivalent conditions to obtain the equivalent properties.

1. Buoyancy force equivalence

The buoyancy force of the net twines was equal to that of the equivalent truss element in unit length.

$$\sum_{n=1}^{4} \mathrm{F}_b = \mathrm{F}_{be} \tag{5-1}$$

$$\sum_{n=1}^{4} \rho g \mathrm{V} = \rho g V_e$$

$$\sum_{\mathrm{n}=1}^{4} \mathrm{V} = \mathrm{V_e}$$

$$4\left(\frac{\pi \mathrm{D}^2}{4}\right) = \left(\frac{\pi \mathrm{D}_e^2}{4}\right)$$

$$4\mathrm{D}^2 = \mathrm{D}_e^2 \tag{5-2}$$

Here, F_b is the buoyancy force of each net twine;

ρ is the density of water, V is the volume of each net twine;

D is the diameter of each net twine;

F_{be} is the buoyancy force of the equivalent truss element from four twines;

V_e is the volume of the equivalent truss element from four twines;

D_e is the diameter of the equivalent truss element from four twines;

2. EA equivalence

The stiffness of the net twines was equal to that of the equivalent truss element in unit length.

$$\sum_{n=1}^{4} \mathrm{EA} = E_e A_e \tag{5-3}$$

From the equation (5-2), we can easily get $\sum_{n=1}^{4} \mathrm{A} = A_e$ (5-4)

So, $\mathrm{E} = E_e$

Here, E and A are elastic modulus and cross section of each twine respectively;

E_e and A_e are elastic modulus and cross section of the equivalent truss element from four twines respectively;

l is the length of the net.

3. Hydrodynamic force equivalence

The hydrodynamic forces were calculated based on Morison's equation, and the forces on four net twines were the same with that on the equivalent truss element. Therefore,

$$\sum_{n=1}^{4} \mathrm{F} = \sum_{\mathrm{n}=1}^{4} \left(\frac{\pi \mathrm{D}^2}{4} \rho \mathrm{C_M} \dot{\mathrm{u}} + \frac{\rho}{2} \mathrm{C_D D u|u|}\right) = \frac{\pi \mathrm{D}_e^2}{4} \rho \mathrm{C_{Me}} \dot{\mathrm{u}} + \frac{\rho}{2} \mathrm{C_{De} D}_e \mathrm{u|u|} \tag{5-5}$$

Here: F is the hydrodynamic force of the twine/bar subject to;

D is the diameter of each net twine;

$\mathrm{C_M}$ and $\mathrm{C_D}$ are the mass and drag coefficient of each net twine respectively;

D_e is the diameter of the equivalent truss element from four twines;

$\mathrm{C_{Me}}$ and $\mathrm{C_{De}}$ are the mass and drag coefficients of the equivalent truss element from

four twines respectively;

Here it should be mentioned that the averaged water particle velocities and accelerations of the four net twines were assumed to be the same as those of the equivalent truss element.

To satisfy Eq. (5-5), we need to make sure:

$$4C_M D^2 = C_{Me} D_e^2 \tag{5-6}$$

$$4C_D D = C_{De} D_e \tag{5-7}$$

From Eq. (5-2) and Eq. (5-7), we can get $C_M = C_{Me} = 2$, $C_{De}=2C_D=2.3$.

Table 5-2 shows the parameters of the truss model with coarse meshes and refined meshes:

Items	Refined	Coarse	Items	Refined	Coarse
Truss length	17.6 mm	70.4 mm	**No. of elements in circumference**	252	63
Twines per truss	1	4	**No. of elements in depth**	81	21
Twine diameter/m	0.002	0.004	**C_D for net**	1.15	2.3
C_M	2	2	**C_D for bottom weights**	1.15	1.15
No. of nodes	20460	3907	**No. of elements**	40588	2599

Table 5-2 Critical Parameters for two truss models

Here it should be mentioned that additional points in the middle of the twines only added in coarse meshes truss model not in the refined meshes truss model. The number of elements has increased approximately 4 times both in circumference and depth from coarse meshes truss to the refined meshes truss, so the element number in refined meshes truss model is about 16 times of that in coarse meshes truss model. The node number in refined meshes truss model should also be 16 times of that in coarse meshes truss model if there were no additional nodes. However, with additional nodes in coarse meshes truss, the number of the nodes nearly tripled. Then the number of nodes in refined meshes truss is approximately 5.3 (or 16/3) times of that in coarse meshes truss.

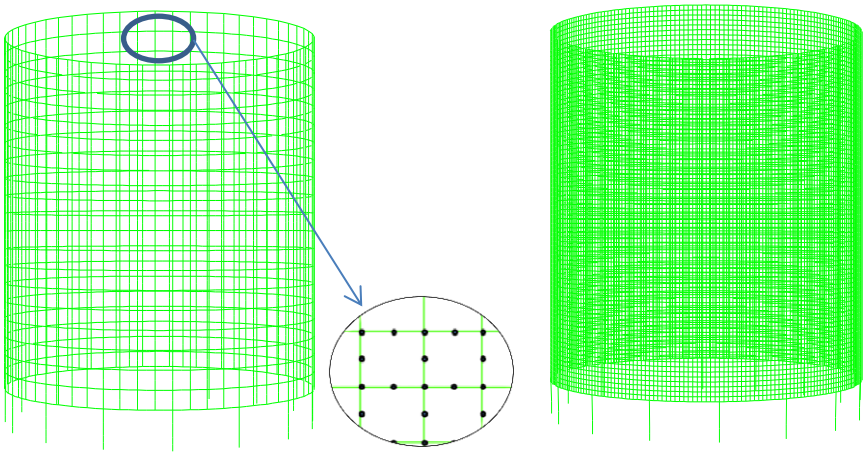

Figure 5-3 Truss model (left: truss model with coarse meshes. Black spots represent nodes. The

additional nodes in the middle of the twines to perform the bending effect) and truss model with refined meshes (right)

5.2.2 Mass spring model

Mass spring model can also represent the fish cage. Set lumped mass point at the knot and at the center of each bar (figure 5-4), then connect each mass point with nonlinear springs. The forces were calculated on equivalent mass points, in which the physical properties such as mass, volume, projected area and hydrodynamic coefficient were equivalent. The mass point at the center of the mesh bar was to represent the properties of the mesh bars and perform the bending of the bar (figure 5-6).

Similar to the truss model, the real net has an enormous number of mass points. We can also apply the equivalent method to reduce the calculation loads, in which several actual meshes were bundled together into a virtual mathematical mesh with the same physical properties. The virtual mass points were considered as small cylinders, but were distinguished as bar cylinders and knot cylinders. The physical properties of the virtual bar cylinders equaled to the actual twines combined together, and physical properties of knot cylinders were the same as the actual knots added together. Here, the spring is without mass, volume or other physical properties, only spring forces need to be taken into consideration. (Lee et al., 2008).
We derive the parameters of the equivalent mass spring model also by applying the equivalent calculation. The equivalent process was the same with truss model simplification. The buoyancy force and hydrodynamic force on four net twines were the same as that on the equivalent bar (or knot) cylinder.

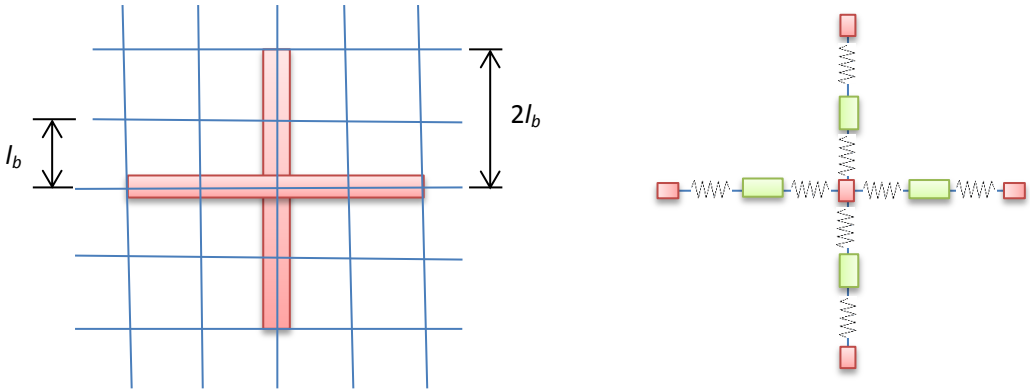

Figure 5-4 Equivalence of the net twines in mass spring model.
(Left side is the truss model, right side is the mass spring model, in mass spring model red rectangles represent the knot cylinder, the green ones mean the bar cylinder)

Properties of nonlinear springs

As the net can only take tension, not compression, we set the spring as nonlinear, as figure 5-6. The stiffness of the spring, $\boldsymbol{k}$, is given by:

$$k = \frac{EA}{l} \tag{5-8}$$

Where E is the Young's modulus of the material, A is the cross section of the equivalent net cylinder from four net twines, ***l*** is the original length of the spring.

Mooring lines were modeled as nonlinear spring. For simplification, we set the pretension of the nonlinear spring as 0.

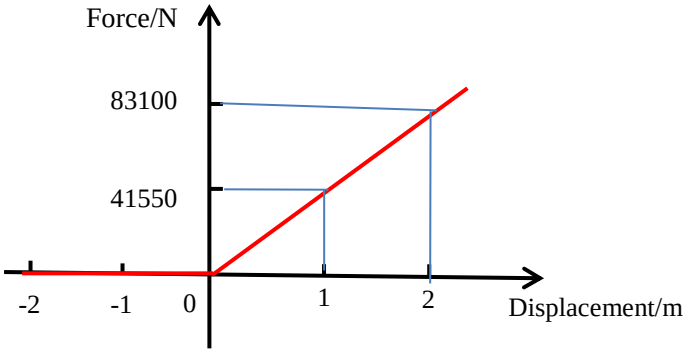

Figure 5-5 The force-displacement relation of nonlinear spring in mass spring model

According to the parameters given in the table 5-2, l_0=0.02483m,

$$\mathrm{k} = \frac{EA}{l_0} = \frac{82 \times 10^6 \times \pi \times 0.004^2/4}{0.02483} \approx 41550N/m$$

Equivalent calculation for mass spring model:

1） Buoyancy force equivalence

As mentioned in Eq. (5-1), we can get:

$$\sum_{\mathrm{n=1}}^{4} \mathrm{V} = \mathrm{V_e}$$

Here, V is the volume of every twine;

V_e is the volume of the equivalent bar (or knot) cylinder from four twines (or knots);

2） Hydrodynamic force equivalence

Equation 5-5 was used for equivalent calculation of the hydrodynamic forces with the same length. For mass spring model, the hydrodynamic force of the twine was equal to that of the equivalent small cylinder with unequal length, so equation 5-5 was not suitable here. Instead, the reference area per unit cylinder length A represented D and cylinder volume per unit cylinder length V represented $\pi D^2/4$. As a result, F(t) is the total force per cylinder length under current condition:

$$\mathrm{F(t)} = F_D + F_I = \rho \mathrm{V} \mathrm{C_M} \dot{\mathrm{u}} + \frac{\rho}{2} \mathrm{C_D A u|u|} \tag{5-9}$$

For twine,

$$\sum_{n=1}^{4} \mathrm{VC}_M = \mathrm{V}_e \mathrm{C}_{\mathrm{Me}}, \quad \sum_{n=1}^{4} \mathrm{C}_M \pi D^2 h = \mathrm{C}_{\mathrm{Me}} \pi {D_e}^2 h_e \tag{5-10}$$

$$\sum_{n=1}^{4} \mathrm{C}_D \mathrm{A} = \mathrm{C}_{\mathrm{De}} \mathrm{A}_e, \quad \sum_{n=1}^{4} \mathrm{C}_D \mathrm{Dh} = \mathrm{C}_{\mathrm{De}} D_e h_e \tag{5-11}$$

$$\mathrm{C_M} = 2,\ \mathrm{C_D} = 1.15,$$

Assume D = 0.004, h = 0.0704

$$\text{So } \mathrm{C_{Me}} = 2,\ \mathrm{C_{De}} = 4.6,\ D_e = 0.008,\ h_e = 0.0176$$

For knot, the equivalent knot cylinder was obtained from four original knot cylinders.

$$\sum VC_M = \mathrm{V}_e \mathrm{C}_{\mathrm{Me}}, \quad \mathrm{C_M} \pi D^3/4 = \mathrm{C}_{\mathrm{Me}} \pi {D_e}^2 h_e/4 \tag{5-12}$$

$$\sum C_D A = \mathrm{C}_{\mathrm{De}} \mathrm{A}_e, \quad \mathrm{C_D} D^2 = \mathrm{C}_{\mathrm{De}} d D_e h_e \tag{5-13}$$

Assume $\mathrm{C_M} = 2,\ \mathrm{C_D} = 1.15,$ D = 0.004

$$\text{So } \mathrm{C_{Me}} = 2,\ \mathrm{C_{De}} = 1.15\ D_e = 0.004, \quad h_e = 0.004$$

Here, F is the hydrodynamic force of the twine/bar subject to;

D is the diameter of every twine;

$\mathrm{C_M}$ and $\mathrm{C_D}$ are the mass and drag coefficient of every twine respectively;

V is the volume of the bar (or knot) cylinder;

A is the area of the bar (or knot) cylinder;

h is the height of the bar (or knot) cylinder;

D_e is the diameter of the equivalent bar (or knot) cylinder from four twines (or knots);

$\mathrm{C_{Me}}$ and $\mathrm{C_{De}}$ are the mass and drag coefficient of the equivalent bar (or knot) cylinder from four twines (or knots) respectively;

$\mathrm{V_e}$ is the volume of the equivalent bar (or knot) cylinder;

$\mathrm{A_e}$ is the area of the equivalent bar (or knot) cylinder;

h_e is the height of the equivalent bar (or knot) cylinder;

So summary of the parameters of the mass spring model:

Equivalent twine cylinder	Inertia coefficient $\mathrm{C_{Me}}$	2
	Drag coefficient $\mathrm{C_{De}}$	4.6
	Cylinder diameter $\mathbf{D_e}$/m	0.008
	Cylinder height $\mathbf{h_e}$/m	0.0176
Equivalent knot cylinder	Inertia coefficient $\mathrm{C_{Me}}$	2
	Drag coefficient $\mathrm{C_{De}}$	1.15
	Cylinder diameter $\mathbf{D_e}$/m	0.004
	Cylinder height $\mathbf{h_e}$/m	0.004
Spring	Stiffness $\mathbf{k}/\ (N/m)$	41550 (only tension)
	Original spring length $\boldsymbol{l_0}$/m	0.02483

Table 5-3 Equivalent parameters for twines and knots in mass spring model

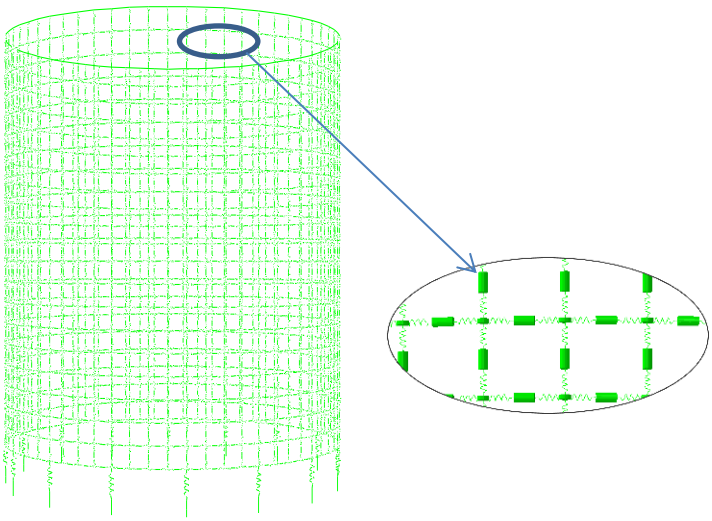

Figure 5-6 Mass spring model
(magnified part shows how the mass points and springs arrange in the model)

5.3 Results and discussions

5.3.1 Cage deformation

The two truss models and mass spring model were simulated under the same conditions (current velocity 0.34 m/s). After 10 seconds simulation, all the models had reached to the balance state. An example can be shown in figure 5-7 when the truss model with 16*800g bottom weight was simulated under current velocity 0.34 m/s, the horizontal displacement of point A reached balance state after 10 seconds simulation.

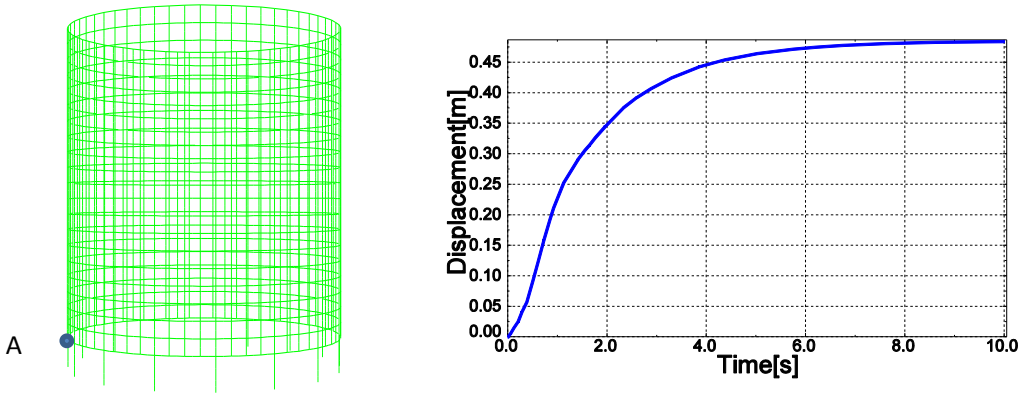

Figure 5-7 Horizontal displacement of point A in 10s simulation

Figure 5-8 shows the deformation of the each numerical model compared with the experimental deformation (Lader & Enerhaug, 2005).

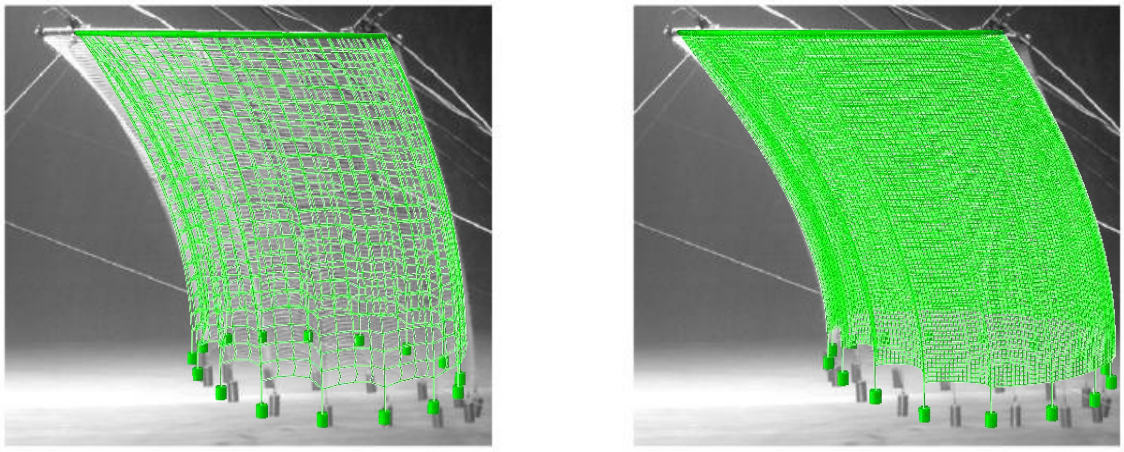

a) b)

c)

Figure 5-8 Fish cage deformation of the truss model with coarse meshes(a), the truss model with refined meshes (b), and mass spring model (c) compared with the experimental deformation from Lader and Enerhaug (2005)

From figure 5-8, we can see that the three models all fit well with the deformation from experiments. The deformation of the truss with coarse meshes and mass spring model seems quite similar. The best fit with the experimental results is the truss model with refined meshes. The different size and position of bottom weights may be one of the reasons for the difference between the deformations from numerical models and experiment.

5.3.2 Convergence study of the truss model

The truss model of coarse meshes and refined meshes were simulated with the same bottom weight 16*800g under 3 different current velocities (0.2m/s, 0.34m/s, 0.5m/s). The hydrodynamic force and relative volume were compared. Here the volume of a deformed fish cage was calculated as the horizontal cross-section multiplied by the average thickness of the section layer (Moe et al., 2010). The MATLAB transcript of calculating the area of the

deformed cross section can be found in Appendix 2 “Polyarea”. The drag force was collected from the sum of horizontal reaction force at the fixed floater, and lift force was the difference between the sum of vertical reaction force and submerged weight.

Figure 5-9 shows the results of the volume reduction and hydrodynamic force from convergence study.

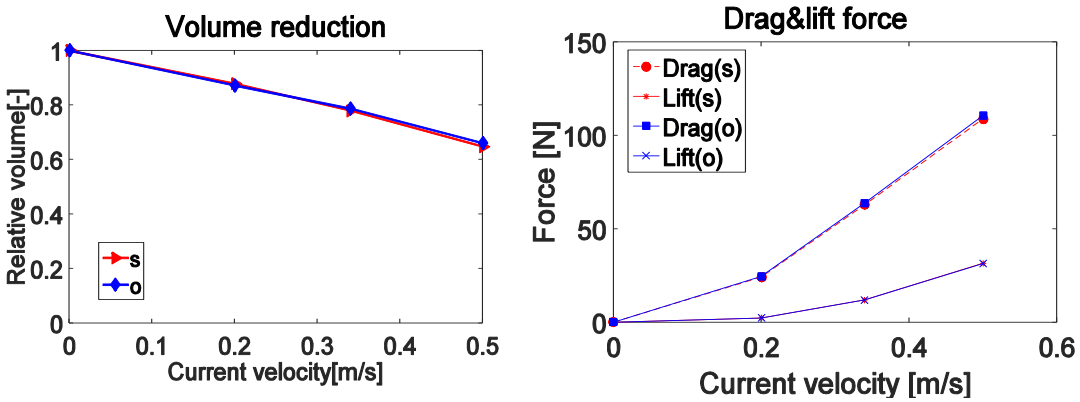

Figure 5-9 Simulation results of the truss model with coarse meshes(s) and refined meshes (o)

From the figure 5-9, the drag and lift forces of the truss model with coarse meshes was approximately less than 1.5% smaller than the truss model with refined meshes, and the relative volume was less than 1.6% smaller when the truss model was refined. So we can conclude that the truss model with coarse meshes is reliable for further study.

5.3.3 Comparison of hydrodynamic forces and volume reduction

The truss model and mass spring model were simulated under different bottom weights (16*400g, 16*600g, 16*800g) and current velocities (0.2m/s, 0.34m/s, 0.6m/s). The hydrodynamic force and volume reduction between these two models were compared in figure 5-10 and 5-11.

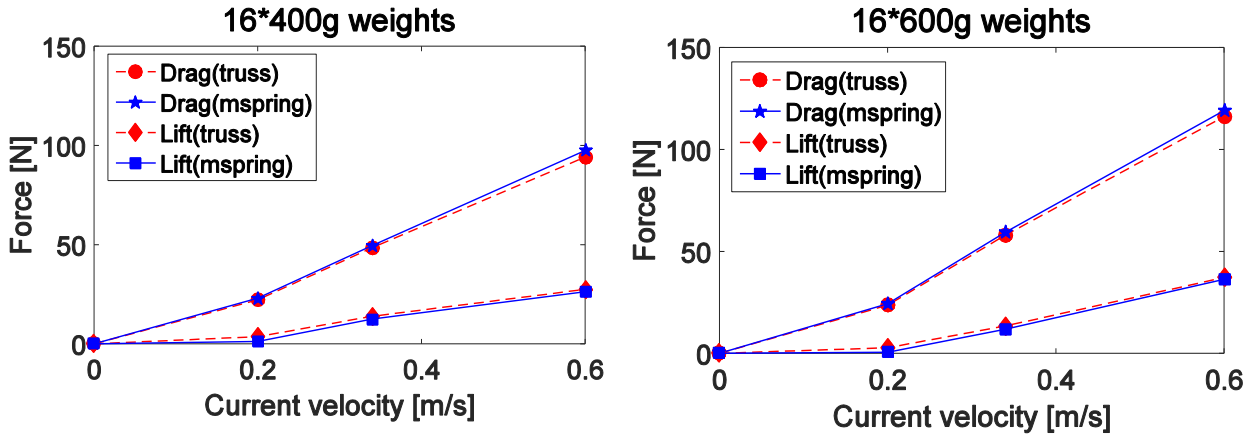

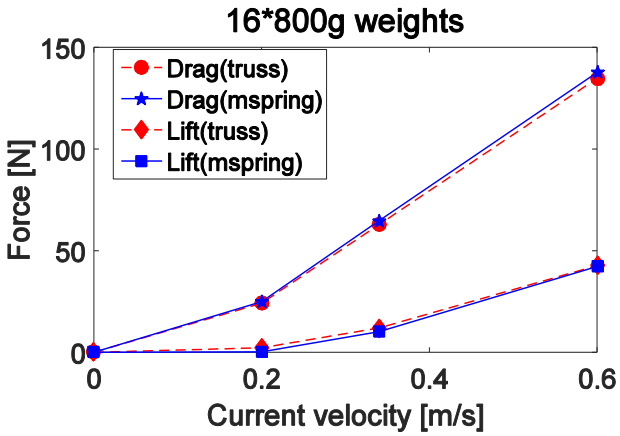

Figure 5-10 Drag and lift force of truss model and mass spring model

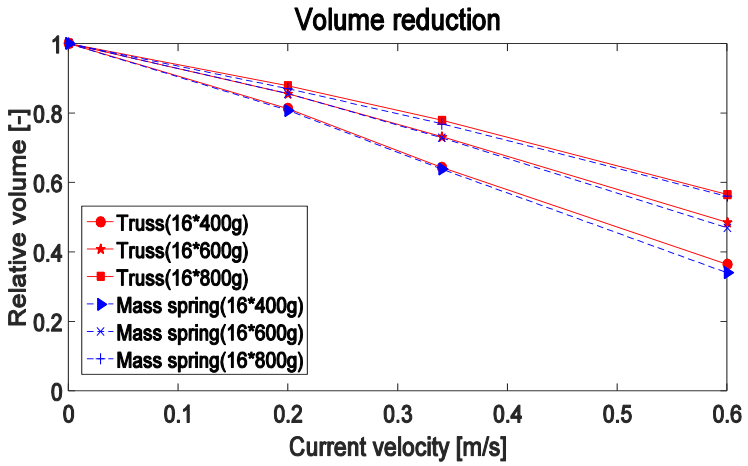

Figure 5-11 Volume reduction of truss model and mass spring model

The hydrodynamic forces and relative volume were almost proportional with the current velocity when the velocity was larger than 0.2 m/s, which was contradict with Morison's equation, the hydrodynamic force should be proportional to the velocity squared. This can be explained by the deformation of the net pen, which starts to become significant when the current velocity exceeds 0.1 m/s. Since the net structure is flexible, the relationship between current velocity and total forces becomes complex since the forces and deformations mutually depend on each other. Different areas in the net structure have different attack angle, and the effective solidity ratio may be altered due to changing forces on the net (Lader & Enerhaug, 2005).

With the increase of the current velocity, the drag and lift force increased significantly, while the volume decreased. The increase of the bottom weight tended to preserve the net volume and slightly increased the drag and lift forces. When the current velocity increased to 0.6m/s, the relative volume deducted significantly to 30%-60% of the original volume.

There were very little differences (less than 3%) between the force and volume results of the truss model and mass spring model. Both truss model and mass spring model can model the net pen and present similar results. Since truss model simulation runs much faster than that of

mass spring, so due to the limited time of the thesis, truss model is chosen for the further simulation.

Then the results of the truss model were compared with the simulation and experimental results from Moe at al.(2010). The hydrodynamic forces comparison is shown in figure 5-12, and relative volume results are in figure 5-13.

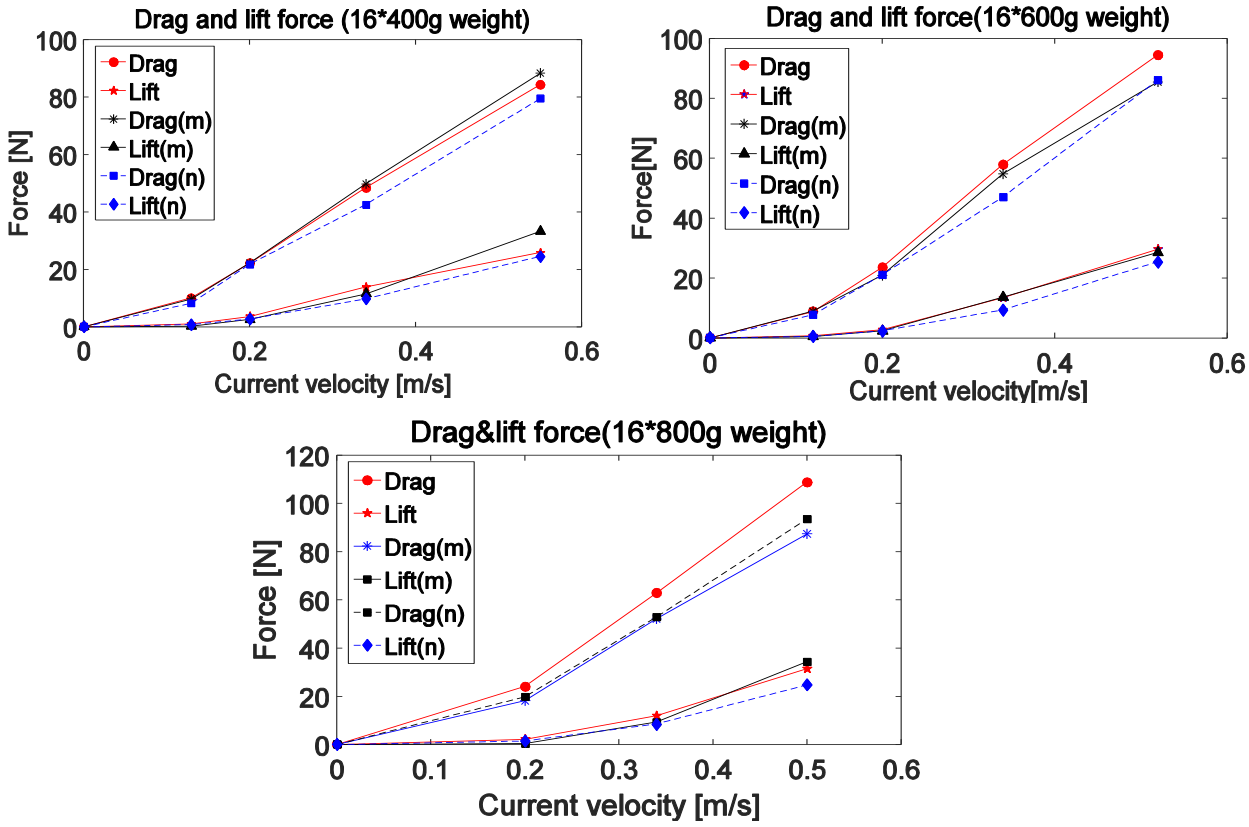

Figure 5-12 Numerical drag and lift force comparison with the model test(m) and numerical simulation(n) from Moe et al. (2010)

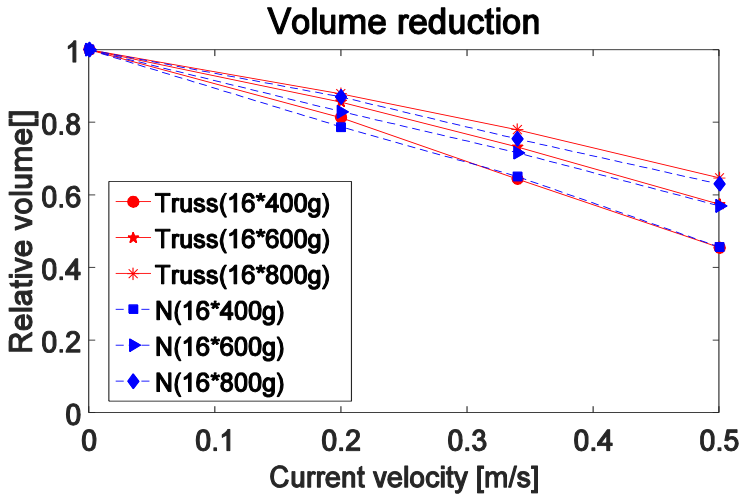

Figure 5-13 Volume reduction of truss model with numerical results from Moe et al. (2010) (red lines : the truss model in the thesis, blue lines: numerical results from Moe)

From figure 5-12 and 5-13, it can be seen that the hydrodynamic forces and the volume reduction are of the same trends, yet a little larger compared with simulation and experiment results from Moe's paper. It is because the truss model in the thesis does not consider the effect of velocity reduction factor. In Moe's truss model, she took the velocity reduction factor as 20% after passing the first net wall, in accordance with the experiments in Lader et al. (2005).

5.4 Summary

In this chapter, both truss and mass spring models were established to represent the fish cage, and the convergence study and sensitivity study were conducted to verify our simulation results with the simulation and experimental results from previous study. Responses of the hydrodynamic forces and volume reduction were compared and good agreements were achieved. Finally truss model was chosen for further study.

From this chapter, we can learn that the drag and lift force increase with the increasing current speed, but decrease with increasing bottom weights. Inversely, the relative volume of the fish cage decrease with the increase of the current velocity, yet increase when the bottom weights increase. The drag, lift force and relative volume are approximately proportional to the current velocity when the velocity is larger than 0.2 m/s, while they should be proportional to the current velocity squared according to Morison's equation.

6. Dynamic analysis of fish cage in full scale size

6.1 Background

A full scale fish cage is introduced in this chapter, truss model is used for the simulation of the full scale fish cage. The full scale fish cage is composed of the floater, the net and the bottom ring.

In chapter 5, we fixed the rigid floater of the fish cage to study the dynamic responses of fish net in pure current conditions. However, in reality the floater is flexible and floating on the waterline, and it will move and deform with wave and current. By the fixed and rigid floater, it will give a larger estimation of the relative volume (Moe et al., 2010). So in this chapter, sensitivity study on the interaction of the net and the floater will be performed first. Then the truss model will be improved with flexible floater considering the interaction effect. Sensitivity study on different solidity ratios, bottom weights and wave-current conditions will be illustrated for further understanding of the dynamic responses in full size fish cage model.

6.2 Numerical model

In the full size fish cage, the floater is a polypropylene pipe with elastic modulus 950MPa and density 953 kg/m^3, it is used to provide the buoyancy force for the whole fish cage. The bottom ring is a solid tube also made of polypropylene, but with a distinct density of 2000 kg/m^3. It is used to preserve the volume. The net with the material of nylon has a negligible bending stiffness. The net is close to neutrally buoyant in water, as its density (1140 kg/m^3) is quite close to that of sea water (1025 kg/m^3).

In this paper, with the current speed from 0 to 0.5 m/s, $Re_n=VD/\nu$, $\nu=1.15\times10^{-6}$m^2/s for sea water, we can get the Reynolds number (0< Re <2174). As seen from Eq. (2-8), we can get the C_D (1.1< Cd<1.29), for simplification, we set the drag coefficient as a constant mean value 1.2. As for inertia coefficient C_M is approximately 2 according to previous experience (figure 2-5).

The parameters of the fish cage are as follows:

	Floater	**Net**	**Bottom ring**
Whole fish cage field diameter(m)	20		
Whole fish cage field depth(m)	19.634		
Outer diameter(m)	0.3	0.005	0.1
Thickness of pipe(m)	0.034		
Bar length/m		0.061	

Table 6-1 Dimensions of the full size fish cage model

To simplify the problem, we use equivalent calculations to let one equivalent twine represents 16 actual twines. Table 6-2 is the net parameters of truss model.

Twine diameter(m)	0.02	**No. of twines (vertical)**	64
Elastic coefficient(MPa)	350	**No. of twines (circumferential)**	19
Density (kg/m^3)	1140	**Cd**	4.8
Bar length(m)	0.980	**Cm**	2
Solidity	0.16	**Net stiffness(MPa)**	350

Table 6-2 Net parameters in the truss model

Some points were chosen on the floater and nets for further analysis of the displacement and stress. Point A, B, C, D, E, F, M, N are all on the net. Point A and C are in the upstream of the net, while point B and D are in the downstream of the net. Point A and B are very close to the floater, point C and D are near the bottom ring. Point **e** is on the floater. Stress on net element AE, BF, CM and DN are very critical, as these are at the joints of the floater to the net and the net to the bottom ring. If the joints failed, the integrity of the whole fish cage would be demaged. Point A, C and E are the first points that contact with the wave and current, and very sensitive to the wave and current. Point B and D are points that are in the direct back of the point A and C.

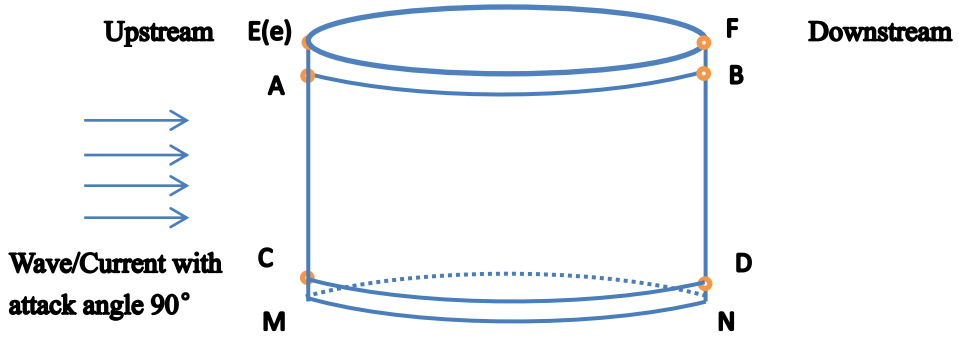

Figure 6-1 Illustration of the fish cage and critical points on the cage

6.3 Sensitive study

Sensitivity study on the interaction between the net and the floater was studied first, then more sensitivity studies on solidity ratio, bottom weight and wave-current condition were performed. The values for all parameters used in the sensitivity study are listed in table 6-3.

Solidity ratio	**bottom weight /Submerged weight**	**Wave-current**		
Sn=0.16	W_s=4725 N	H=1m, T=4s	H=1m, T=8s	H=1m, T=12s
Sn=0.25	W_s=7145 N	H=2m, T=4s	H=2m, T=8s	H=2m, T=12s

Sn=0.34	W_s=9566 N	H=3m, T=4s	H=3m, T=8s	H=3m, T=12s

Table 6-3 Sensitivity study on the full scale fish cage

6.3.1 Interaction of the net and the floater

The effect of the net to floater and the floater to the net will be investigated to see whether the interaction effect can affect the responses of the floater or the net. Three models were established to study the interaction, and their details are listed in Table 6-4, and M2 and M3 are shown in Figure 6-2.

Models	Model compositions	Floater condition	Mooring system	Boundary conditions
M1	Only floater	Flexible	With	Mooring system connected to fixed points
M2	Floater+net+bottom	Flexible	With	Mooring system connected to fixed points
M3	Floater+net+bottom	Rigid	Without	Floater fixed

Table 6-4 Models to study the interaction of the net and floater

All these three models were put into pure regular wave condition (H=5m, T=8s), the displacement and stress were compared.

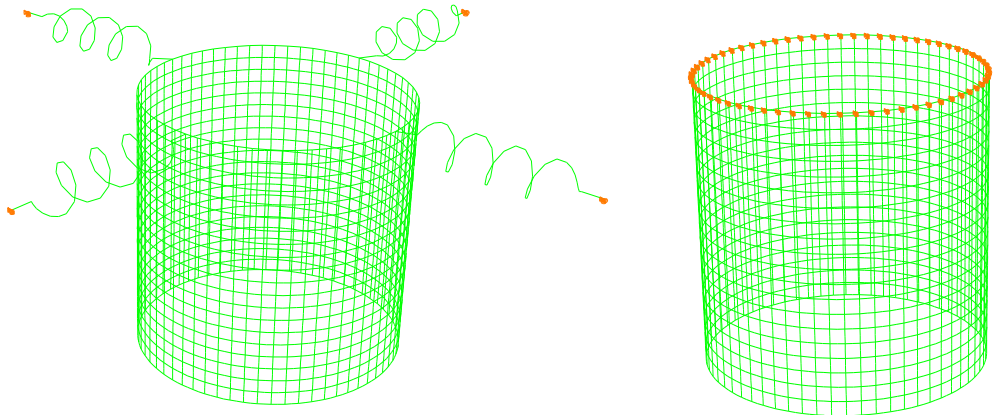

Figure 6-2 Two fish cage models M2 and M3 (left: M2 Mooring system connected to fixed points and flexible floater, right: M3 rigid and fixed floater. Red points signify the boundary condition)

1. Effect of the net to the floater

Responses of M1 and M2 model were compared here through displacement of point **e** on the floater. Figure 6-3 shows the variation of horizontal and vertical displacements of point **e**.

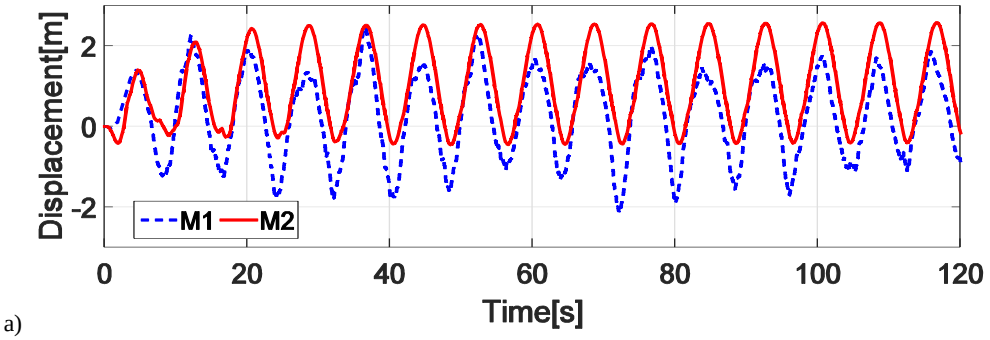

a)

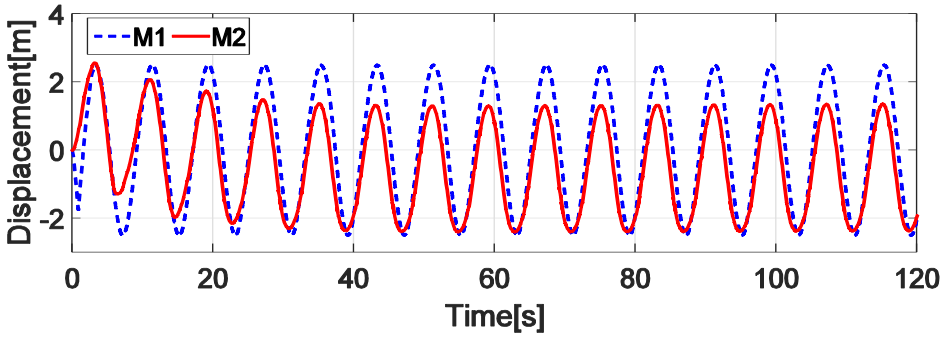

b)

Figure 6-3 Horizontal (a) and vertical (b) displacements of point **e** under pure regular wave condition (H=5m, T=8s)

In figure 6-3, point **e** in M1 tends to have larger motion than M2 both horizontally and vertically. Horizontal displacement of point **e** of M2 is larger than that of M1 in +X direction. The mean position of point **e** in M2 has moved to about 1m in +X direction. This can be explained from figure 3-3, when the wave height is large compared to the structure size, the mean wave force on the fish cage is larger in the wave direction than in the opposite wave direction, thus moves the floater to a new mean position. Lader et al. (2007) also mentioned this phenomena from mechanics of a regular wave. The structure on the wave crest relative to the trough, the maximum horizontal velocity is larger, also the net area exposed to the fluid velocity is larger.

The vertical displacement of point **e** in M2 is smaller than that of M1. The net induced large damping forces on the vertical motion, thus reduces the floater motion in vertical direction (Lader & Enerhaug, 2005).

Figure 6-3 shows the stress variation of point **e** in two models.

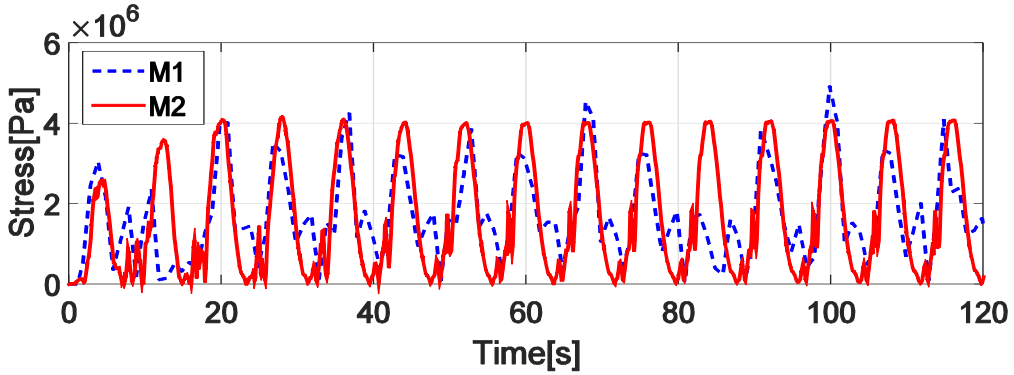

Figure 6-4 Stress variations of point E in M1 and M2

The stress of point **e** in M2 tends to change harmonically, while that of M1 does not act periodically, sometimes there are very large stresses. Mostly the stress of M2 is smaller than that of M1 except when there is large impact. This is because the only floater can offset some wave energy by large displacement and deformation. However for M2, vertical motion of the top point is closely related to the load on the net and bottom, thus increase the stress of point **e** on the floater.

2. Interaction of the floater to the net

Response of two fish cage model M2 and M3 were compared. Displacement and net stress on critical places were studied. Figure 6-5 shows the displacement variations in model M2 and M3 both horizontally and vertically.

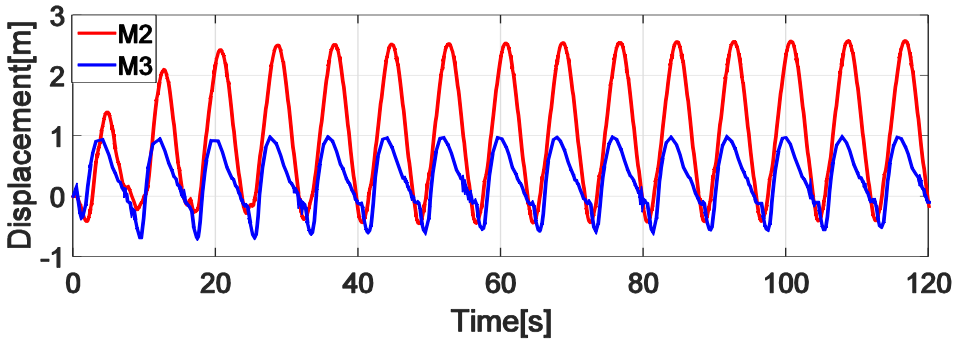

a)

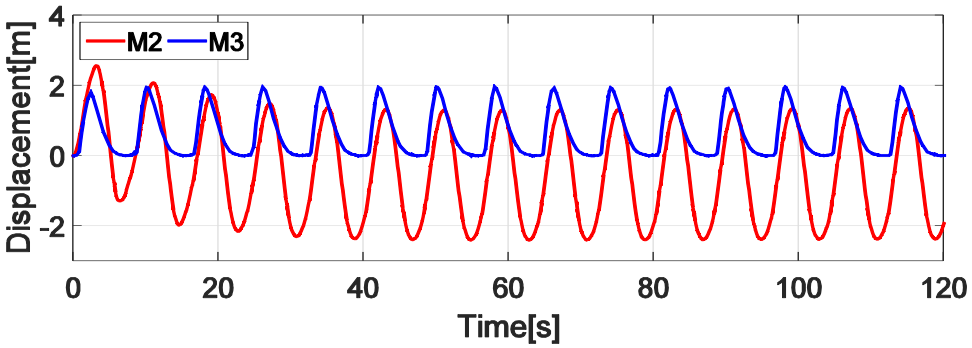

b)

Figure 6-5 Horizontal (a) and vertical (b) displacement of point A in two fish cage models

In figure 6-5, it can be easily detected that the displacement of point A in M2 is much larger

than M3 both horizontally and vertically. The displacement variations of point A both horizontally and vertically in M2 are almost twice as M3. The mean horizontal displacement of point A in M2 is about 1m in +X direction, while that in M3 is almost 0. That is because the motion of the net is closely related to the floater. In M2, the floater has moved to the new mean position of 1m in +X direction, while in M3, the floater is fixed with respect to the earth.

There is almost no negative value in vertical displacement of M3. The motion of point A is constraint by the fixed floater, so it is impossible for the net to move downwards due to lift force. In M2, the floater is moored in horizontal directions, yet it is free to move in vertical directions, so vertical displacement of point A in M2 is larger than M3. It can be concluded that the motion of the floater can cause large displacement both horizontally and vertically on the net.

Figure 6-5 shows the displacement variation of point C in M2 and M3 models.

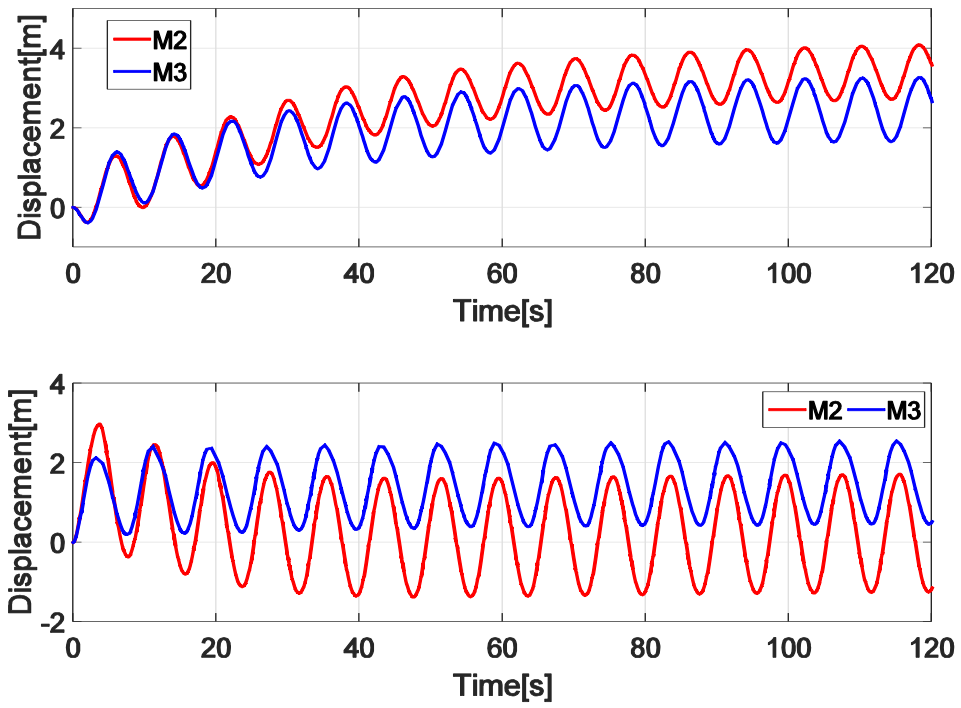

Figure 6-6 Horizontal (a) and vertical (b) displacement of point C in two fish cage models

The mean position of point C moves in +X direction horizontally both in M2 and M3, but point C in M2 moves a little further than M3. For the displacement of M2 relative to that of M3, it is smaller both horizontally and vertically. The point C is lifted to a new position at around 1.5 meters in +Z direction in M3, while it stays at around 0 in M2. Compared with figure 6-5, it is easy to find that the vertical displacement of point C is smaller than that of point A. That is because the floater in M2 moves downward in figure 6-5 (b), and the net and the bottom ring move with it. This downward effect and the lifting effect finally make the

mean position of the bottom ring stay at 0. The floater in M3 is fixed, there is only lifting effect, so the bottom ring is lifted up to a new mean position in +Z direction.

Figure 6-5 shows the stress variation of element AE, BF, CM and DN in two models. Stress on these elements are very important for the integrity of the fish cage.

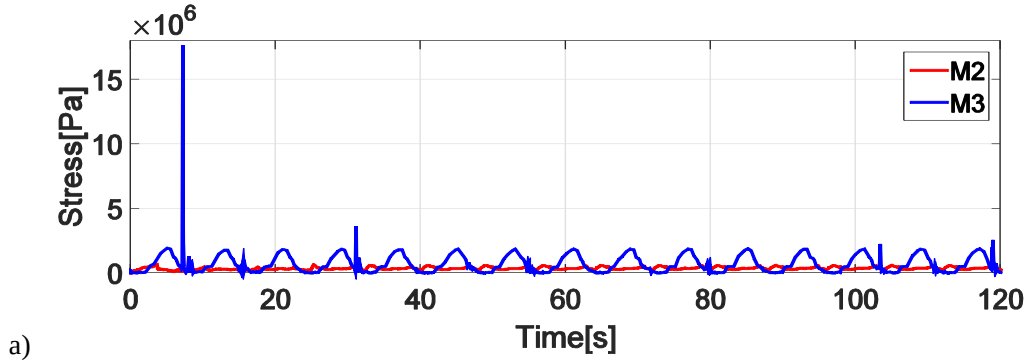

a)

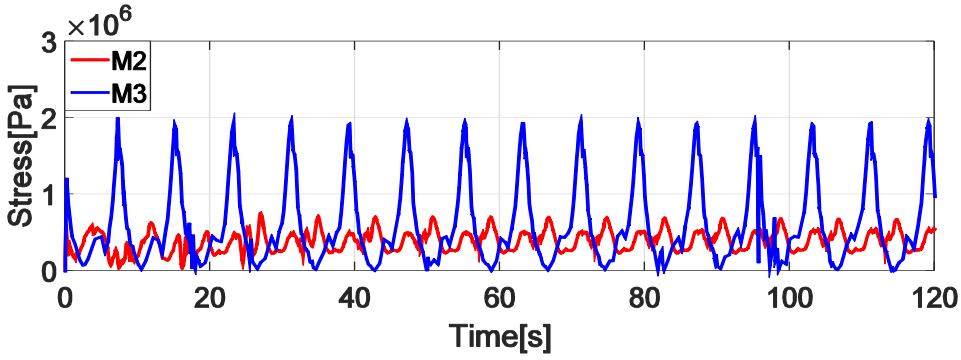

b)

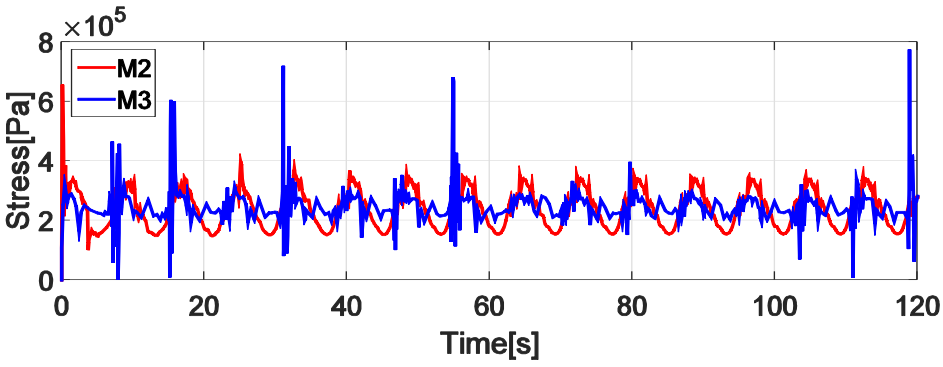

c)

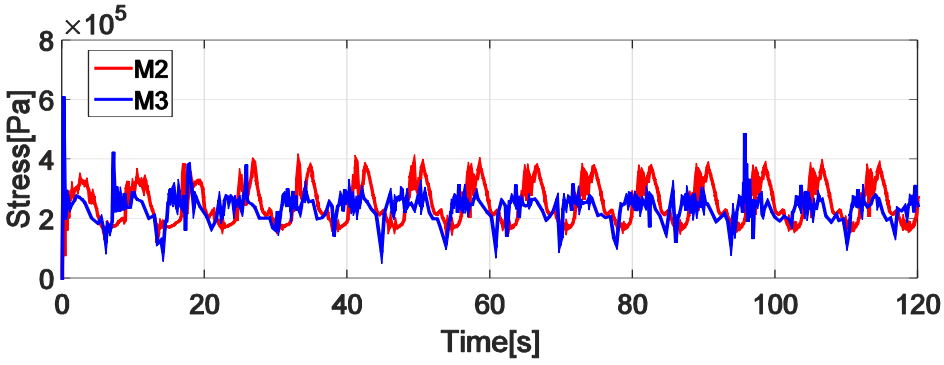

d)

Figure 6-7 Stress at element AE(a), BF(b), CM(c), DN(d) in M2 and M3

In figure 6-7 the stresses in these four elements (AE, BF, CM, DN) are almost the same in M2, but the stresses varies in M3. Stress vibration near the floater (element AE and BF) in M3 is much larger than in M2. The stress near the floater in M3 sometimes goes to zero (figure 6-7 b). This indicated there is slack on the net of M3, and large stresses are triggered. Apart from the extreme value caused by slack, the maximum stress of M2 is almost 3 times of that in M3. It can be due to that wave energy consumed by the large displacements in M2, which results in smaller stress in the net. The floater in M3 is constrained, the displacement of point A closely related to the floater is small, so some of the wave energy is used to extend the net, thus induces large stress on the net.

Stresses at element CM and DN are a little larger in M2 than in M3 if the slack effect is not considered. Lifting force acts on the bottom ring and the net in M3, but in M2 the lifting force on the structure is used to lift the bottom ring, net and the floater, so stress in element CM in M2 is a little larger in M3.

3. Improvement of the truss model

The effect of the floater to the net is much larger than that of the net to the floater. So modelling the responses of the floater are very crucial for obtaining the accurate responses of the whole fish cage.

ABAQUS cannot predict the buoyancy force correctly when the body is submerged(as discussed in chapter 4), so in ABAQUS the floater cannot stay half submerged in water as it should be in dynamic analysis, but will continually move up and down the waterline. This will give a heavy load to the calculation (for pure current condition, about 20 hours is needed for 24s simulation). To fix this problem, the buoyancy force were given a value in +Z direction according to the gravity minus the lift force (lift force can be obtained by trying from the lift force when the floater is fixed), then the simulation was much faster (for 500s simulation, it takes only 20 minutes or so, overview of the simulation is in Appendix 1).

Figure 6-8 shows the vertical displacement of point **e** on the floater under 0.5 m/s with the improved truss model. At the beginning, the floater sank quickly, but with the increase of lifting force, it raised up gradually until the balanced position in the waterline. So the responses before the floater reached to the balanced position may have some deviations with its true responses, but the responses in the final balanced state can well represent responses in reality.

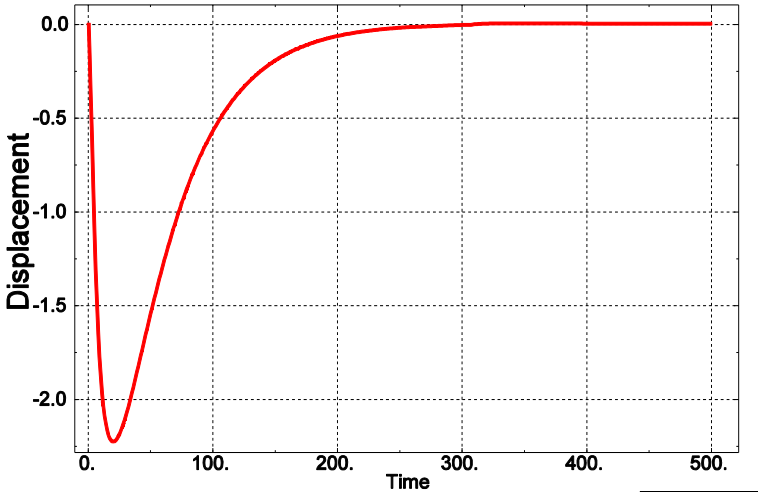

Figure 6-8 Vertical displacement of point E under current 0.5 m/s

6.3.2 Sensitive study on solidity ratio

Biofouling is a serious problem that has always troubled the fish farmers in recent years. Biofouling can grow very fast and thick. Not only it can affect the exchange rate of the fresh water within and outside the net pen, it can also be the fertilizer of some microorganism, which may endanger the health of the fish groups. In some cases, on the heavily fouled nets the drag can be increased by up to 900% in rough seas and high current conditions. This will significantly affect cage structure and behavior. The increased stress on the netting could weaken the netting and also endanger the safety of fish cages (Kassah, 2012).

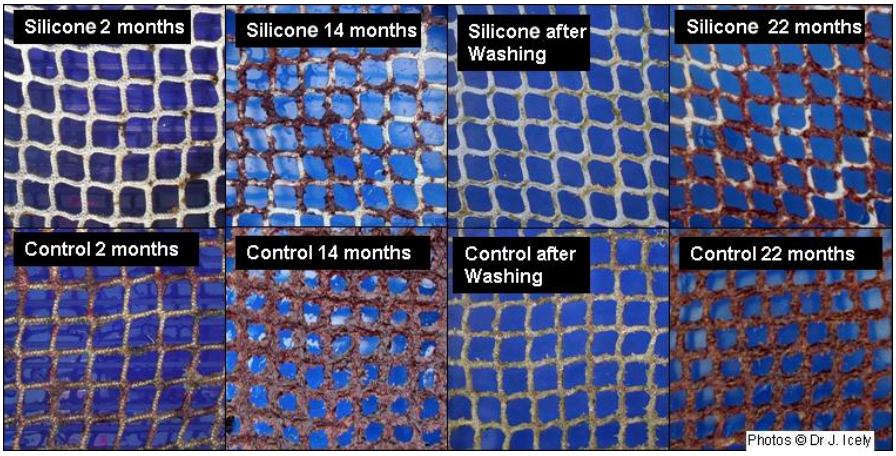

Figure 6-9 Comparison of biofouling with silicone coating and non-coated control netting
http://www.crabproject.com/index.php/107/testing-materials/

Solidity ratio is the ratio between the solid area of the net $\mathbf{A_s}$ and the total area enclosed by the net **A**. Biofouling will increase the solid area of the net, and increase the Sn. Fouling can be modelled as an increase in the net solidity, and by comparing nets with different solidity ratios, the effect of bio-fouling can be estimated (Lader & Fredheim, 2006). Here we are going to compare the responses in 3 different solidity ratios: 0.16, 0.25, 0.34. Figure 6-10 shows the

dimension of one knotless mesh of the net pen, and the relation of Sn and the dimension of the mesh can be expressed in Eq. (6-1).

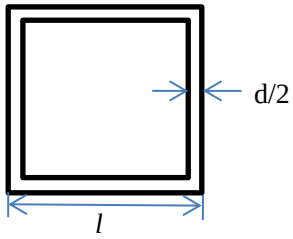

Figure 6-10 One knotless mesh of the net pen

$$Sn = \frac{\mathrm{As}}{\mathrm{A}} = \frac{4*(\frac{d}{2})(l-\frac{d}{2})}{l^2} \approx \frac{2d}{l} \qquad (d \ll l) \qquad (6\text{-}1)$$

Here, d is the diameter of the twine, l is truss length. Then the relative diameter can be found from the Eq. 6-1 (shown in table 6-5).

Sn	$Sn1$=0.16	$Sn2$ =0.25	$Sn3$ =0.34
d	d1=0.005m	d2=0.007625m	d3=0.01037m

Table 6-5 Various solidity ratio with related twine diameter

The models with different solidity ratio were simulated under current velocity from 0.1-0.5 m/s for 500s, when the models in all states have reached to the balance state (overview of simulation in Appendix 1). The deformation, hydrodynamic force, mooring tension and stresses in critical place were studied. Figure 6-11 shows the deformation as a result of the numerical simulation with various solidity ratio and current velocities.

Sn1 Sn2 Sn3

v=0.1m/s

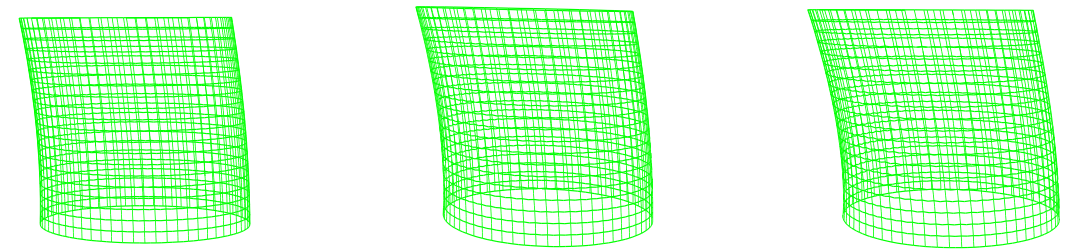

v=0.2m/s

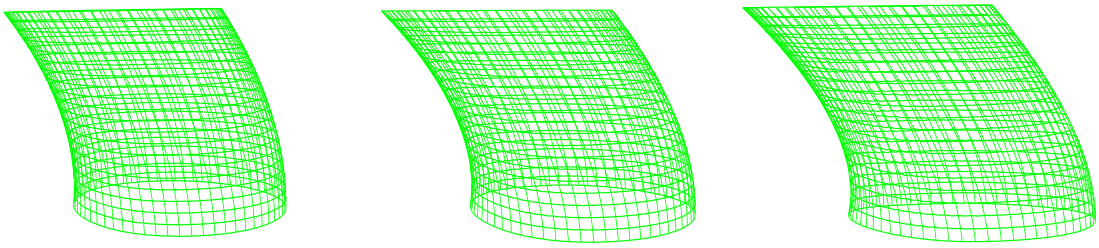

v=0.3m/s

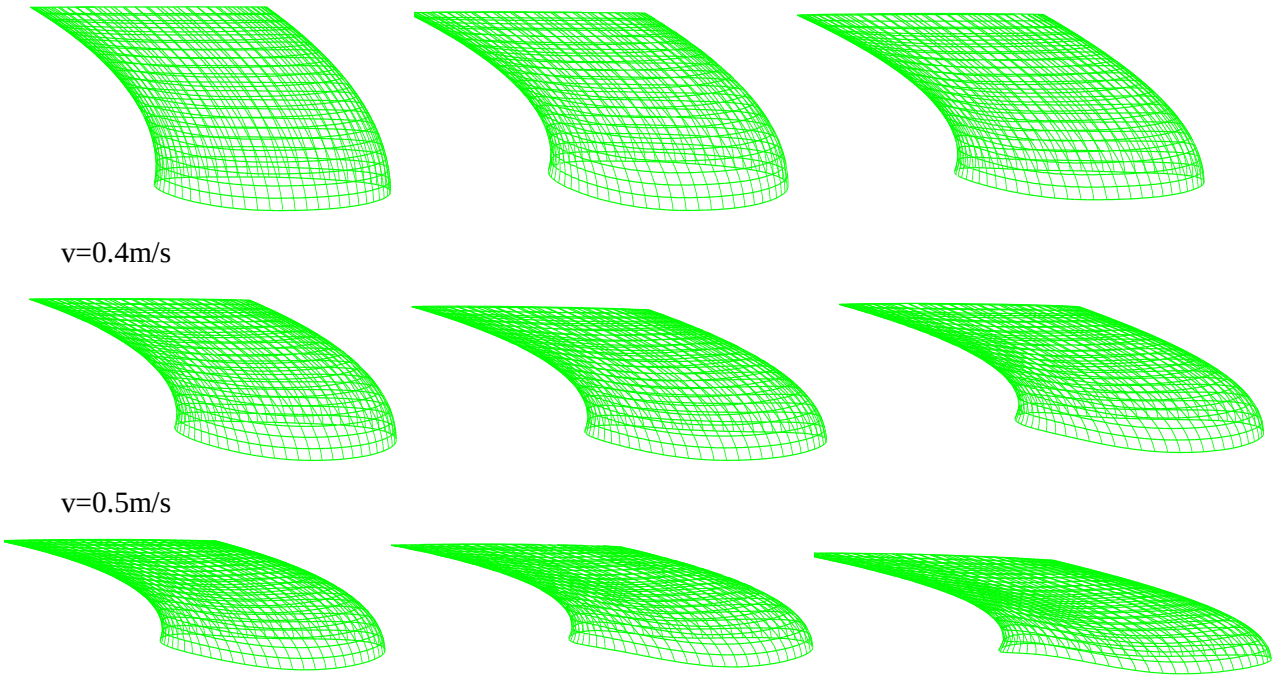

Figure 6-11 Deformations of model cage as a result of the numerical simulation various solidity ratio and current velocities

From figure 6-11, it can be seen that when the velocity is 0.1m/s, we can hardly see the deformation of the fish cage. However, with the increasing velocity speed, the relative volume of the fish cage decreases. The volume reduction reaches to approximately 50% of the original volume (from figure 6-11) when the velocity is 0.5 m/s, in which level the fishes would have low probability to survive. When the solidity ratio increases, the volume decreases a little, although the effect to the relative volume is not so obvious as the current velocity.

Figure 6-12 shows the volume reduction, and figure 6-13 demonstrates the drag and lift forces.

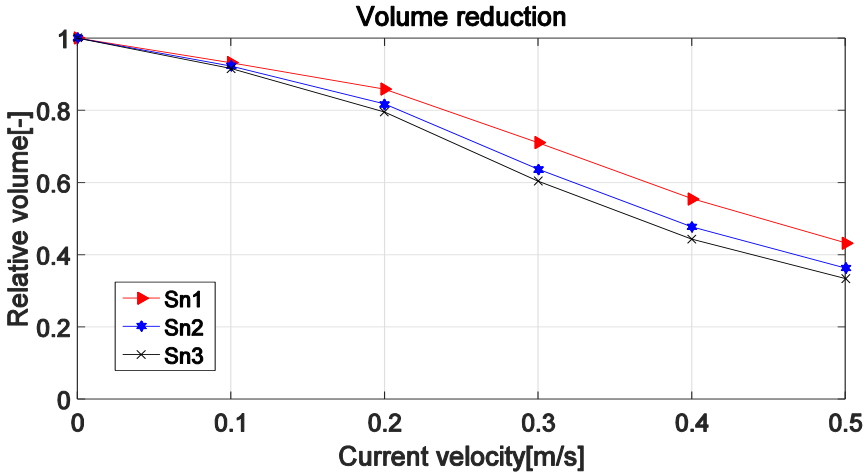

Figure 6-12 Volume reduction under various solidity ratio (Sn=0.16, 0.25, 0.34) and current velocities (0-0.5m/s)

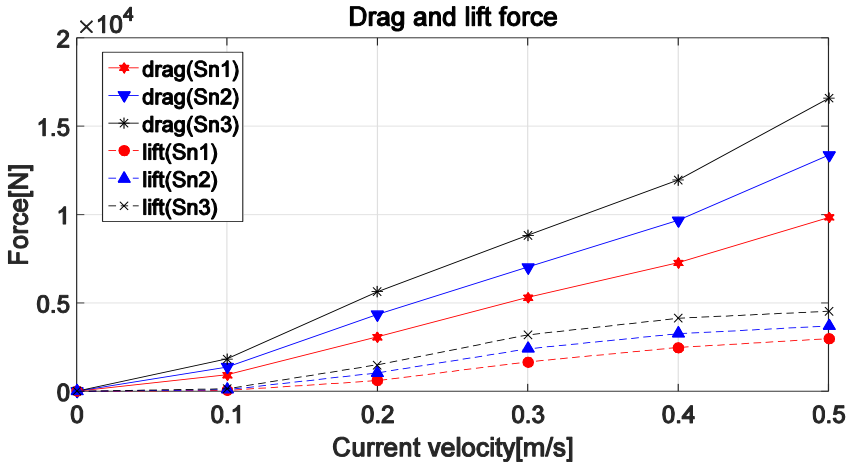

Figure 6-13 Drag and lift force under various solidity ratio (Sn=0.16, 0.25, 0.34) and current velocities (0-0.5m/s)

In figure 6-13, the drag and lift force seem to increase proportionally with the current velocity when the velocity is larger than 0.1 m/s. Figure 6-12 demonstrates that the relative volume decreases significantly, especially when the current velocity reaches to 0.5 m/s, the volume has deducted to around 40% of the original volume. The drag force tends to have larger increase than the lift force. It is also noticed that when the solidity ratio doubles (increase from 0.16 to 0.34), the drag force increases by 69% , the lift force increases by 52% under current velocity 0.5 m/s, yet the relative volume decreases by 11%. However, when the current velocity doubles (from 0.1m/s to 0.2m/s or 0.2m/s to 0.4m/s), the hydrodynamic forces and volume reduction almostly doubles, too. Then we can conclude that current velocity has a larger impact on the volume reduction than solidity ratio. Figure 6-14 shows how the maximum mooring tension changes with the current velocity and solidity ratio.

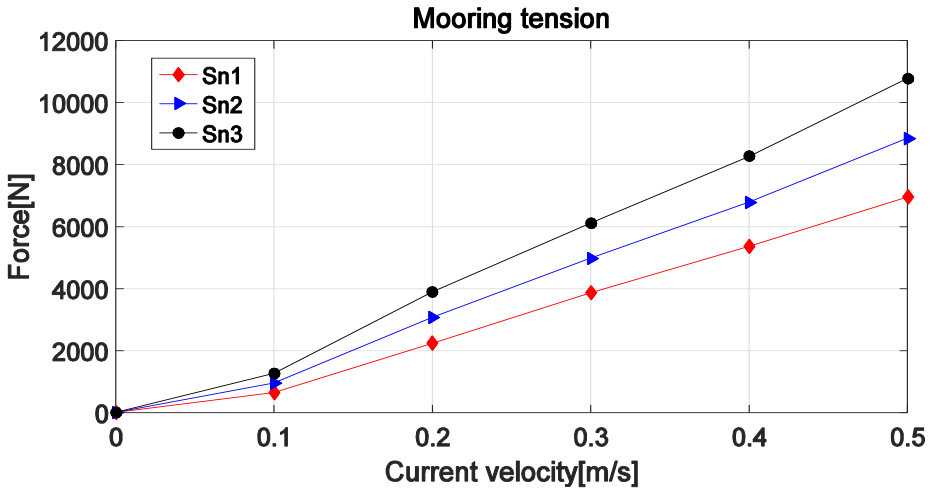

Figure 6-14 Maximum mooring tension under various solidity ratio (Sn=0.16, 0.25, 0.34) and current velocities (0-0.5m/s)

From figure 6-14, it can be observed that the maximum mooring tension is almost proportional to the current velocity when current velocity is more than 0.1 m/s, and increases

with the increasing current velocity and solidity ratio. When Sn=0.34, the mooring tension increases significantly by 9 times when current velocity increases from 0.1 m/s to 0.5 m/s. However, when the Sn almost doubles (increase from 0.16 to 0.34), mooring tension increases less than 57%. The current effect to the hydrodynamic force is much larger than solidity ratio.

6.3.3 Sensitive study on bottom weights

To investigate the effect of the various bottom weights to the fish cage, 3 different bottom weights were chosen. Here we increase the weight of bottom ring by its density, so that the hydrodynamic force in the bottom ring won't change accordingly. The relative floater parameters also changed to let the floater half submerged in the water (Table 6-6).

Models	Floater		Bottom weights		
	Radius/m	Thickness/m	Radius/m	Density/(kg/m^3)	Submerged weight/N
b1(Original)	0.15	0.034	0.05	2000	4725
b2	0.15	0.0293	0.05	2500	7145
b3	0.15	0.0239	0.05	3000	9566

Table 6-6 Parameters of the fish cage models

The models with different bottom weights were simulated under current velocity from 0.1-0.5 m/s for 500s, when all the models have reached to the balance state (overview of simulation in Appendix 1). The deformation, hydrodynamic force, mooring tension and stresses in critical place were studied. Figure 6-13 shows the deformation as a result of the numerical simulation with various solidity ratio and current velocities.

b1 b2 b3

v=0.1m/s

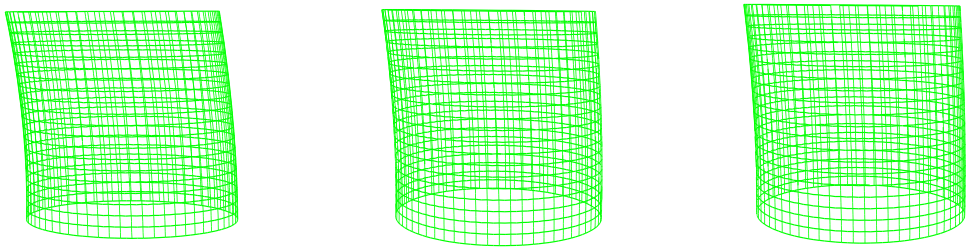

v=0.2m/s

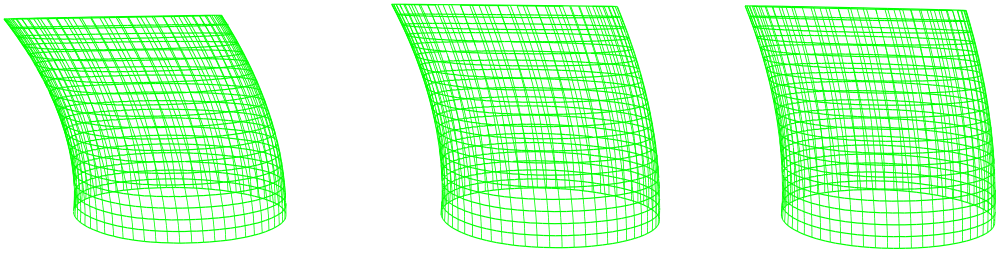

v=0.3m/s

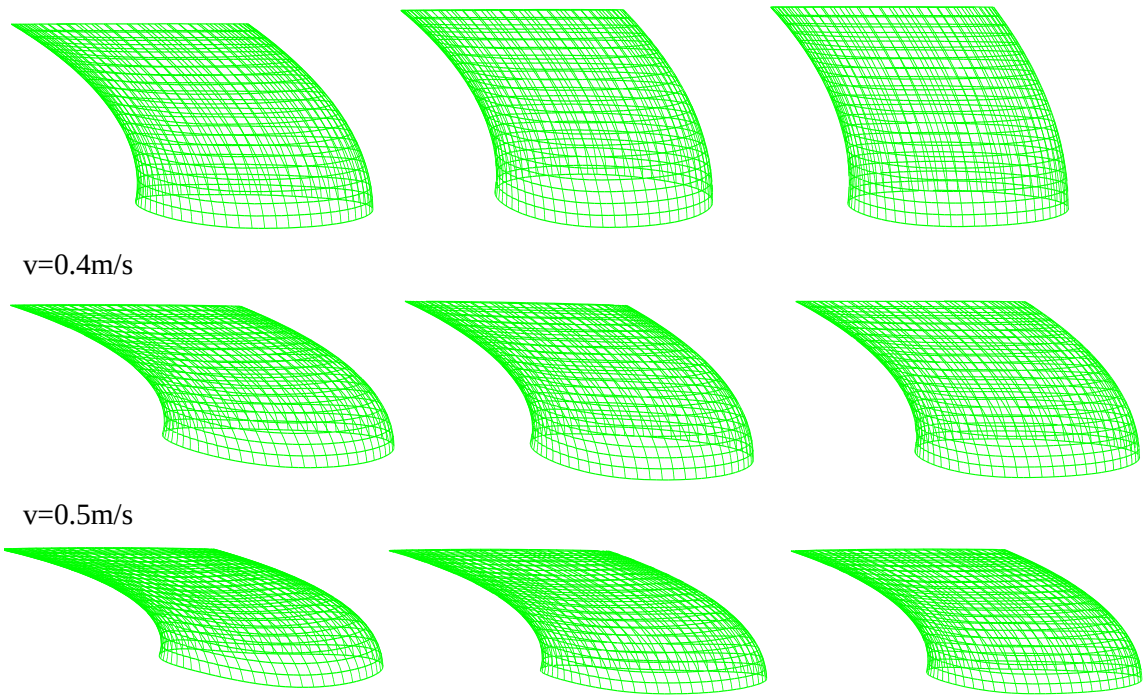

Figure 6-15 Net pen deformations as a result of numerical simulation with three bottom weights and current velocities (0-0.5m/s)

Figure 6-15 shows that the increasing bottom weights tends to preserve the volume, although this effect may not be so obvious. Current velocity seems to have much more obvious effect to the relative volume. Figure 6-16 shows the relative volume under various current velocity and bottom weight. Figure 6-17 compares the drag and lift force in various bottom weight condition.

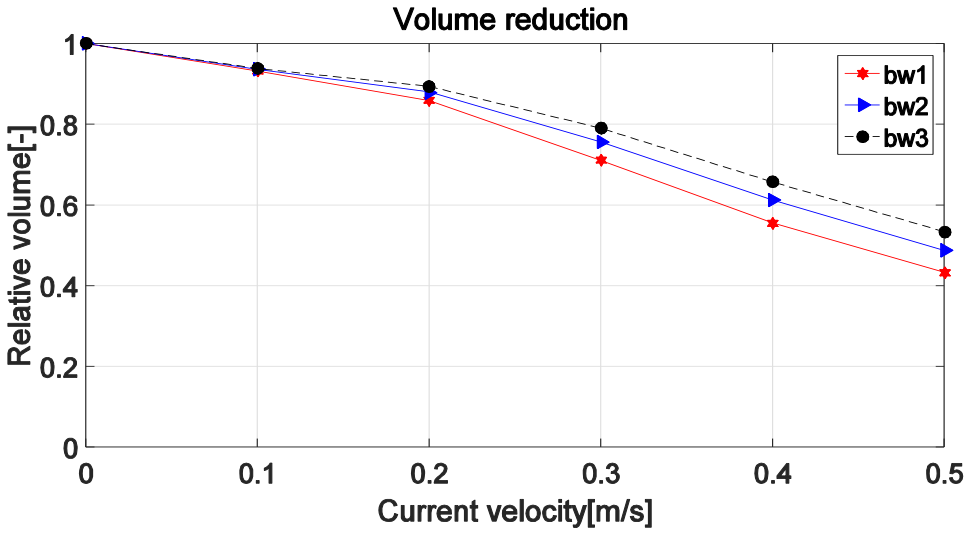

Figure 6-16 Volume reduction with three bottom weights and current velocities (0-0.5m/s) (bw represent bottom weight)

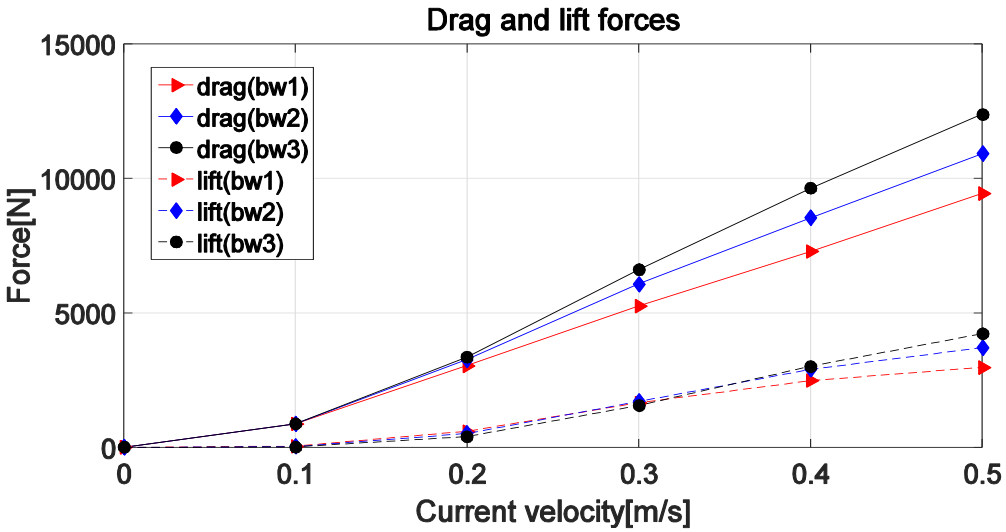

Figure 6-17 Drag and lift forces with three bottom weights and current velocities (0-0.5m/s)

In figure 6-16, it can be seen that with the increase of the bottom weights, the drag force increases almost proportionally with the current velocity when current velocity is larger than 0.1 m/s, but relative volume of the fish cage decreases proportionally with the current velocity when current velocity is larger than 0.2 m/s.

Under the velocity less than 0.3m/s, the lift force with the smallest bottom weight is largest. With the increase of the bottom weight, the inclination of the net truss decreases, the relative lift force decreases with the decreasing inclination angle. However, when the current speed is larger than 0.3 m/s, the lift force increases with the increasing bottom weight. Both the drag and lift force increases with increasing current speed and are approximately proportional with the velocity larger than 0.1 m/s.

When the bottom weight increases from bw1 to bw3 under the current velocity 0.5m/s, the drag force increases by 31%, and lift force increases by 42%, yet the relative volume has been enlarged by only 10% of the original volume. Compared with the sensitivity study on the solidity ratio, we can see that the interaction of the hydrodynamic force and deformation is complex. There is no direct relation with the hydrodynamic force and relative volume. The increase of the drag and lift force does not mean the relative volume will increase (or decrease).

Figure 6-18 and 6-19 shows that the stresses in critical place changes with different bottom weights under various current conditions.

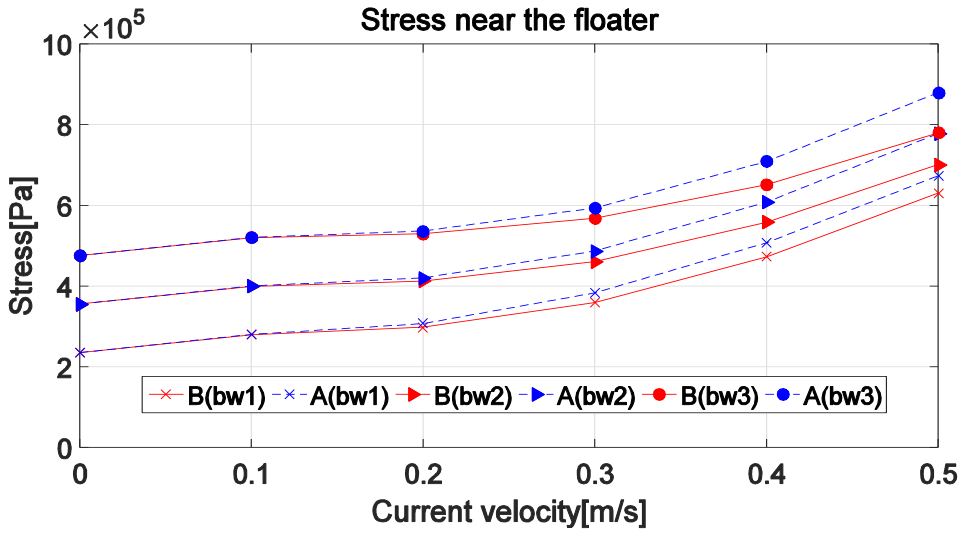

Figure 6-18 Stresses on the net element AE and BF near the floater with three bottom weights and current velocities (0-0.5m/s)

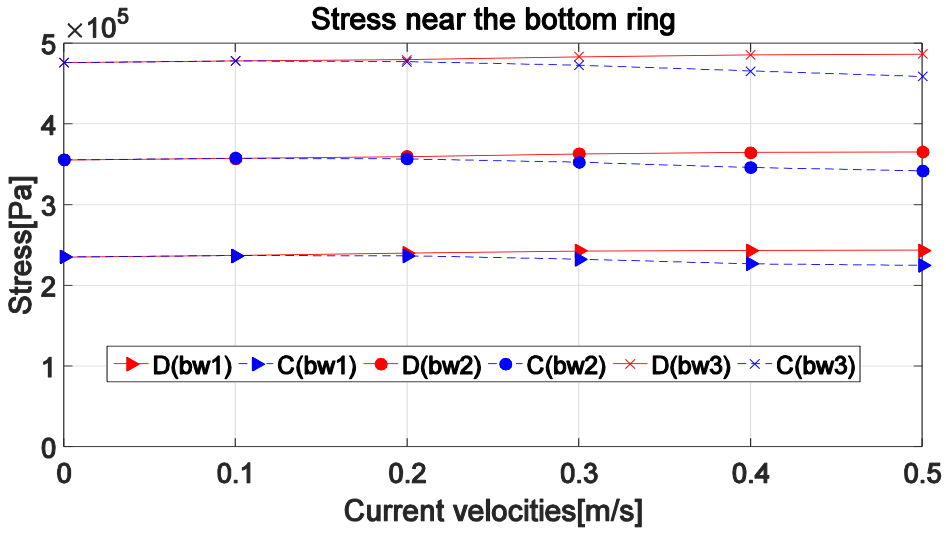

Figure 6-19 Stresses on the net element CM and DN near the bottom of the bottom ring with three bottom weights and current velocities (0-0.5m/s)

The stress at AE which is in the front net is larger than BF which lies in the rear net, and the difference goes larger as the current velocity increases. The stress at DN is a little larger than that at CM. That is due to the increasing lift force tends to incline the floater and bottom ring, the deformation will be enlarged when the current velocity increases, causing unequal stress on the net with the same height but different positions.

Compared between the figure 6-18 and 6-19, it is easy to find the stress on the net near the floater increase significantly with the increase of the current velocity while that near the bottom ring does not change much. The motion of the floater is confined horizontally due to the mooring lines, so larger stress is induced when current velocity is high. However, the bottom ring is free to move both horizontally and vertically, so the wave energy on the bottom ring is transferred to the kinetic energy of the bottom ring without causing much stress variation on the net close to it.

The stress near the floater increases with the current velocity, and is nearly proportional to the current velocity squared. The stress near the bottom rings does not seem to change much in the front.

Figure 6-20 illustrates the maximum mooring tension changes under three bottom weights and current (v=0-0.5m/s) conditions.

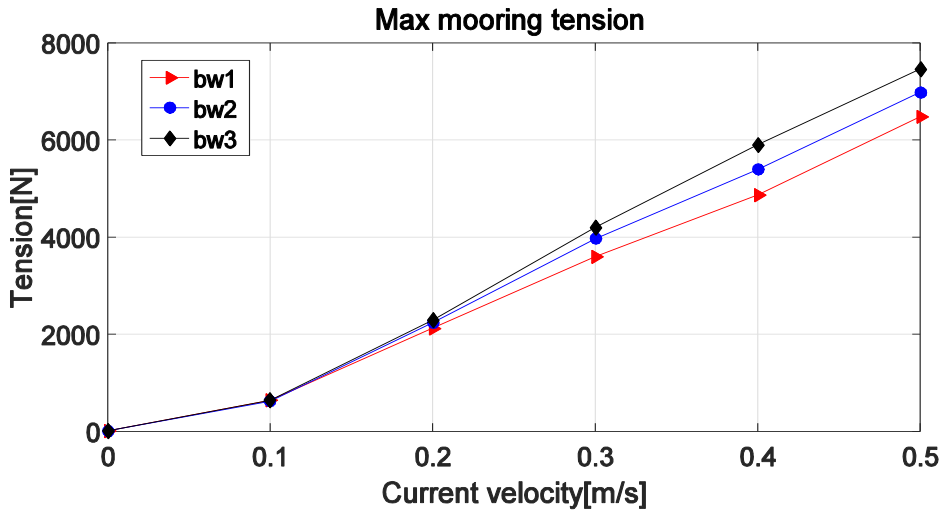

Figure 6-20 Maximum mooring tensions for fish cage with three bottom weights and current velocities (0-0.5m/s)

Figure 6-20 shows that the maximum mooring tension also increases with the current velocity and added weight of bottom ring. When the submerged weight of the bottom ring nearly doubles (from bw1 to bw3), the maximum mooring tension increases by 15% at the current velocity 0.5 m/s. The current velocity has a larger effect to maximum mooring tension than the added weight of the bottom ring. The mooring tension is approximately 0.7 times of the drag force, and it shares the similar trend as the drag force.

6.3.4 Sensitive study on wave-current conditions

When the fish cage is in the open sea, the wave and current usually happen together. Here the responses of the fish cage under waves (Table 6-7) and currents (v=0-0.5 m/s) were studied. The model was simulated in every condition for 500 seconds (overview of simulation in Appendix 1), when the models in all states have reached to balance. Response of deformation, hydrodynamic force, mooring tension and stresses in critical place were studied. Figure 6-19 shows the deformation in one period as a result of the numerical simulation when the fish cage is under wave (H=3m, T=8s) and current (v=0.3m/s).

Waves		
H=1m, T=4s	H=1m, T=8s	H=1m, T=12s
H=2m, T=4s	H=2m, T=8s	H=2m, T=12s
H=3m, T=4s	H=3m, T=8s	H=3m, T=12s

Table 6-7 Wave conditions with different heights and periods

A. Deformation

Figure 6-21 describes the deformation of the fish cage under wave (H=3m, T=8s) and current (v=0.3m/s) in one period when the fish cage has reached to balance.

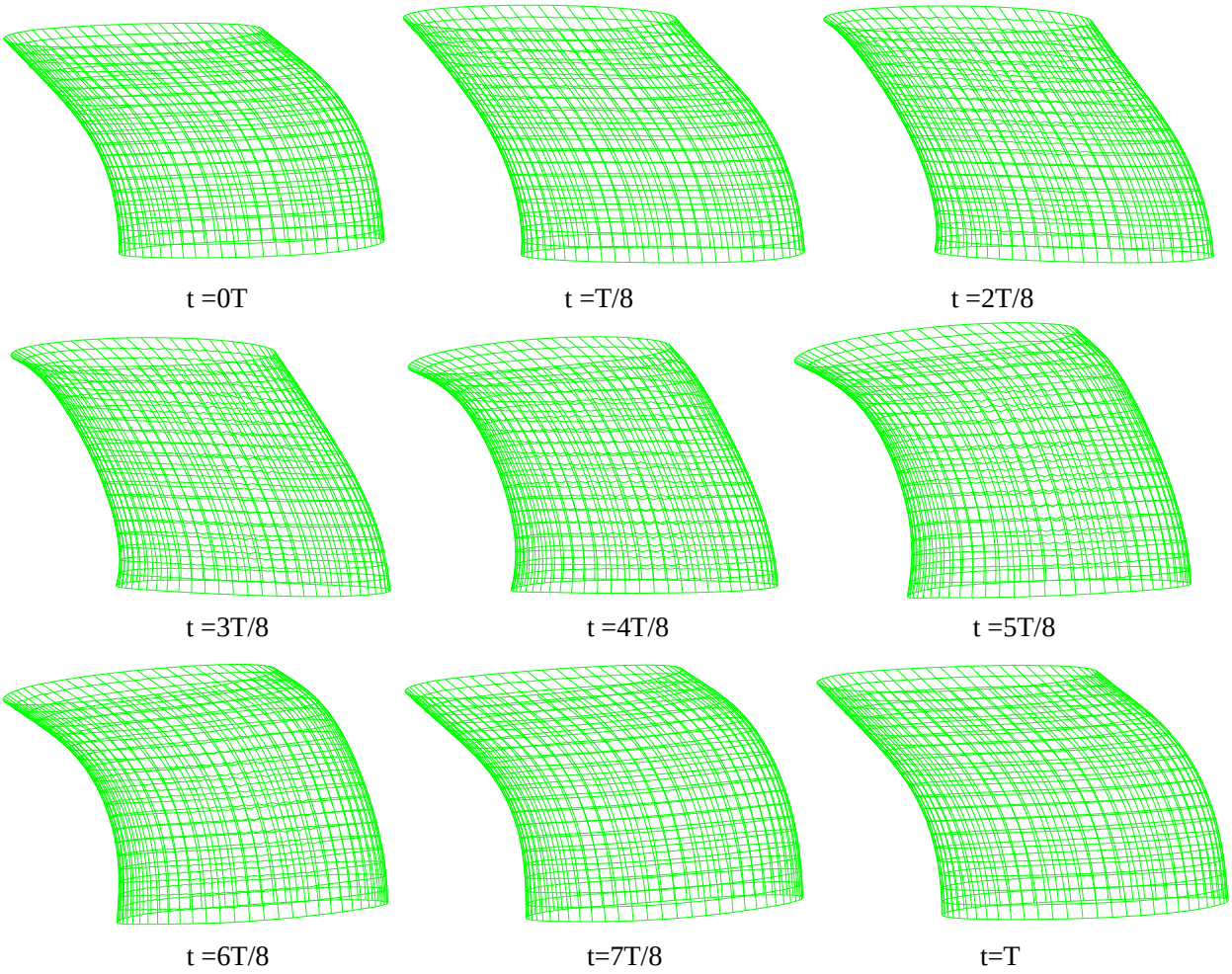

Figure 6-21 Deformation of fish cage under wave (H=3m, T=8s) and current (v=0.3m/s) in one wave period when the fish cage reached to balance

Figure 6-21 shows that the deformation of the floater is very obvious, but the bottom ring does not deform much. It seems the net deformation does not synchronize with the floater, but the inclination of the net is very obvious at every time point. The net inclination is mainly due to the current effect. The shape of the cage is changing all the time in a wave period, but the volume of the fish cage does not seem to change much.

B Mooring tensions

Mooring tension was estimated under wave and current. Figure 6-22 and 6-23 shows how the mooring tension reacts with different wave heights and periods after the model has reached to the balance state.

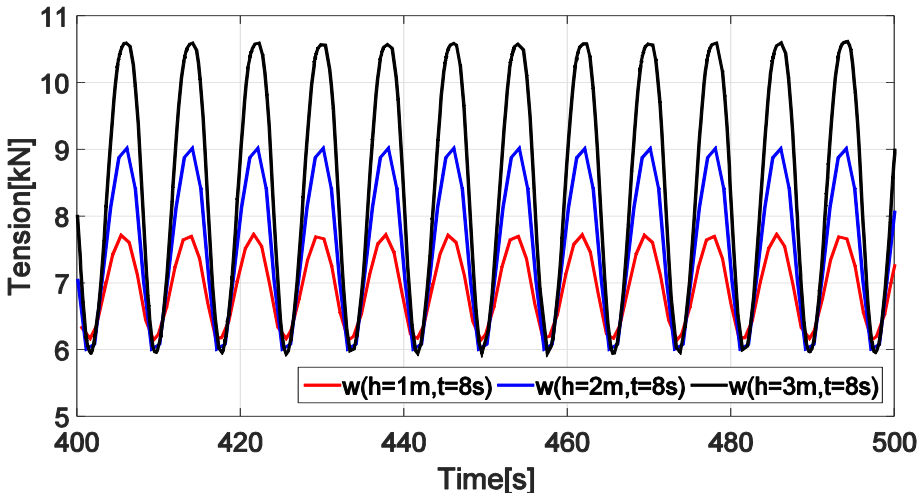

Figure 6-22 Mooring tension under wave (h=1m, 2m, 3m, t=8s) and current (v=0.4m/s)

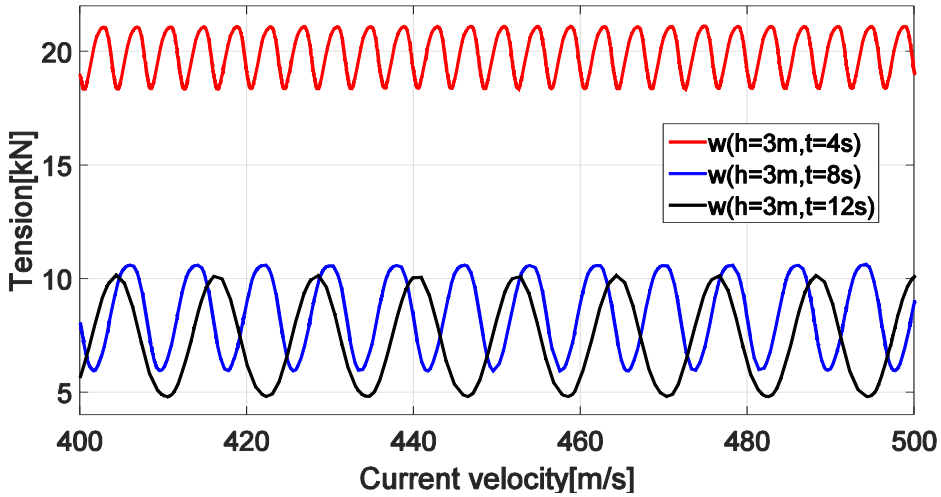

Figure 6-23 Mooring tension under wave (h=3m, t=4s, 8s, 12s) and current (v=0.4m/s)

Under the same period, the mooring line with the largest wave height has the maximum mooring tension and maximum tension variation. If we set the wave height as a constant, the mooring tension has its maximum value when the period is shortest, and maximum variation when the period is largest. The variation of the mooring tension between the maximum value and the minimum value does not change much when the wave period increases from 8s to 12s. The mooring line suffers the tension variation when there is wave, which would induce fatigue problem for the mooring line.

The maximum mooring tension is an important parameter when we study the failure of the mooring line. Figure 6-24 shows how the wave period has affected the maximum mooring tension when the wave height is set as a constant.

a)

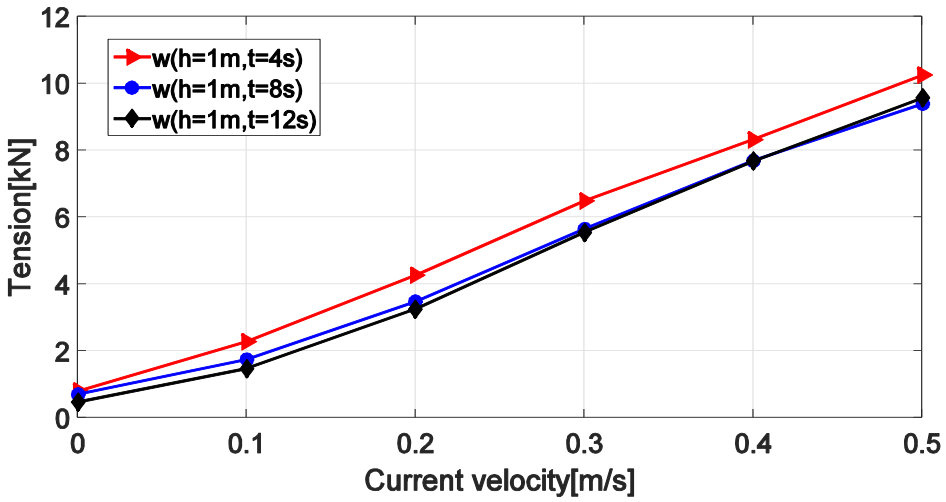

b)

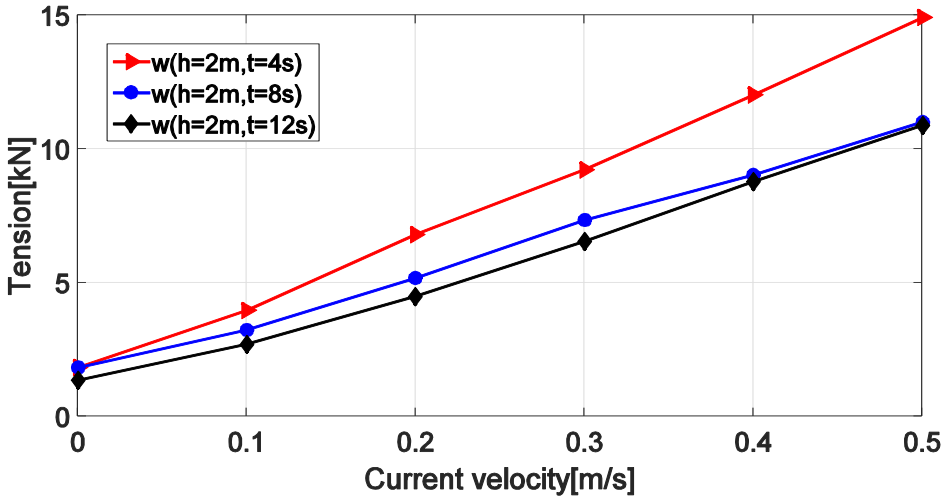

c)

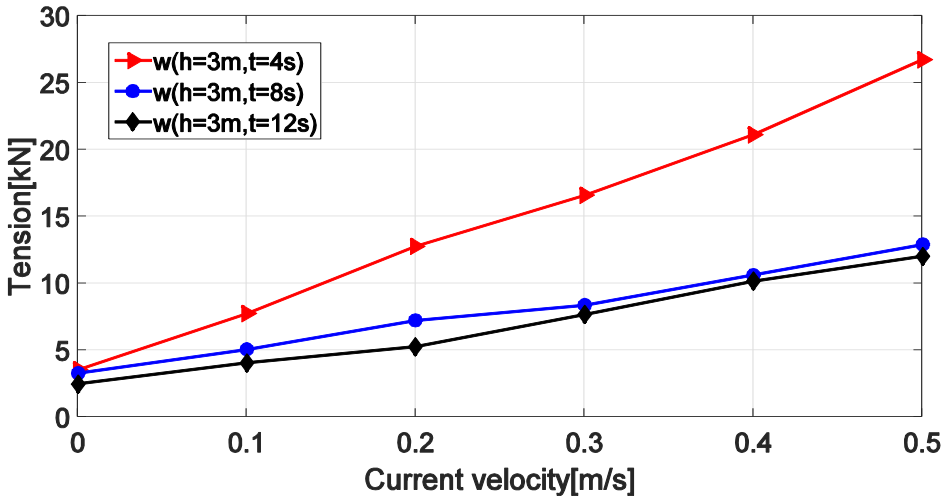

Figure 6-24 Maximum mooring tension under wave (different period) and current

From the figure 6-24, we can detect that irrespective of the wave height, the maximum mooring tensions are quite similar under longer wave (T=8s, 12s) and current condition.

However, with the shorter period (T=4s), the maximum mooring tension increases significantly, and reaches its highest ($2.67*10^4$ N) when the wave height is largest (H=3m). In this case, the shorter wave period could induce the largest maximum mooring tension, while the maximum mooring tension does not change much under wave with longer period and current condition.

Figure 6-25 shows the how maximum mooring tension varies under wave and current when the wave height increases and the wave period is a constant.

a)

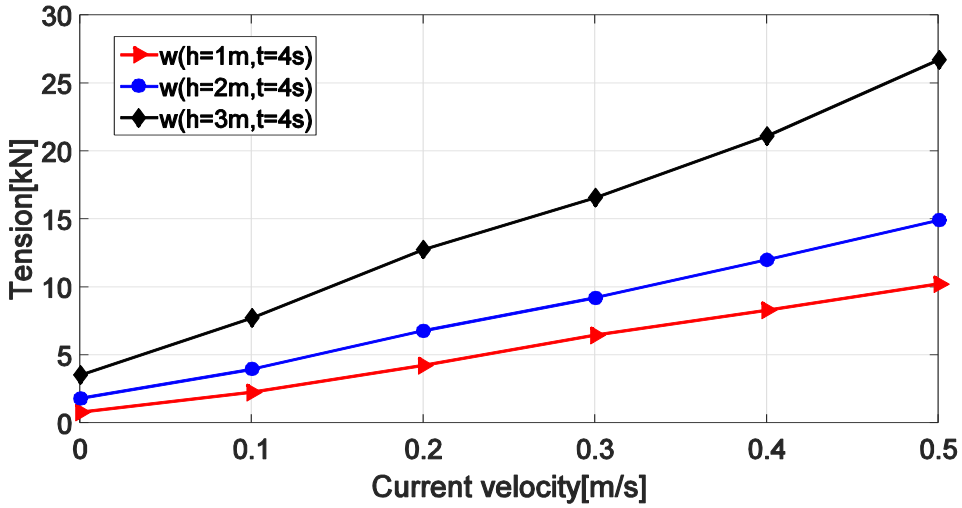

b)

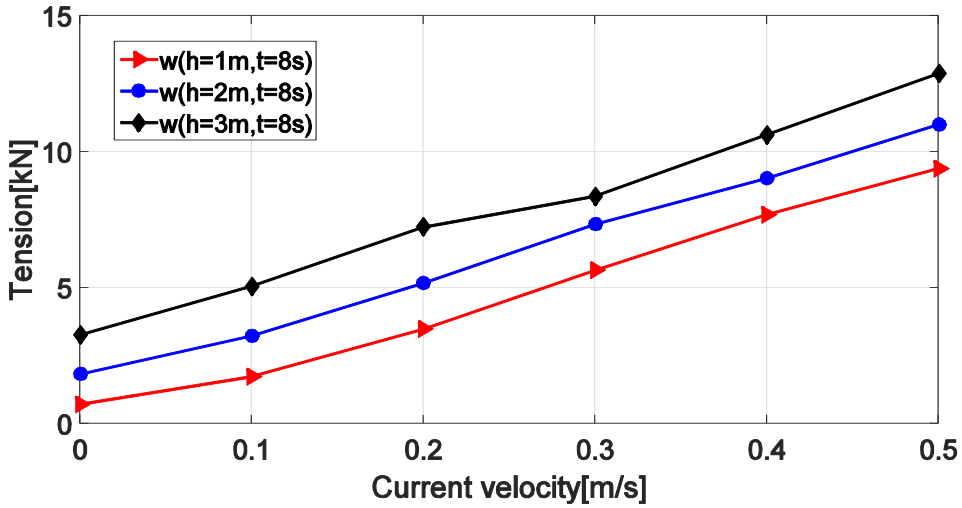

c)

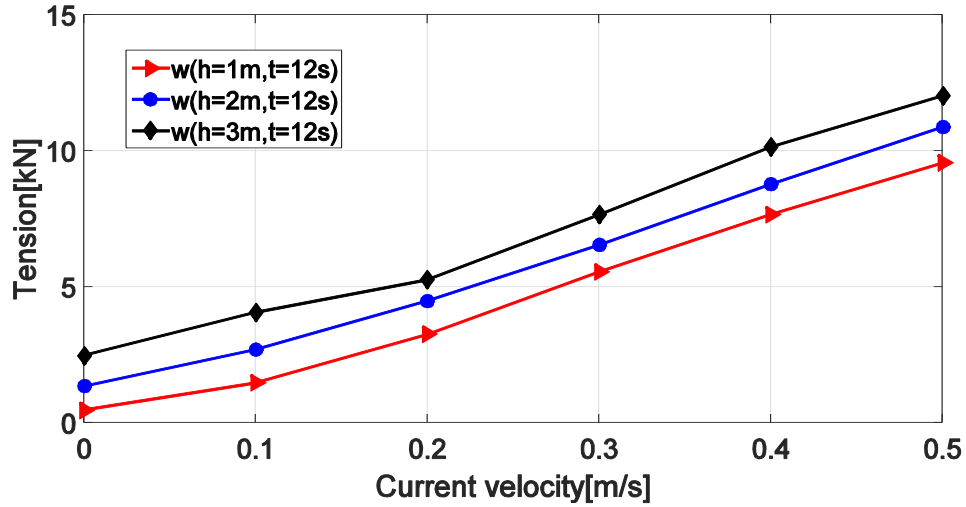

Figure 6-25 Maximum mooring tension under wave (different heights) and current

In figure 6-25, we can conclude that the higher the wave height is, the larger the maximum mooring tension is. Compared with figure 6-25, we could also find the wave height has larger impact to the maximum mooring line than wave period.

In all, the wave with higher wave height and shorter period will have maximum mooring tension. Here higher wave height and longer period can also be explained as higher wave steepness (H/L), as the wave length is proportional to the wave period T according to the airy wave theory. This phenomenon can be explained from Morison's equation (2-16). The shortest wave period has the fastest fluid particle speed, and the larger speed means the larger drag force which in turn will be transmitted to larger mooring tension.

C Maximum stress in critical place

Figure 6-26 and 6-27 shows the maximum stress in element AE and BF under wave (different wave height) and current. When current velocity is 0, there is wave only.

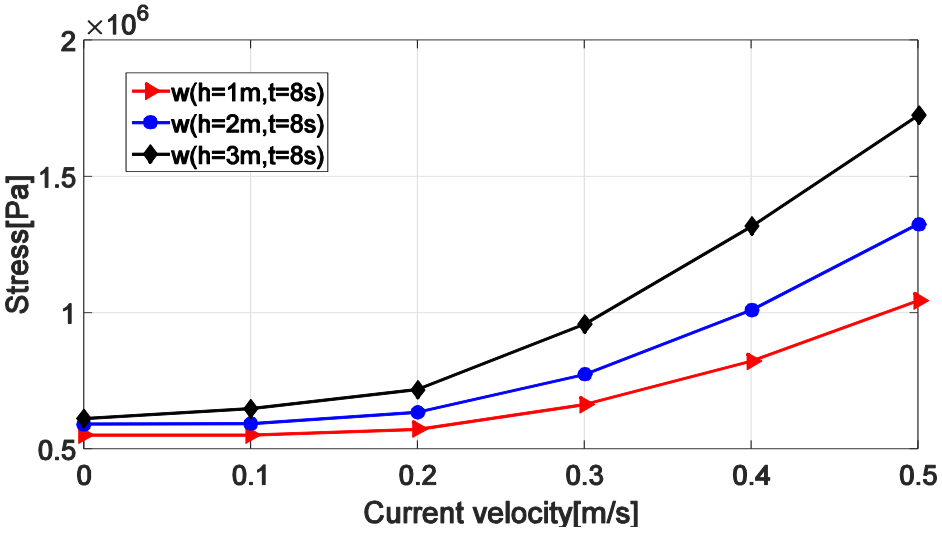

Figure 6-26 Maximum stresses in element AE under wave and current

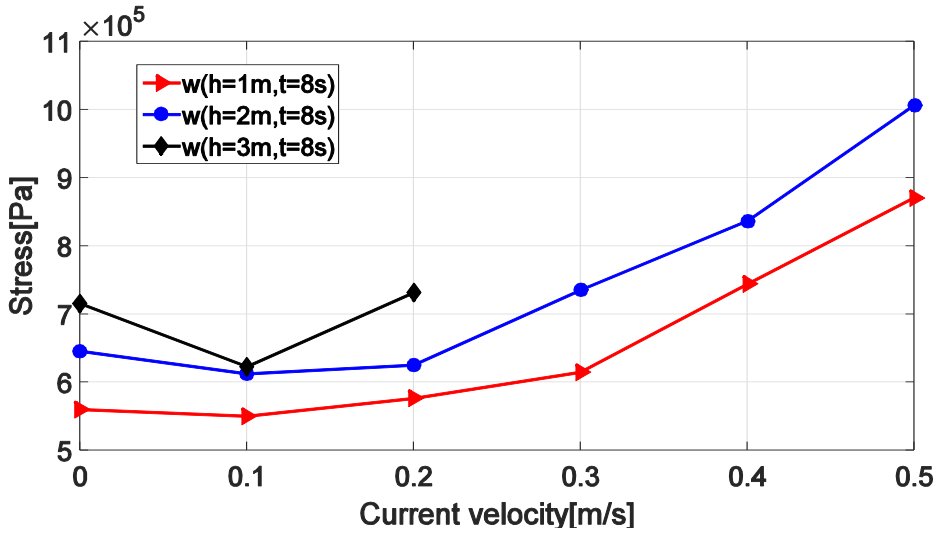

Figure 6-27 Maximum stresses in element BF under wave and current

Figure 6-26 shows steady increase of stress on element AE with current velocity and wave height. Stress is almost proportional to the current velocity squared. The stress increases by less than 59% when the wave height triples (from h=1m to 3m). In figure 6-27, the stress is larger in pure wave condition than in wave-current (v=0.1 m/s) condition, especially when the wave is large. It can be concluded that small current in wave-current (v=0.1 m/s) condition can help to reduce the stress in the rear part of the fish cage due to pure wave in large wave condition.

There is severe slack under wave (H=3m, T=8s) and current (v=0.3m/s), which can be seen in figure 6-28. The net is more likely to have slack problem near the floater than near the bottom ring in large wave and current condition as the movement on the floater is much larger than the bottom ring. Slack is more likely to happen when the movement of the floater is too large. Slack can induce very large stress suddenly causing severe consequence to the net such as fatigue or even broken, especially on the joints of the floater and the net, which needs to be avoided in designing the fish cage.

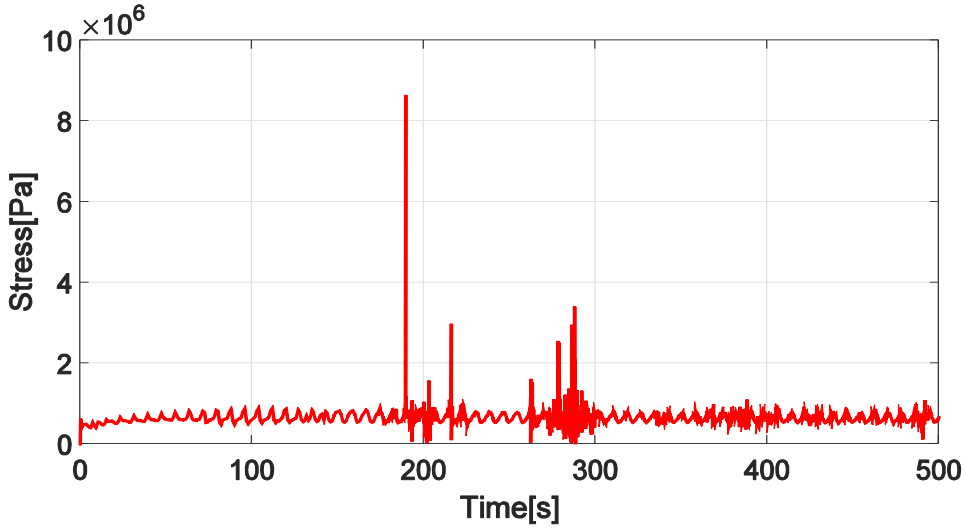

Figure 6-28 Stress in element BF under wave (H=3m, T=8s) and current (v=0.3m/s)

D Hydrodynamic force

As we know, the wave could increase the maximum hydrodynamic force for the net pen according to Morison's equation. Figure 6-29 shows the maximum drag and lift force of the net pen under wave-current condition compared with that in pure current condition. The trend of the maximum drag and lift under wave-current conditon seemed to be parallel with that under pure current. That could be explained as the wave exerted the same hydrodynamic force to the net pen irrespective of current velocity. The wave induced larger drag force than lift force.

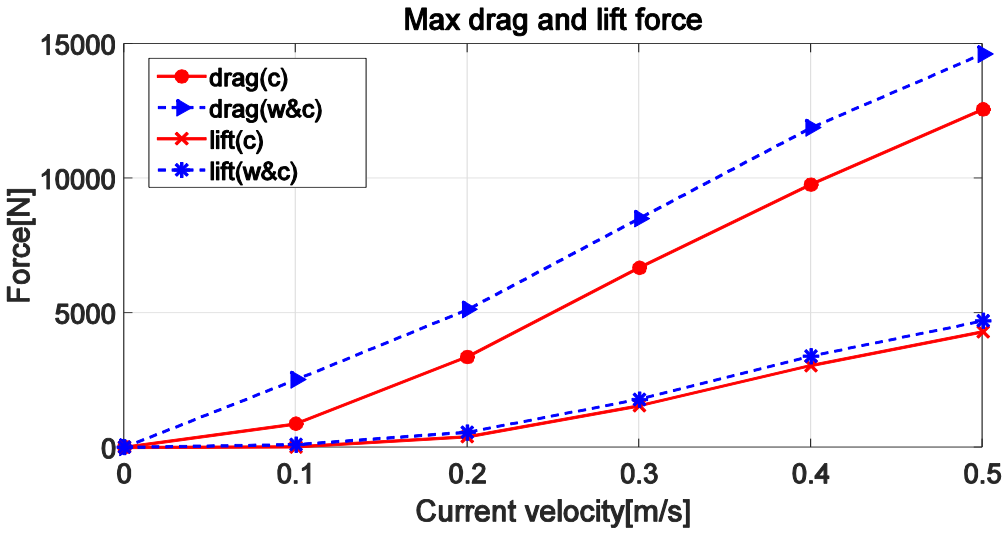

Figure 6-29 Maximum drag and lift forces of the fish cage under wave (H=1m,T=8s) and current

6.4 Summary

In this chapter, the truss model was applied in the full scale fish cage. Sensitivity study on the interaction of the floater and the net was study first. It was found that the interaction was critical when predicting the responses of the whole fish cage. Then the truss model was improved using a flexible floater. Sensitivity study on different bottom weights, solidity ratios and wave-current conditions were discussed. Response of deformation, volume, hydrodynamic force, maximum mooring tension and stresses were compared.

We can conclude that bio-fouling is a serious problem that can induce large hydrodynamic force and mooring tension, resulting in severe volume reduction. Added bottom weight can help to preserve the volume of the net. The wave can cause heavy load to the mooring tension, drag and stresses, yet has less influence to the net pen volume. The hierarchy of the parameters that affect the responses of the net pen is current velocity, wave height and wave period.

7. Conclusions and future work

7.1 Conclusions

This thesis has addressed the dynamic analysis of gravity based fish cage under various environment conditions. Firstly, this thesis illustrated the state-of-art technology development of fish cages and current research progress on the dynamic responses. Then the basis theories to analyze the dynamic responses of fish cage were presented. Before studying the complex responses of the fish cage, the methodology was verified with a simple beam. Response of the only floater under wave and current was studied, too. For the whole fish cage model, both truss and mass spring model were established to test the responses on a model scaled fish cage, and validated with the numerical and experimental results from previous study. Finally responses of the full scale fish cage were studied through truss model. Sensitivity study on the interaction of the floater and the net, solidity ratio, bottom weights, and wave-current condition were studied. The conclusions are as follows:

1. Morison's equation is the main method to calculate the hydrodynamic force on the fish cage. Drag and mass coefficient are very crucial to decide the hydrodynamic force.

2. The single floater will move and deform under wave and current, and this will affect the responses of the net. Inversely, the responses of the net will also influence the floater. The interaction effect needs to be taken into consideration when studying the responses of the fish cage.

3. Both truss model and mass spring model can well simulate the responses of a scaled fish cage under current. Numerical results are in accordance with the numerical and experimental results from previous study.

4. Sensitivity study about a full scale model on solidity ratio, bottom weight and wave-current effect shows that the hydrodynamic force and deformation influence each other, and there is deviation between the simulation force results and that calculated from Morison's equation. Increasing solidity ratio will enlarge the hydrodynamic force, and decrease the relative volume of net pen. Added bottom weight will increase both the hydrodynamic force and the relative volume of the net pen. The wave can cause heavy load to the mooring tension, drag and stresses, yet has less influence to the net pen volume.

5. Compared the responses of the fish cage induced by current velocity, wave height and wave period seperately, the current velocity has the largest effect, then wave height. The wave period has least influence.

7.2 Error Sources

Due to inexperience and limited knowledge, there are some possible errors in the thesis.

1. When extracting the stress data from the truss model, the nodal stress value calculated from two adjacent elements were compared, there was deviation between two stress values at the same point. This indicates that the model mesh needs to be refined until the nodal stress values calculated from different element are close enough.

2. During simulation, we take hydrodynamic coefficients as fixed values, but in reality it changes with different solidity ratio Sn, Reynolds number Re, and attack angle Θ, so the hydrodynamic force results may include some uncertainties.

3. Truss model and mass spring model only compare in pure current condition with attack angle 90 degree, yet we do not know how these two models behave in other environmental conditions such as different attack angles, or wave conditions. More comparisons in various conditions are required.

4. Current velocity will be reduced after it passed the front net in the cage. However, this velocity reduction factor is not considered in the thesis model, so the responses may have some deviations with its true response.

5. Time domain curves showed in thesis may not quite smooth, and this may affect the maximum value. It is because the maximum increment size is set as 0.1, if the maximum increment size is to be set as 0.01 or smaller, the results will be much better, although the calculation will be much slower.

7.3 Suggestions for future work

This thesis has provided the preliminary study of the responses of fish cage under wave and current. In the future, the following work is recommended:

1) The floater model needs to be updated in ABAQUS program to improve the buoyancy calculation when the structure is partly submerged. In ABAQUS the floater is not stable in static analysis as it should be when half submerged. Apart from the buoyancy distribution method, the user defined function may be a good solution for this problem.

2) The drag coefficient C_D and mass coefficient C_M changes with different solidity ratio Sn, Reynolds number Re, and attack angle Θ. The hydrodynamic coefficients should be changing according to various conditions. To correctly define the hydrodynamic coefficient in ABAQUS is very crucial for the simulation.

3) More sensitivity study on wave condition, various attack angles or other conditions should be involved to decide which model between truss and mass spring is better for fish cage simulation.

4) In the mass spring model, the knots are modeled as cylinders. Large error will come up when the flow angle is changed, and it will be more accurate if the knot cylinder is modeled as spherical, although in this thesis it matters not as we only simulate under the current with 90 °attack angle.

5) In this thesis, we have discussed the responses of fish cage in regular wave and current. However, regular wave rarely exists in reality; so study of responses in irregular wave is more significant for designing the structure in open ocean area. Response of fish cage in irregular wave and how the mooring lines behave with the responses will be studied in the future.

6) A fish farm normally contains several fish cages with certain distances, and the responses of one cage will affect the responses of others. Or when a boat passes by a fish cage, responses of the fish cage will be affected. How large this will affect the responses of the fish cage and the layout of the fish farm need to be investigated.

7) In the fish cage model, we have considered the horizontal mooring lines, but in fact, the mooring lines of the fish cages are consisted of horizontal mooring lines and vertical mooring lines (as in figure 1-2). The reaction of the vertical mooring lines will be included in the future. In the model that had been built, we take the horizontal mooring as a nonlinear spring to simplify the problem, but it cannot fully represent the dynamic behavior of the mooring line. The model of the mooring lines needs to be updated.

8) Wake flow means flow velocity reduction will happen when the flow passes a piece of net, the drag force will be reduced, and deformation of the rear net will be less severe. How large this phenomenon has affected the deformation of the fish cage and how this effect will help decide the array of the fish farms will need to be studied further.

References

Kassah, J. E. (2012). Development of biofouling on salmon cage nets and the effects of anti-fouling treatments on the survival of the hydroid. MS thesis. Institutt for biologi,

Lader, P. F., & Enerhaug, B. (2005). Experimental investigation of forces and geometry of a net cage in uniform flow. IEEE Journal of Oceanic Engineering, 30(1), 79-84.

Li, L., Fu, S., Xu, Y., Wang, J., & Yang, J. (2013). Dynamic responses of floating fish cage in waves and current. Ocean engineering, 72, 297-303.

Al-Hammoud,A.(2016)https://www.quora.com/What-is-the-main-and-most-important-difference-between-a-beam-and-a-truss

BadinottiGroup(2011). Gravity based fish cage. http://www.badinotti.com/pord_sub_cage.html

Berstad, A. J., Tronstad, H., Sivertsen, S.-A., & Leite, E. (2005). Enhancement of design criteria for fish farm facilities including operations. 825-832.

Cook, R., Malkus, D., Plesha, M., & Witt, R. (2002). Concepts and applications of finite element analysis. 407-416.

DeCew, J., Tsukrov, I., Risso, A., Swift, M., & Celikkol, B. (2010). Modeling of dynamic behavior of a single-point moored submersible fish cage under currents. Aquacultural Engineering, 43(2), 38-45.

DNV. (2008). Environmental conditions and environmental loads (RP-C205). 56-57.

Ellmer, W (2011). ocean station cage. https://discuss.seasteading.org/t/offshore-aquaculture-realistic-projects-big-business-seafood-ocean-colonization-ocean-ranching-oceanic-investment-world-food-security-oceanic-business-alliance/1631/16

Eurofish. (2014). Overview of the Norwegian fisheries and aquaculture sector. 8-9

Fei, L. (2014). Research and Analysis on Design and Simulation of Navigable and elevating hydraulic cage System. Master thesis, Zhejiang Marine College, China.

Fisheries, F. A. O. (2016). The state of world fisheries and aquaculture 2016. 12-14

Fredriksson, D. W., DeCew, J. C., & Irish, J. D. (2006). A field study to understand the currents and loads of a near shore finfish farm. 1-9.

Gudmestad, O. T. (Ed.). (2015). Marine Technology and Operations theory &practice: WITpress.

Huang, C.C., Tang, H.J., & Liu, J.Y. (2008). Effects of waves and currents on gravity-type cages in the open sea. Aquacultural Engineering, 38(2), 105-116.

Kristiansen, T., & Faltinsen, O. M. (2012). Modelling of current loads on aquaculture net cages. Journal of Fluids and Structures, 34, 218-235.

Løland, G. (1991). Current forces on and flow through fish farms: Institutt for Marin Hydrodynamikk.

Lader, F., & Enerhaug, B. (2005). Experimental investigation of forces and geometry of a net cage in uniform flow. IEEE Journal of Oceanic Engineering, 30(1), 79-84.

Lader, F., & Fredheim, A. (2006). Dynamic properties of a flexible net sheet in waves and current—A numerical approach. Aquacultural Engineering, 35(3), 228-238.

Lader, F., Jensen, A., Sveen, J. K., Fredheim, A., Enerhaug, B., & Fredriksson, D. (2007). Experimental investigation of wave forces on net structures. Applied Ocean Research, 29(3), 112-127.

Lee, C.-W., Kim, Y.-B., Lee, G.-H., Choe, M.-Y., Lee, M.-K., & Koo, K.-Y. (2008). Dynamic simulation of a fish cage system subjected to currents and waves. Ocean engineering, 35(14), 1521-1532.

Li, L. (2013). Dynamic response of deep water floating cage structure under wave and current. Graduation thesis,Shanghai Jiao Tong University, China(Graduation thesis).

MathWorks.(2009) https://se.mathworks.com/products/matlab.html

Milne, P. H. (1972). Fish and shellfish farming in coastal waters.

Moe, H., Fredheim, A., & Hopperstad, O. (2010). Structural analysis of aquaculture net cages in current. Journal of Fluids and Structures, 26(3), 503-516.

Msangi, S., Kobayashi, M., Batka, M., Vannuccini, S., Dey, M., & Anderson, J. (2013). Fish to 2030: prospects for fisheries and aquaculture. World Bank Report(83177-GLB).

Refamed. (2010a). tension leg cage. http://www.refamed.com/gabbie_mare/tlc_system.html

Refamed. (2010b). TLC Brochure. http://www.refamed.com/archivio/TLC%20brochure.pdf

SIMULIA. (2016). Get started with Abaqus/CAE.

Staniford, D. (2002). Sea cage fish farming: an evaluation of environmental and public health aspects (the five fundamental flaws of sea cage fish farming). European Parliament's Committee on Fisheries public hearing on 'Aquaculture in the European Union: Present Situation and Future Prospects', 1st October.

Version, A. (2013). 6.13. Analysis User's Guide, Dassault Systems.

Ye, X., Chen, X., Chen, S., & Wang, T. (2014). Research on the visual dynamic simulation technology of fishing net. Paper presented at the Mechatronics and Automation (ICMA), 2014

IEEE International Conference.

Zhao, Y.-P., Li, Y.-C., Dong, G.-H., Gui, F.-K., & Teng, B. (2007). A numerical study on dynamic properties of the gravity cage in combined wave-current flow. Ocean engineering, 34(17), 2350-2363.

Tsukrov, I., Eroshkin, O., Paul, W., & Celikkol, B. (2005). Numerical modeling of nonlinear elastic components of mooring systems. IEEE Journal of Oceanic Engineering, 30(1), 37-46.

Appendices

Appendix 1: Overview of the simulation

All the simulations are done in a 8-cores work station with 32GB memories. The details of the simulations are listed as below.

Items	Models	Responses	Environment conditions	Boundary conditions	Incremental size	Time	Approximate time needed
Response of the single floater	Single floater	Deformation/displacement	Wave(H=5m,T=8s) and current(v=1m/s)	Mooring fixed	Initial=0.0001,min=10^{-6},max=0.01	24s	20 mins
Convergence study on model scaled fish cage	Fish cage (truss)	Deformation/drag/lift/volume reduction	Current (v= 0.21,0.34,0.5 m/s)	Floater fixed	Initial=0.0001,min=10^{-6},max=0.01	10s	10-40 mins
Sensitivity study on model scaled fish cage	Fish cage (mass spring)	Deformation/drag/lift/volume reduction	Current (v= 0.12,0.21,0.34,0.52 m/s)	Floater fixed	Initial=0.0001,min=10^{-6},max=0.01	10s	8-16 hours
Sensitivity study on full scale cage (interaction of the net and floater)	Single floater	Displacement/Stress	Wave(H=5m,T=8s)	Mooring fixed	Initial=0.0001,min=10^{-6},max=0.1	120s	3 hours
	Fish cage (truss)			Mooring fixed		120s	24 hours
	Fish cage (truss)			Floater fixed		120s	10-40 mins
Sensitivity study on full scale cage (solidity ratio)	Fish cage (improved truss)	Deformation/drag/lift/volume reduction/critical stress /mooring load	Current (v= 0-0.5 m/s)	Mooring fixed		500s	10-40 mins
Sensitivity study on full scale cage (bottom weights)	Fish cage (improved truss)	Deformation/drag/lift/volume reduction//critical stress /mooring load				500s	10-40 mins
Sensitivity study on full scale cage (wave-current condition)	Fish cage (improved truss)	Deformation/drag/lift/stress in critical/maximum mooring load	Wave(H=1m,2m,3m,T=4s,8s,12s) and current(v=0-0.5m/s)	Mooring fixed		500s	2-6 hours

Appendix 2: MATLAB transcripts

a) Current force

This transcript uses MATLAB CALFEM module to calculate the current force on the beam.

```
clear all
close all
clc
Edof=[1 1 2 3 4 5 6;2 4 5 6 7 8 9] %define the dof of beams
Ex1=[0 0]
Ey1=[0 5]
Ex2=[0 0]
Ey2=[5 10]
E=2.1e11%Elastic modulus, steel
A=3.14e-4%cross section area of beam
I=7.85e-9%inertia of beam
ep=[E A I]
eq=[0,-10.25]%uniform current force
[Ke1,fe1]=beam2e(Ex1,Ey1,ep,eq)%% calculate stiffness and force of beam element1
[Ke2,fe2]=beam2e(Ex2,Ey2,ep,eq)%% calculate stiffness and force of beam element2
K=zeros(9)%% define the stiffness matrix
f=zeros(9,1)%% define the matrix of force
[K,f]=assem(Edof(1,:),K,Ke1,f,fe1)%% add the stiffness contr. from element 1
[K,f]=assem(Edof(2,:),K,Ke2,f,fe2)%% add the stiffness contr. from element 2
BC=[1 0;2 0;3 0;7 0;8 0;9 0]%Boundary conditions
[a,r]=solveq(K,f,BC)%calculate the displacement
r=K*a-f%get the reaction force
Ed=extract(Edof,a)%add displacement
es1=beam2s(Ex1,Ey1,ep,Ed(1,:),eq,11)%add displacement contr.
es2=beam2s(Ex2,Ey2,ep,Ed(2,:),eq,11)%add displacement contr.
figure(1)
ploTar1=[2 4 1];ploTar2=[1 2 1]
eldraw2(Ex1,Ey1,ploTar1)%draw the original element 1
eldraw2(Ex2,Ey2,ploTar1)%draw the original element 2
sfac=scalfact2(Ex2,Ey2,Ed(2,:),0.2)%define the vector of displacement
eldisp2(Ex1,Ey1,Ed(1,:),ploTar2,sfac)%draw the deformed element 1
eldisp2(Ex2,Ey2,Ed(2,:),ploTar2,sfac)%draw the deformed element 2
```

```
figure(2)
ploTar2=[2 4]
sfac=scalfact2(Ex2,Ey2,es2(:,2),0.2)
eldia2(Ex1,Ey1,es1(:,2),ploTar2,sfac)%draw the shear force of element 1
eldia2(Ex2,Ey2,es2(:,2),ploTar2,sfac)%draw the shear force of element 2
figure(3)
sfac=scalfact2(Ex2,Ey2,es2(:,2),0.2)
eldia2(Ex1,Ey1,es1(:,3),ploTar2,sfac)%draw the moment of element 1
eldia2(Ex2,Ey2,es2(:,3),ploTar2,sfac)%draw the moment of element 2
```

b) wave force (linear stretching 1)

This transcript is used to calculate the wave force using the linear stretching 1 method (as in figure 3-1).

```
D=0.1;p=1025;CM=2;g=9.8;k=0.5236;w=2.2652;d=10;H=1.5;
CD=1;
syms z t;
f1=(pi*(D^2)/4)*p*CM*(H/2)*g*k*exp(k*z)*cos(w*t); %inertia force
f2=p*CD*D*((H/2)*g*k/w)^2*exp(2*k*z)*sin(w*t)*abs(sin(w*t))/2; %drag force
f3=(pi*(D^2)/4)*p*CM*(H/2)*g*k*cos(w*t);
f4=p*CD*D*((H/2)*g*k/w)^2*sin(w*t)*abs(sin(w*t))/2;
   t=0:0.1:6;
   if (sin(w*t) < 0) %linear stretching
     f=int(f1+f2,z,'0.75*sin(2.2652*t)',-10);
   else
      f=int(f1+f2,z,0,-10)+int(f3+f4,z,'0.75*sin(2.2652*t)',0);
   end;
 F=subs(f);
f5=f1+f2;
t=0:0.1:6;
f6=int(f5,z,'H*sin(w*t)/2',-10);
F1=subs(f6);
plot(t,F,t,F1,'--k','linewidth',2)
xlabel('Time/s');
ylabel('Force/N');
title('Wave force when H=1.5m')
```

c) wave force (linear stretching 2)

This transcript is used to calculate the wave force using the linear stretching 2 method (as in figure 3-1).

```
D=0.3;p=1025;CM=2;g=9.8;k=0.063;w=0.785;d=60;H=*;
CD=1;
syms z t;
f1=(pi*(D^2)/4)*p*CM*(H/2)*g*k*(exp(k*z))*cos(w*t); %inertia force
f2=p*CD*D*((H/2)*g*k/w)^2*(exp(2*k*z))*sin(w*t)*abs(sin(w*t))/2; %drag force
f=f1+f2; %wave force
t=0:0.1:20;
f3=int(f,z,0.5,-60);
F=subs(f3);
subplot(211)
plot(t,F)
xlabel('Time/s'),
ylabel('Force/N'),
title('Wave force when H=*m')
maximum(F)
```

d) Polyarea

The relative volume is the sum of the horizontal cross-section multiplied by the average thickness of the section layer. This transcript is used to calculate the area of the section layer.

```
clear;clc;
a=xlsread('test1.xlsx','10m'); % coordinates of all the points in the deformation fish cage
for i=1:1:64
X(i)=a(i,9);
Y(i)=a(i,10);
Z(i)=a(i,11);
H(1)=sum(Z)/64;
B(1)=polyarea(X,Y) % polyarea of the floater
end
for k=0:1:19
```

```
for i=1:1:128
X(i)=a(i+128*k+64,9);
Y(i)=a(i+128*k+64,10);
Z(i)=a(i+128*k+64,11);
end
X(129)=a(1+128*k+64,9);
Y(129)=a(1+128*k+64,10);
H(k+2)=sum(Z)/128; % average height of every net layer
B(k+2)=polyarea(X,Y) % polyarea of the every net layer
end
```

Appendix 3: ABAQUS transcripts

a) Scaled truss model

This transcript is used to build the scaled truss fish cage model.

*Heading

** Job name: scaled truss model Model name: Model-1

** Generated by: ABAQUS/CAE 6.11-1

*Preprint, echo=NO, model=NO, history=NO, contact=NO

**

** PARTS

**

*Part, name=Part-1

*Node% define the coordinate of the nodes

1, 0.7040, 0.0000, 0.0000

2, 0.7005, 0.0701, 0.0000

3, 0.6900, 0.1395, 0.0000

…….

3907, 0.6727, -0.2075, -1.5534

*Element, type=B31

1, 1, 2% define the element of thefloater

2, 2, 3

3, 3, 4

……

63, 63, 1

5136, 3860, 3876% define the element of the bottom ring

5137, 3861, 3877

5138, 3862, 3878

5139, 3863, 3879

5140, 3864, 3880

……..

5166, 3890, 3906

5167, 3891, 3907

*Element, type=T3D3% define the element of the 3-D truss

64, 64, 65, 66

65, 66, 67, 68

66, 68, 69, 70

67, 70, 71, 72

…….

2599, 2578, 3859, 3875

*Nset, nset=floatingcollar, internal, generate

 1, 63, 1

*Elset, elset=floatingcollar, internal, generate

 1, 63, 1

 *Nset, nset=truss, internal, generate

 64, 3843,1

*Elset, elset=truss, internal, generate

 64, 2599,1

*Nset, nset=bottomweight, internal

3860, 3861, 3862, 3863, 3864, 3865, 3866, 3867, 3868, 3869, 3870, 3871, 3872, 3873, 3874, 3875,

3876, 3877, 3878, 3879, 3880, 3881, 3882, 3883, 3884, 3885, 3886, 3887, 3888, 3889, 3890, 3891,

3892, 3893, 3894, 3895, 3896, 3897, 3898, 3899, 3900, 3901, 3902, 3903, 3904, 3905, 3906, 3907,

*Elset, elset=bottomweight, internal

5136, 5137, 5138, 5139, 5140, 5141, 5142, 5143, 5144, 5145, 5146, 5147, 5148, 5149, 5150, 5151,

5152, 5153, 5154, 5155, 5156, 5157, 5158, 5159, 5160, 5161, 5162, 5163, 5164, 5165, 5166, 5167,

** Section: Section-1 Profile: Profile-2

*Solid Section, elset=truss, material=truss

0.00001256

** Section: Section-3 Profile: Profile-2

*Beam Section, elset=bottomweight, material=bottomweight, temperature=GRADIENTS, section=CIRC

0.0252

0,1,0

** Section: Section-1 Profile: Profile-1

*Beam Section, elset=floatingcollar, material=floatingcollar, temperature=GRADIENTS, section=CIRC

0.02

0.,0.,-1.

*End Part

**

** ASSEMBLY

**

*Assembly, name=Assembly

```
**
*Instance, name=Part-1-1, part=Part-1
                0.,                 0.,                 2.
*End Instance
**
*Nset, nset=floatingcollar, instance=Part-1-1, generate
     1,    63,    1
*Elset, elset=floatingcollar, instance=Part-1-1, generate
     1,    63,    1
*Elset, elset=truss, instance=Part-1-1, generate
  64,    2599,    1
*Nset, nset=bottomweight, instance=Part-1-1
3860, 3861, 3862, 3863, 3864, 3865, 3866, 3867, 3868, 3869, 3870, 3871, 3872, 3873, 3874, 3875,
3876, 3877, 3878, 3879, 3880, 3881, 3882, 3883, 3884, 3885, 3886, 3887, 3888, 3889, 3890, 3891,
3892, 3893, 3894, 3895, 3896, 3897, 3898, 3899, 3900, 3901, 3902, 3903, 3904, 3905, 3906, 3907,
*Elset, elset=bottomweight, instance=Part-1-1
5136, 5137, 5138, 5139, 5140, 5141, 5142, 5143, 5144, 5145, 5146, 5147, 5148, 5149, 5150, 5151,
5152, 5153, 5154, 5155, 5156, 5157, 5158, 5159, 5160, 5161, 5162, 5163, 5164, 5165, 5166, 5167,
*End Assembly
**
** MATERIALS
**
*Material, name=floatingcollar
*Density
953.,
*Elastic
  9.5e+8, 0.3
*Material, name=truss
*Density
1125.,
*Elastic
  8.2e+07, 0.3
*Material, name=bottomweight
*Density
4000.,
*Elastic
```

9.5e+8, 0.3

*AQUA

-1,2,9.8,1025

0.13,0,0,2

** --

**

** STEP: Step-1

**

*Step, name=Step-1, nlgeom=YES, inc=100000000

*Dynamic

0.0001,10.,1e-6,0.1

**

** BOUNDARY CONDITIONS

**

** Name: BC-1 Type: Symmetry/Antisymmetry/Encastre

*Boundary

floatingcollar, PINNED

**

** LOADS

**

** Name: Load-1 Type: Gravity

*Dload

bottomweight, GRAV, 9.8, 0., 0., -1.

bottomweight, PB, 1, 0.0504

bottomweight, FDD, 1, 0.0504, 2.3

** Name: Load-2 Type: Gravity

*Dload

truss, GRAV, 9.8, 0., 0., -1.

truss, PB, 1, 0.004

truss, FDD, 1, 0.004, 2.3

**

** OUTUT REQUESTS

**

*Restart, write, frequency=0

**

** FIELD OUTUT: F-OuTut-1

**

*Output, field

*Node Output

RF, U

**

*End Step

b) Scaled mass spring model

This transcript is used to build the scaled mass spring fish cage model.

**Heading

** Job name: 0311 Model name: Model-2

** Generated by: ABAQUS/CAE 6.10-1

*Preprint, echo=NO, model=NO, history=NO, contact=NO

**

** PARTS

**

*Part, name=Part-1

*Node

1, 0.7070, 0.0000, 1.9736

2, 0.7070, 0.0000, 1.9648

……

60, 0.7070, 0.0000, 0.6184%define the knot cylinder nodes

*Element, type=B31

1, 1, 2

2, 2, 3

……

40, 59, 60%define the knot cylinder elements

*Nset, nset=_PickedSet20, internal, generate

1, 60, 1

*Elset, elset=_PickedSet20, internal

1, 2, 3, 4, 5, 6, 7, 8, 9, 10, 11, 12, 13, 14, 15, 16,

17, 18, 19, 20, 21, 22, 23, 24, 25, 26, 27, 28, 29, 30, 31, 32,

33, 34, 35, 36, 37, 38, 39, 40

** Section: Section-1 Profile: Profile-1

*Beam Section, elset=_PickedSet20, material=truss, temperature=GRADIENTS, section=CIRC

0.004

0,1,0

*End Part

**

*Part, name=Part-2

*Node

1, 0.7066, 0.0265, 1.9296

2, 0.7061, 0.0352, 1.9296

……

189, 0.7066, -0.0265, 1.9296%define the twine cylinder nodes

*Element, type=B31

1, 1, 2

2, 2, 3

……

126, 188, 189%define the twine cylinder elements

*Nset, nset=_PickedSet24, internal, generate

1, 189, 1

*Elset, elset=_PickedSet24, internal, generate

1, 126, 1

*Nset, nset=_PickedSet25, internal, generate

1, 189, 1

*Elset, elset=_PickedSet25, internal, generate

1, 126, 1

** Section: Section-1 Profile: Profile-1

*Beam Section, elset=_PickedSet24, material=truss, temperature=GRADIENTS, section=CIRC

0.004

0, 0, -1

*End Part

**

*Part, name=Part-3

*Node

1, 0.7070, 0.0000, 2.0000

2, 0.7035, 0.0704, 2.0000

……

63, 0.7035, -0.0704, 2.0000

*Element, type=B31

1, 1, 2

2, 2, 3

……

63, 63, 1

*Nset, nset=_PickedSet3, internal, generate

1, 63, 1

*Elset, elset=_PickedSet3, internal, generate

1, 63, 1

** Section: Section-3 Profile: Profile-3

*Beam Section, elset=_PickedSet3, material=floatingcollar, temperature=GRADIENTS, section=CIRC

0.005,

0.,0.,-1.

*End Part

**

*Part, name=Part-4

*Node

1, 0.7070, 0.0000, 0.4966

2, 0.6515, 0.2746, 0.4966

……

48, 0.6756, -0.2084, 0.4466

*Element, type=B31

1, 1, 17

2, 2, 18

……

32, 32, 48

*Nset, nset=_PickedSet4, internal, generate

1, 48, 1

*Elset, elset=_PickedSet4, internal, generate

1, 32, 1

*Nset, nset=_PickedSet5, internal, generate

1, 48, 1

*Elset, elset=_PickedSet5, internal, generate

1, 32, 1

** Section: Section-3 Profile: Profile-3

*Beam Section, elset=_PickedSet4, material=bottomweight, temperature=GRADIENTS, section=CIRC

0.0252,

0.,1.,0.

*End Part

**

*Part, name=Part-5

*Node

1, 0.7070, 0.0000, 1.9316

2, 0.7070, 0.0000, 1.9296

3, 0.7070, 0.0000, 1.9276

……

60, 0.7070, 0.0000, 0.59

*Element, type=B31

1, 1, 2

2, 2, 3

3, 4, 5

……

40, 59, 60

*Nset, nset=_PickedSet20, internal, generate

 1, 60, 1

*Elset, elset=_PickedSet20, internal, generate

 1, 40, 1

** Section: Section-1 Profile: Profile-1

*Beam Section, elset=_PickedSet20, material=truss, temperature=GRADIENTS, section=CIRC

0.004

0,1,0

*End Part

**

** ASSEMBLY

**

*Assembly, name=Assembly

**

*Instance, name=Part-1-1, part=Part-1

*End Instance

**

……

*Instance, name=Part-5-1-rad-63, part=Part-5

0,0,0

0,0,0,0,0,1,354.2680

*End Instance

**

*Nset, nset=mass1, internal, instance=Part-1-1, generate

1,60,1

……

*Nset, nset=mass2, internal, instance=Part-5-1-rad-63, generate% generate all the nodes

1,60,1

*Elset, elset=mass1, internal, instance=Part-1-1, generate

1,40,1

……

*Elset, elset=mass2, internal, instance=Part-5-1-rad-63, generate% generate all the elements

1,40,1

*Spring, elset=Springs/Dashpots-2-spring,nonlinear

0,-1

0,-0.5

0,0

41550,1

83100,2

*Element, type=SpringA, elset=Springs/Dashpots-2-spring% generate the springs

1,Part-3-1.1,Part-1-1.1

2,Part-3-1.2,Part-1-1-Rad-2.1

3,Part-3-1.3,Part-1-1-Rad-3.1

……..

5040,Part-5-1-Rad-63.59,Part-2-1-lin-20-1.187

*Spring, elset=Springs/Dashpots-2-spring,nonlinear

0,-1

0,-0.5

0,0

8460,1

16920,2

*Element, type=SpringA, elset=Springs/Dashpots-2-spring

5041,Part-5-1.60,Part-4-1.1

5042,Part-5-1-rad-5.60,Part-4-1.2

……..

5056,Part-5-1-rad-61.60,Part-4-1.16% generate the springs used to hang the bottom weights

*End Assembly

**

** MATERIALS

**

*Material, name=floatingcollar

*Density

953.,

*Elastic

 9.5e+8, 0.3

*Material, name=truss

*Density

1125.,

*Elastic

 8.2e+07, 0.3

*Material, name=bottomweight

*Density

4000.,

*Elastic

9.5e+8, 0.3

*AQUA

-1,2,9.8,1025

0.5,0,0,2

** --

**

** STEP: Step-1

**

*Step, name=Step-1, nlgeom=YES, inc=1000000

*Dynamic

0.0001,10.,1e-8,0.01

**

** BOUNDARY CONDITIONS

**

** Name: BC-1 Type: Symmetry/Antisymmetry/Encastre

*Boundary

floater, PINNED

** LOADS

**

** Name: Load-1 Type: Gravity

*Dload

mass1, GRAV, 9.81, 0., 0., -1. % gravity for mass 1

mass1, PB, 1, 0.008 %buoyancy for mass 1

mass1, FDD, 1, 0.008, 4.6%drag for mass 1

mass2, GRAV, 9.81, 0., 0., -1.

mass2, PB, 1, 0.004

mass2, FDD, 1, 0.004, 1.15

bottom, GRAV, 9.81, 0., 0., -1.

bottom, PB, 1, 0.0504

bottom, FDD, 1, 0.0504, 1.15

**

** OUTUT REQUESTS

**

*Restart, write, frequency=50

**

** FIELD OUTUT: F-OuTut-1

**

*Output, field

*Node Output

RF, U

**

*End Step